Interplay of Intrinsic and Extrinsic Factors in Gastric Metaplasia: miR-148a in Chief Cells and the Involvement of Telocytes

By

Yoojin Sohn

Dissertation

Submitted to the Faculty of the

Graduate School of Vanderbilt University

in partial fulfillment of the requirements

for the degree of

DOCTOR OF PHILOSOPHY

in

Cell and Developmental Biology

May 10, 2024

Nashville, Tennessee

Approved:

Christopher V. Wright, D. Phil.

Chin Chiang, Ph.D.

Michelle Southard-Smith, Ph.D.

Richard M. Peek, Jr., M.D.

James R. Goldenring, M.D., Ph.D.

ACKNOWLEDGEMENTS

First and foremost, I extend my deepest gratitude to God the Father Almighty for guiding me through my graduate journey. His omnipresent guidance and omniscient love have been my strength and motivation during the most challenging times. I give all the glory and praise to Him.

I must thank my mentor and advisor, Dr. Jim Goldenring. I am forever grateful for your guidance and support. I have been exceptionally fortunate to have you as my mentor, and you are the best mentor I could have asked for. Your unparalleled expertise, wisdom, and unwavering support have been pivotal in shaping my academic and personal growth. I cherish our scientific discussions, and I fondly recall our brainstorming sessions in your open office, where your insights always illuminated my path.

Special thanks to my dissertation committee members: Dr. Chris Wright, Dr. Chin Chiang, Dr. Michelle Southard-Smith, and Dr. Rick Peek. Their insightful questions and valuable suggestions have enriched my research and honed my critical thinking and analytical skills. I am particularly grateful to Dr. Chris Wright, whose exceptional support and collaborative spirit have been instrumental in overcoming numerous challenges I faced.

Additionally, I was incredibly fortunate to have had Dr. Eunyoung Choi in the lab next door. Her mentorship and advice have been invaluable to me. Witnessing her meticulous approach and dedication to science has been nothing short of inspiring.

My journey would not have been the same without the incredible support from the members of the Goldenring and Choi Labs. To each current and former member, your friendship and shared enthusiasm for science have created an enriching and enjoyable environment. Thank you for being an integral part of my journey.

Lastly, and most importantly, I am deeply grateful to my family. To my amazing wife, Yoona, your love, patience, and understanding have been the cornerstone of my resilience and perseverance. Your unconditional support has been my greatest blessing. Thank you for being my home during the most restless times. I would not have been where I am today without you. To my parents, Kwangsik Sohn and Seonghye Kim, I extend my heartfelt thanks for your endless love and sacrifices. Your support and belief in my dreams has been my driving force. My brother, Yuhyun, thank you for being there for me, always.

This dissertation stands as a testament not just to my academic pursuits but to the collective effort and support of many. Thank you all.

TABLE OF CONTENTS

ACKNOWLEDGEMENTS iii
LIST OF TABLES vi
LIST OF FIGURES vii

CHAPTERS
I. INTRODUCTION 1
1.1 Gastric Cancer 1
1.2 Preneoplastic Lesions in Stomach 1
1.3 Characterization of Gastric Pathology 3
1.3.1 Gastritis 3
1.3.2 Oxyntic Atrophy 3
1.3.3 Pyloric Metaplasia 4
1.3.4 Intestinal Metaplasia 5
1.3.5 Dysplasia and Cancer 5
1.4 Spasmolytic Polypeptide-Expressing Metaplasia 6
1.5 Chief Cell Transdifferentiation 7
1.6 Metaplastic Microenvironment 10
1.7 Conclusion 12

II. DECREASE IN MIR-148A EXPRESSION DURING INITIATION OF CHIEF CELL TRANSDIFFERENTIATION 14
2.1 Introduction 15
2.2 Results 18
2.3 Discussion 38
2.4 Materials and Methods 43

III. TELOCYTE RECRUITMENT DURING THE EMERGENCE OF A METAPLASTIC NICHE IN THE STOMACH 52
3.1 Introduction 53
3.2 Results 56
3.3 Discussion 77
3.4 Materials and Methods 80

IV. CONCLUSIONS AND FUTURE DIRECTIONS 84
4.1 Conclusions 84
4.2 Future Directions 88
4.2.1 miR-148a Downregulation in Chief Cell Transdifferentiation 88
4.2.2 Telocyte Involvement in Metaplasia Development 94

REFERENCES 106

LIST OF TABLES

Table

1. miRNAs highly expressed in mouse chief cells 20
2. miRNAs downregulated in ImSPEM cells compared with ImChief cells 22
3. miRNAs upregulated in ImSPEM cells compared with ImChief cells 24
4. Candidate miRNAs and their targeted genes related to SPEM development 32
5. List of qPCR primers used in Chapter II 50

LIST OF FIGURES

Figure

1. Development of metaplasia and cancer in the stomach 2
2. Ordered sequence of events during chief cell transdifferentiation 9
3. Ordered sequence of events during chief cell transdifferentiation with miR-148a downregulation 14
4. miRNAs related to SPEM development 19
5. miR-148a expression in normal mouse stomach 25
6. miR-148a expression during chief cell transdifferentiation into SPEM cells 27
7. miR-148a expression in human stomach 28
8. The involvement of miR-148a in the initiation of chief cell transdifferentiation 30
9. The upregulation of Dnmt1 in chief cells during chief cell transdifferentiation via the downregulation of miR-148a 34
10. miR-148a downregulation during chief cell transdifferentiation process 37
11. Recruitment of telocytes in metaplasia development in the stomach 52
12. Telocytes in the stomach express FOXL1 and PDGFRα 57
13. FOXL1+/PDGFRα+ double-positive telocytes are increased during the metaplasia development in the stomach 59
14. Telocytes show altered distribution near the expanding proliferative zone in DMP-777-treated mouse stomach 62
15. L635 treatment promotes a shift in telocyte distribution corresponding with proliferative zone expansion 64
16. Telocytes exhibit a consistent proximity to the proliferative cell zone during recovery 66
17. Telocytes are increased during Kras-driven metaplasia development in the stomach 68
18. Telocytes are only found at the base of the gland when metaplasia develops in that region 71
19. Telocytes are actively recruited during metaplasia development 73
20. *Wnt5a* expression co-localizes with PDGFRα-positive telocytes and reflects the telocyte distribution shift in metaplasia 76
21. Major discoveries of the thesis 87
22. FOXL1+/PDGFRα+ double-positive telocytes with other cell markers in stroma 97

CHAPTER I

INTRODUCTION

Gastric Cancer

The incidence of gastric cancer has experienced a marked reduction in the United States in recent years, as reported by the National Cancer Institute; however, its global impact remains significant (*National Cancer Institute*, 2023). The disease stands as the fifth most frequently diagnosed cancer worldwide and positions itself as the fourth leading cause of cancer-related deaths (Sung et al., 2021). Gastric cancer is typically categorized into two main types: the diffuse-type, recognized by its poorly differentiated, dys-cohesive cancer cells that mostly invade as individual cells; and the more common intestinal-type, displaying cancer cells with varying differentiation levels that assemble in tubular or gland-like formations (Ajani et al., 2022). The development of intestinal-type gastric cancer stems from an inflammation-driven sequence within the stomach mucosa, which transitions from gastritis to complete cancer. In this context, a strong risk factor for gastric cancer in humans is an infection with *Helicobacter pylori*. (Nam et al., 2010). Dr. Pelayo Correa has described the histopathologic progression of gastric cancer post *H. pylori* infection, encompassing stages like chronic gastritis, gastric atrophy, intestinal metaplasia, dysplasia, and ultimately cancer (Blaser & Parsonnet, 1994; Correa & Piazuelo, 2012; Correa et al., 2010).

Preneoplastic Lesions in Stomach

Intestinal metaplasia (IM), characterized by the appearance of intestinal-type cells, notably goblet cells within the stomach, has been strongly associated with intestinal-type gastric cancer (Correa et al., 2010). Alongside IM, another metaplasia, pyloric metaplasia (PM), has

been identified in the human stomach. PM emerges as an initial response to gastric epithelium damage, and it is characterized by mucous-secreting glands, which closely resemble the antral glands, taking the place of oxyntic glands in the stomach's corpus region (Goldenring, 2023). Within PM, spasmolytic polypeptide-expressing metaplasia (SPEM) lineage cells mark their presence at the base of the gland. This metaplastic phenotype, observed both in human and mouse stomachs, shares a close relation with gastric cancer onset (Halldorsdottir et al., 2003; Weis et al., 2013; Yamaguchi et al., 2002). Notably, PM encompassing the SPEM lineage is also perceived as a precursor to IM, and both these metaplastic changes stand out as preneoplastic lesions with a strong correlation to gastric cancer (Figure 1) (Nam et al., 2009; Schmidt et al., 1999). Therefore, understanding the factors that promote initiation and progression of metaplasia holds the key to pioneering early interventions that can mitigate gastric cancer risks.

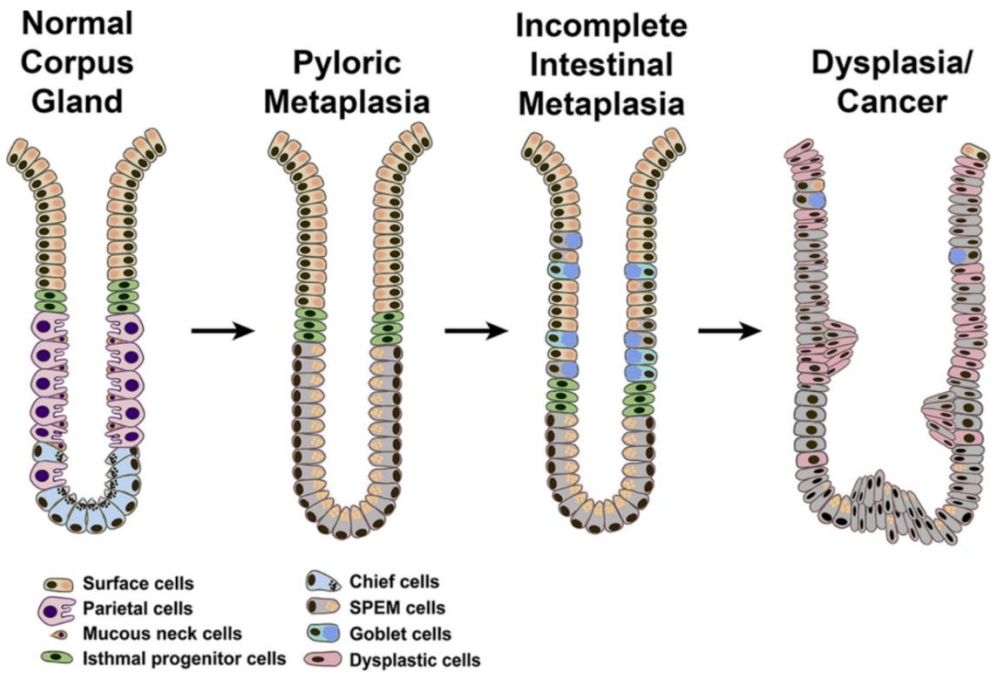

Figure 1. Development of metaplasia and cancer in the stomach.
A schematic representation of the metaplasia development pathway in stomach leading to cancer. (Adapted from (Goldenring, 2023))

Characterization of Gastric Pathology

Gastritis

Gastritis, the inflammatory reaction of the stomach's lining, in humans is primarily an aftermath of a persistent infection with the gram-negative bacterium, *Helicobacter pylori*, but it can also stem from gastric autoimmunity (Annibale et al., 2020; Blaser & Parsonnet, 1994; Marshall & Warren, 1984). The discovery of *H. pylori*-induced gastritis involved an experiment where a researcher willingly consumed a culture of the bacterium, leading to the onset of gastritis (Marshall et al., 1985). Histology remains the gold standard for detecting premalignant changes in the stomach, including atrophic gastritis, intestinal metaplasia, and dysplasia. Gastritis can be identified using hematoxylin and eosin (H&E) staining techniques or via specialized immunohistochemical staining procedures (Sepulveda & Patil, 2008).

Oxyntic atrophy

Oxyntic atrophy is characterized by the loss of acid-secreting parietal cells, which initiates a cascade of epithelial changes and metaplastic transformations in the stomach (Goldenring et al., 2010). In both humans and mice, chronic *Helicobacter* infection leads to oxyntic atrophy in the stomach's corpus over time (Fox et al., 1996; Fox et al., 2003; Wang et al., 1998). Oxyntic atrophy in rodents can be effectively modeled through *Helicobacter* infections or by pharmacologically eliminating parietal cells (Petersen et al., 2017). Diagnosing oxyntic atrophy generally involves the observation of absent eosinophilic parietal cells in H&E-stained tissue sections, supplemented by parietal cell-specific markers like H/K-ATPase immunostaining, providing deeper insights into parietal cell depletion. It is important to note that

oxyntic atrophy triggers mucosal changes, leading to the emergence of hyperplastic and metaplastic lesions in the gastric mucosa.

Pyloric Metaplasia

Metaplasia is an adaptive mechanism of the body where one mature cell type undergoes transformation to another, generally as a protective response to environmental stimuli, such as physical or chemical damages. In the stomach's main body or corpus, the glandular composition spans various cell lineages, such as the acid-secreting parietal cells and zymogen-secreting chief cells. Located at the gland's base, the chief cells are terminally differentiated and predominantly non-proliferative in normal physiological conditions. Nonetheless, in instances of mucosal injury, such as *H. pylori*-induced oxyntic atrophy, these chief cells can undergo transdifferentiation, evolving into mucous-secreting SPEM cells. Consequently, these metaplastic glands adopt the characteristics and structure of the mucin-secreting glands found in the distal stomach, such as the antral/pyloric glands and Brunner’s glands, with TFF2/Muc6-expressing SPEM cells at their bases and TFF1/Muc5AC-expressing surface cells towards the lumen (Goldenring, 2018).

Pyloric metaplasia exemplifies the stomach's innate ability to adapt and heal, highlighting the implication of cellular plasticity and reprogramming. While metaplasia serves as a physiological response to local injury, aiming to promote healing, chronic inflammation and continuous damage can shift PM towards the induction of IM, eventually paving the way for intestinal-type gastric cancer (Goldenring et al., 2010). Hence, a deep understanding of these cellular shifts is paramount for the enhanced management and prevention of related gastric pathologies.

Intestinal Metaplasia

Intestinal metaplasia (IM) denotes a preneoplastic lesion in the stomach, marked by the native gastric mucosa being substituted by an intestinal-type mucosa, especially evident through the emergence of goblet cells. The distinct morphology of these goblet cells, when labeled with MUC2 and TFF3, serves as an indication of intestinal metaplasia (Goldenring et al., 2010). Furthermore, the expression of nuclear Cdx1 and Cdx2 has been observed in instances of IM in humans (Busuttil & Boussioutas, 2009; Eda et al., 2002). IM is a heterogeneous lesion based on its histology and the types of mucins secreted, and it can be further categorized into either complete IM (small intestinal type) or incomplete IM (colonic type) (Busuttil & Boussioutas, 2009).

Glands with complete IM are characterized by prominent goblet cells, Paneth cells and enterocyte-like cells and are perceived as a protective lineage with marginal pre-neoplastic potential (Correa et al., 2010). On the other hand, glands with incomplete IM display immature goblet cells and also feature SPEM cell lineages at their bases (Lee et al., 2022). It is important to note that IM is linked with dysplasia and intestinal-type gastric cancer, and of the two IM types, the incomplete IM is associated with a higher risk of gastric cancer compared to complete IM (Correa et al., 2010; Gonzalez et al., 2013; Shao et al., 2018).

Dysplasia and Cancer

Dysplasia refers to the abnormal development or growth of cells that are largely non-invasive. Within the gastrointestinal tract, dysplasia is recognized as a precursor to cancer and serves as a significant indicator of heightened cancer risk (Sharma & Montgomery, 2013). Traditional diagnostic techniques have relied on pathologists identifying dysplastic phenotypes through the cellular and glandular morphologies observable on H&E staining. However, recent

advancements have highlighted the emergence of specific markers like TROP2 and CEACAM5, that indicate the shift from incomplete intestinal metaplasia to dysplasia in the stomach, allowing for more accurate identification and diagnosis (Lee et al., 2023; Riera et al., 2020).

More than 95% of gastric cancers are adenocarcinomas, and they are defined by cells with aberrant, invasive, and metastatic characteristics (Ajani et al., 2022). Intestinal-type gastric cancer is detected in H&E stained tissue samples through irregular patterns, including multilayered cell formations, altered nuclear shape and placement, and invasion into the submucosa. Previous studies have also noted the upregulation of CEACAM5 in gastric cancers, establishing it as a marker indicative of a poor prognosis in gastric cancer (Zhou et al., 2015).

In sum, gastric carcinogenesis entails a multi-step trajectory, wherein *Helicobacter pylori* infection sets off a cascade of events, spiraling from gastritis to dysplasia and ultimately cancer. Recognizing the preneoplastic lesions, like intestinal and pyloric metaplasia, and how it progresses to dysplasia and cancer, offers us an opportunity to devise innovative preventive strategies and early detection frameworks that can make a difference in managing the threats of gastric cancer.

Spasmolytic Polypeptide-Expressing Metaplasia

The term SPEM (Spasmolytic Polypeptide-Expressing Metaplasia) was coined in 1999, named for its distinct expression of the Trefoil factor-2 (TFF2, also known as spasmolytic polypeptide) (Schmidt et al., 1999). The exact origins of SPEM cells have been a topic of debate in recent years—whether from chief cells or from progenitor cells (Bockerstett et al., 2020; Caldwell et al., 2022; Choi et al., 2016; Choi et al., 2019; Hata et al., 2020; Hayakawa et al., 2015; Kinoshita et al., 2018; Nam et al., 2010). While there has been discussion around their origin, studies have indicated that SPEM cells have both morphological and gene expression

profiles that are intermediate between digestive enzyme-secreting chief cells and mucous-secreting cells (Nam et al., 2010; Weis et al., 2013). Adding depth to this understanding, lineage-tracing studies have confirmed that SPEM cells primarily arise from transdifferentiating chief cells rather than normal progenitor cells (Caldwell et al., 2022; Leushacke et al., 2017; Nam et al., 2010).

The SPEM cells are a critical component of pyloric metaplasia. Their mucous-secreting ability offers a protective barrier against the continued aggression of factors like *H. pylori*, thereby providing a reparative and adaptive response to maintain the stomach's integrity and function. Furthermore, the SPEM cells serve as progenitor-like proliferative cells, generating surface cells (Caldwell et al., 2022). A comprehensive grasp of the mechanisms behind the transdifferentiation of chief cells into the SPEM lineage is crucial, as it could provide valuable insights into pathways central to the onset and progression of gastric cancer.

Chief Cell Transdifferentiation

The transdifferentiation of chief cells into SPEM cells is a finely orchestrated process. This involves dismantling the secretory architecture inherent to chief cells and facilitating pronounced transcriptional changes, marked by the increased expression of GSII-lectin, TFF2, MUC6, CD44v9, and AQP5 (Goldenring, 2018; Lee et al., 2022; Meyer et al., 2019). Beyond transdifferentiation, SPEM cells exhibit the potential to re-enter the cell cycle, as shown by the expression of proliferation markers like Ki67 and PCNA (Petersen et al., 2018; Yamaguchi et al., 2002).

The process of chief-cell transdifferentiation involves an organized sequence of changes in chief cells that lead to the development of SPEM cells (Mills & Sansom, 2015; Petersen et al., 2018; Shimizu et al., 2020; Willet et al., 2018). These changes are illustrated in Figure 2.

Following oxyntic atrophy, there is an early loss of the expression of the chief cell maturation-specific transcription factor, Mist1 (Petersen et al., 2018; Weis et al., 2013). During this phase, there is also a decline in the levels of miR-148a, the most abundant miRNA in chief cells (Shimizu et al., 2020). Progressing further, an upregulation of SPEM cell markers, AQP5 and CD44v9, is observed (Lee et al., 2022). Significantly, CD44v9 facilitates cellular adaptability to stresses, such as Reactive Oxygen Species (ROS), functioning as both an activator and stabilizer for the xCT cystine transporter (Ishimoto et al., 2011; Meyer et al., 2019; Wada et al., 2013). The increased cellular stress is associated with augmented autophagy that is necessary for breaking down the zymogen granules (Meyer et al., 2019; Willet et al., 2018). Concurrently, a dynamic fluctuation in mTORC1 activity is observed. There is an initial decline post-injury, followed by a reactivation alongside the elevated expression of damage-associated metaplastic genes, such as Sox9, synchronous with the onset of the cell cycle (Willet et al., 2018).

Importantly, the trajectory of transdifferentiation can be interrupted at different stages, highlighting a plasticity governed by an intricate, sequentially organized order. (Petersen et al., 2018; Willet et al., 2018). In autophagy-defective Gnptab$^{-/-}$ mouse model, metaplasia-associated gene expression changes were incomplete, and increased instances of apoptosis was observed at gastric gland bases (Willet et al., 2018). This indicates that maintaining regular lysosomal function and autophagy is crucial during transdifferentiation. Additionally, when mTORC1 is inhibited using rapamycin, it hinders the proliferation of SPEM cells, while permitting autophagy and induction of metaplastic gene (Willet et al., 2018). This suggests the reactivation of mTORC1, which occurs at the later stage of chief-cell transdifferentiation into SPEM cells, is required for re-entering the cell cycle. These insights highlight that the process of chief-cell transdifferentiation into proliferative SPEM cells follows a step-by-step program with specific

intervening checkpoints in place. Moreover, the transdifferentiation of chief cells and metaplasia development is not an isolated event, and it is influenced by and reliant on the surrounding microenvironment.

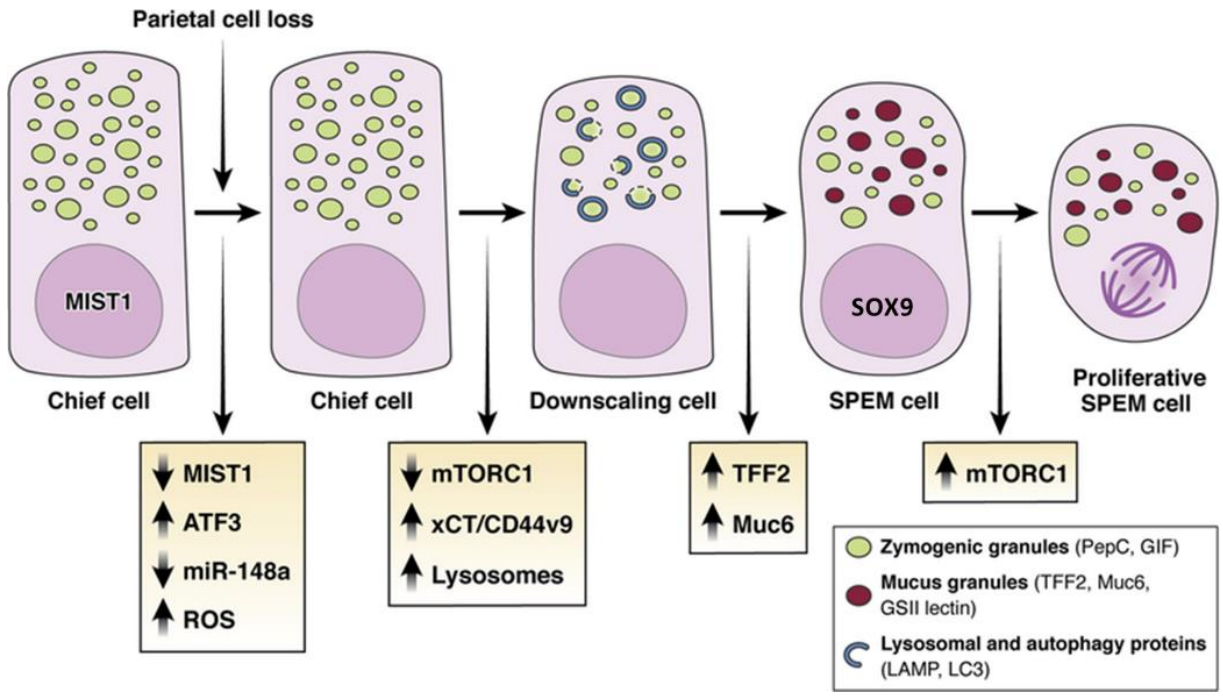

Figure 2. Ordered sequence of events during chief cell transdifferentiation.
Transdifferentiation of Chief cells into SPEM cells occurs through an orderly set of cellular transitions. (Adapted from (Goldenring & Mills, 2022))

Metaplastic Microenvironment

The microenvironment is composed of a diverse array of cell types, such as immune cells, fibroblasts, and endothelial cells, which coordinate to maintain homeostasis in the normal gastric mucosa (Busada et al., 2019; Sigal et al., 2017). Among these, immune cells have emerged as key players in the context of metaplasia development in the stomach.

Prior research has emphasized the significance of immune cells, notably type 2 innate lymphoid cells (ILC2) and M2 macrophages, in the development of metaplasia (Busada et al., 2019; Meyer et al., 2020; Petersen et al., 2014). Following damage to the gastric mucosa, epithelial cells initiate a response by releasing interleukin 33 (IL-33). Both IL-33 and its receptor, ST2, found in ILC2s, have been implicated as essential components for the onset of metaplasia, as neither IL-33 knockout nor ST2 knockout mice develop metaplasia, even after parietal cell loss (Petersen et al., 2018). Furthermore, the type II cytokine IL-13, predominantly released by ILC2s, plays an essential role in this transformation. Evidence suggests that mice deprived of IL-13 do not develop metaplasia even post parietal cell loss, but, introducing recombinant IL-13 to ST2 knockout mice reestablishes the metaplasia following injury (Petersen et al., 2018). It is evident that ILC2 cells, being the primary source of IL-13, are crucial for a well-coordinated response to severe injury in the gastric epithelium, including facilitating macrophage activation or infiltration post-injury (Meyer et al., 2020). Additionally, M2 macrophages play a significant role in advancing metaplasia to the more advanced SPEM phenotype (Petersen et al., 2014). In summary, the role of immune cells in metaplasia development, especially in the gastric environment, is not just integral but pivotal. These discoveries reinforce the importance of continuous research in this domain, potentially reshaping our approach to gastric pathologies and their treatment.

In addition to immune cells, fibroblasts are important components of the microenvironment and play key roles in tissue homeostasis, disease progression, and wound healing processes. A growing body of literature highlights the significance of fibroblasts, especially as cancer-associated fibroblasts, within the tumor microenvironment. These fibroblasts influence various functions, including cancer cell proliferation, tumor immunity, extracellular matrix remodeling, and drug resistance (Biffi & Tuveson, 2021). However, there is a discernible gap in literature when it comes to their precise roles in the development and progression of preneoplastic lesions in the stomach. The precise dynamics of fibroblasts within this context still require thorough investigation.

The recent discovery of the interaction between fibroblasts and metaplastic epithelial cells, steering the progression from metaplasia to dysplasia, has broadened our perspective (Lee et al., 2023). Single-cell RNA sequencing has illuminated the heterogeneous nature of fibroblasts within the gastric environment. The identification of four distinct fibroblast subsets, each characterized by its own set of markers and functional implications, underlines the complexity of the stromal cell environment. Intriguingly, telocyte-like fibroblasts are noteworthy both for their distinct morphology and their role in the early stages of carcinogenesis. While the fibroblasts have been recognized for their structural role in shaping the extracellular matrix, they also produce a wide array of secretory factors. These potentially include WNT ligands, a diverse array of cytokines/chemokines, and essential growth factors (Biffi & Tuveson, 2021; Lee et al., 2023). This underscores their potential importance in maintaining tissue homeostasis on one hand and influencing carcinogenic pathways on the other. The expanding research into these cells' multifaceted roles is promising, opening avenues for new preventive and therapeutic strategies targeting the early stages of carcinogenesis. A comprehensive understanding of how stromal cells

integrate into standard homeostasis and influence early carcinogenesis, especially in the initiation of metaplasia, is imperative.

Conclusion

The development of metaplasia in response to injury or infection represents a delicate balance between reparative mechanisms and processes that potentially drive carcinogenesis. The metaplastic response can be reparative following injury allowing protection and restoration of the stomach after damage. However, this physiological cellular response can be problematic if it persists in the presence of persistent inflammation and injury, predisposing to cancer development.

Identifying and gaining a clear understanding of the factors involved in the development of metaplasia and progression to cancer in the stomach is crucial. The Spasmolytic Polypeptide-Expressing Metaplasia (SPEM) cells have gained notable attention due to their adaptive and reparative response roles, especially in relation to mucosal damage. The potential link with the onset and progression of gastric cancer underscores the importance of understanding their transdifferentiation. The orchestrated process of chief cells transdifferentiation into SPEM cells is illuminated by their gene expression alterations. Comprehending this process is essential not just for the implications it has on gastric integrity but for the broader understanding of gastric cancer onset.

The gastric microenvironment, populated by immune cells, fibroblasts, and endothelial cells, has profound implications for metaplastic development. Both immune and stromal cells in the gastric environment interact closely with epithelial cells, indicating a complex interplay between homeostasis and metaplasia initiation and progression. The subsequent chapters of this

thesis will focus on identifying key factors and mechanisms underlying chief-cell transdifferentiation and the development of metaplasia in the gastric mucosa. This exploration is crucial for advancing our understanding of gastric pathologies and developing targeted therapeutic interventions for the early stages of carcinogenesis and metaplastic transformations in the stomach.

CHAPTER II

DECREASE IN MIR-148A EXPRESSION DURING INITIATION OF CHIEF CELL TRANSDIFFERENTIATION

This chapter is adapted from: Shimizu T*, **Sohn Y***, Choi E, Petersen CP, Prasad N, Goldenring JR. Decrease in MiR-148a Expression During Initiation of Chief Cell Transdifferentiation. *Cell Mol Gastroenterol Hepatol*. 2020;9(1):61-78. (*co-first author)

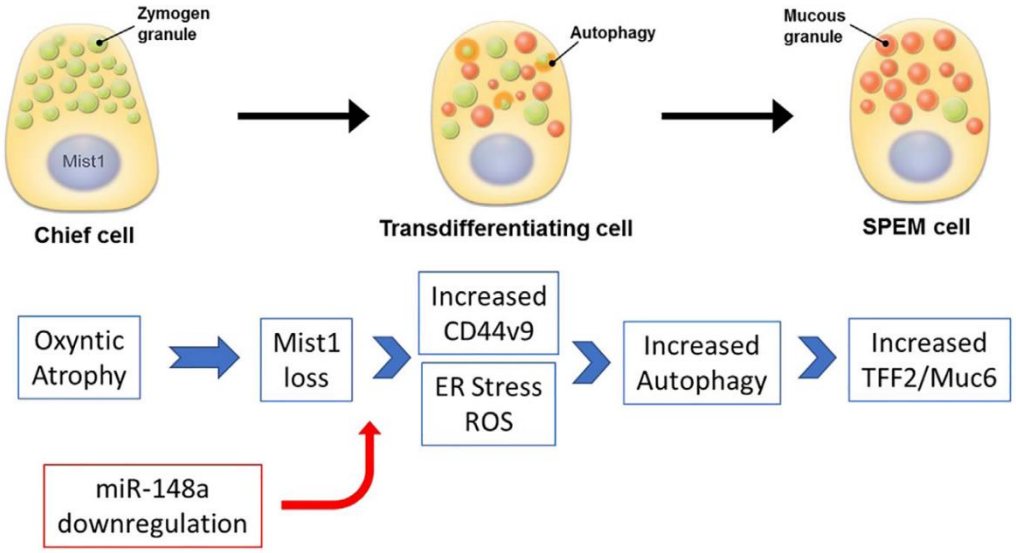

Figure 3. Ordered sequence of events during chief cell transdifferentiation with miR-148a downregulation.
This is the graphical abstract describing how miR-148a downregulation occurs early in the process of chief cell transdifferentiation into SPEM cells.

Introduction

In the stomach mucosa, gastric chief cells are located at the base of oxyntic glands and express secretory zymogens. Chief cells differentiate from mucous neck cells in the lower half of corpus glands without cell division and remain in a fully differentiated state under normal conditions with a lifetime of over 60 days (Weis et al., 2016). Previous studies demonstrated that some transcription factors, including XBP1 and MIST1 are required for the differentiation from mucous neck cells into chief cells and the maintenance of chief cells (Bredemeyer et al., 2009; Goldenring et al., 2011; J. K. M. Lennerz et al., 2010). On the other hand, parietal cell loss and inflammation induce chief cells to transdifferentiate into mucous cell metaplasia, designated spasmolytic polypeptide-expressing metaplasia (SPEM), with the loss of zymogen granules and the formation of Muc6-containing mucous granules (Goldenring et al., 2011; Mills & Sansom, 2015). SPEM is considered a likely precursor lineage for intestinal metaplasia (IM) development, and these metaplasias are possible precursor lesions of gastric cancer (Goldenring et al., 2010; J. K. M. Lennerz et al., 2010). However, the regulatory mechanisms for the chief-cell transdifferentiation process have not been fully elucidated.

MicroRNAs (miRNAs) are critical post-transcriptional regulators of gene expression (Bartel, 2004; Ha & Kim, 2014). miRNAs are involved in the developmental process of various organs as well as cancer progression (Calin & Croce, 2006; Esquela-Kerscher & Slack, 2006). Dysregulation of miRNAs has been reported in human gastric cancer (Ueda et al., 2010) and *Helicobacter pylori* (*H. pylori*)-induced gastritis (Matsushima et al., 2011; Zabaleta, 2012), contributing to gastric epithelial cell proliferation. We previously reported an analysis of miRNAs in laser capture microdissected human chief cells, SPEM cells and IM cells, suggesting that miR-30a downregulation and miR-194 upregulation were related to metaplasia progression

through regulation of the transcription factors HNF4γ and NR2F2 (Sousa et al., 2016). However, it remains unclear whether miRNAs are involved in the initiation of SPEM development.

Chief-cell transdifferentiation and the transition to SPEM cells occur through a series of ordered events. Our group and others have identified a number of events that chief cell undergo in order to transdifferentiate from zymogen secreting cells into mucous secreting metaplastic cells. Acute oxyntic atrophy induces an early loss of the chief cell maturation-specifying transcription factor, Mist1 (Petersen et al., 2018; Ramsey et al., 2007; Weis et al., 2013) and upregulation of the specific splice variant of CD44, CD44 variant 9 (CD44v9) (Meyer et al., 2019; Petersen et al., 2018; Wada et al., 2013). CD44v9 is an activator and a stabilizer of xCT, a cystine transporter, which promotes adaptation to Reactive Oxygen Species (ROS) and cellular stress (Ishimoto et al., 2011; Meyer et al., 2019; Wada et al., 2013). The increased cellular stress is associated with an increase in autophagy, which is necessary for breaking down the zymogen granules (Willet et al., 2018). Importantly, the process of transdifferentiation can be arrested at different stages (Meyer et al., 2019; Petersen et al., 2018; Willet et al., 2018), suggesting that chief-cell transdifferentiation occurs through a set of stepwise events that are coordinated and maintained in a defined order.

Here we investigated the influence of miRNAs on the initiation of chief-cell transdifferentiation into SPEM cells. We performed miRNA profiling specifically on mouse chief cells and compared miRNA expression with that in conditionally immortalized mouse chief cell and SPEM cell lines. Interestingly, several miRNAs were highly expressed in normal chief cells, but downregulated in SPEM cells. Among them, miR-148a was the most highly expressed miRNA by over 10-fold in chief cells. Loss of miR-148a was associated with the early initiation of chief-cell transdifferentiation. In addition, the loss of miR-148a led to upregulation of an early

SPEM marker, CD44 variant 9 and one of its target genes, Dnmt1. The loss of miR-148a was found early during the chief-cell transdifferentiation process, preceding upregulation of CD44v9. These findings suggest that miR-148a is an early regulator in reprogramming chief cells during transdifferentiation into SPEM.

Results

The miRNA profile of *in vivo* mouse chief cells and immortalized chief cell and SPEM cell lines.

In a previous study, our group reported the miRNA profile of human SPEM and IM in comparison to chief cells from normal stomach (Sousa et al., 2016). In those studies, we identified miRNAs related with human intestinal metaplasia progression; however, no miRNAs related to SPEM development were confirmed. We therefore sought to investigate miRNAs during the initiation of SPEM development using mouse models. First, to profile miRNAs from mouse chief cells, we crossed Mist1$^{CreERT2/+}$mice with R26R^{mTmG} reporter mice. After Tamoxifen injection, immunostaining analyses of these mouse stomachs showed that most of GFP-positive cells were chief cells at the base of glands with only occasional labeled cells in the isthmus regions (Figure 4A) (Weis et al., 2016). We sorted GFP-positive cells from two mice and performed miRNA sequencing (Figure 4B). 43 miRNAs were highly expressed in mouse chief cells (read values >500 in both mice) (Table 1). Among them, miR-148a-3p was the most highly expressed miRNA (read values > 150,000) in chief cells, over 10-fold higher than other highly expressed miRNAs, such as miR-375-3p, let-7 family (let-7b-5p, let-7c-5p, let-7f-5p and let-7a-5p) and miR-200b-3p (read values >8,000). Interestingly, these miRNAs have already been reported as downregulated in human gastric cancer tissues and related to gastric cancer progression (Motoyama et al., 2008; Qiu et al., 2017; Tang et al., 2013; Tsukamoto et al., 2010).

To investigate miRNAs related to metaplasia development, we examined miRNA expression profiles for conditionally immortalized mouse chief cell (ImChief) and SPEM cell (ImSPEM) lines, previously established from Immortomice (Weis et al., 2014). ImChief cells express chief cell markers, such as Pepsinogen C (*Pgc*) and *Mist1*, and produce characteristic

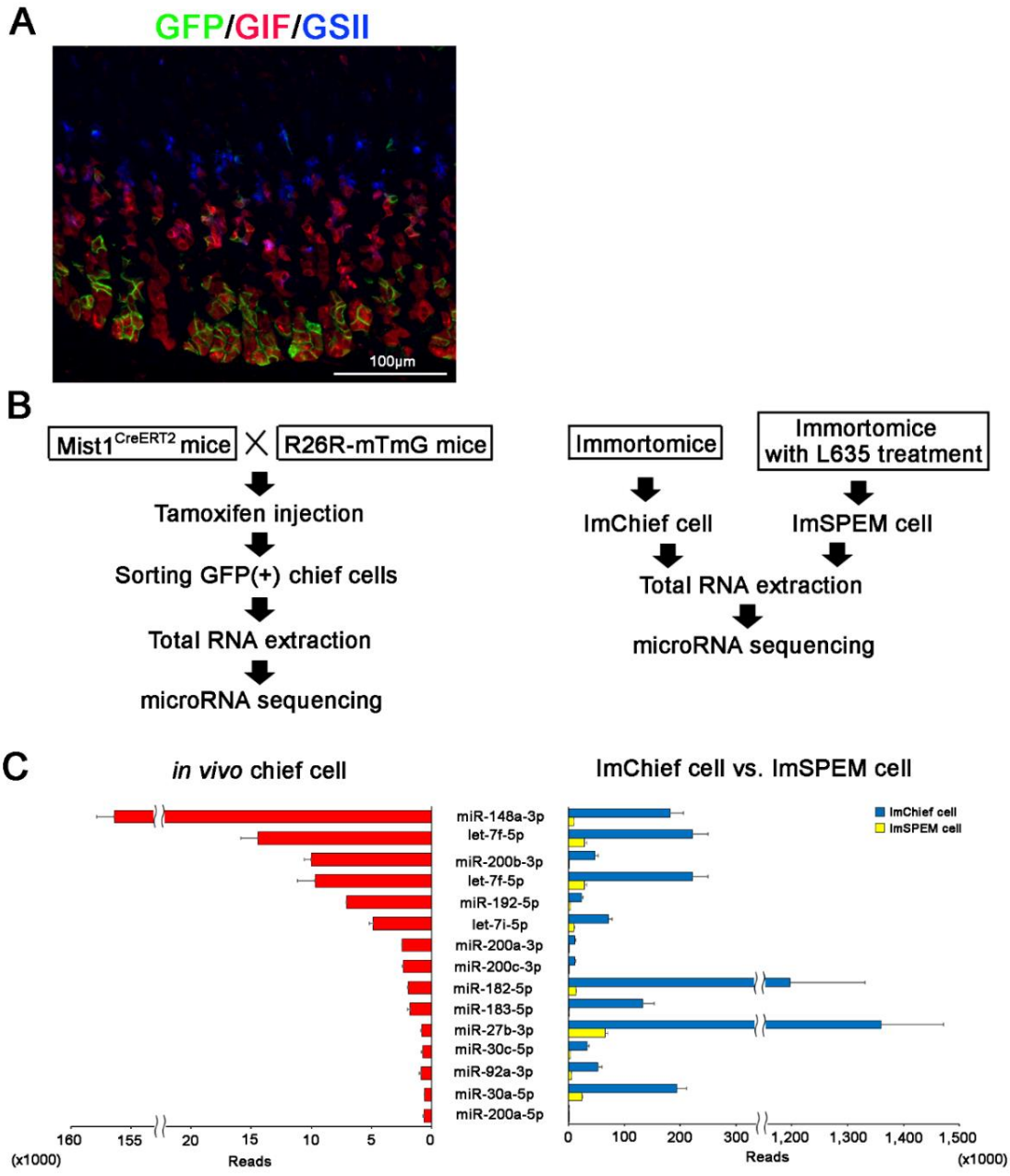

Figure 4. miRNAs related to SPEM development.
A. Immunofluorescence staining in Mist1CreERT2/+;R26RmTmG/+ mice.
Membrane-associated GFP was expressed in GIF-positive chief cells and occasionally in the isthmus regions at 10 days after Tamoxifen injection.
B. Schemes of miRNA sequencing experiments. (left) miRNAs from sorted chief cells of Mist1-mTmG mice. (right) miRNAs from ImChief cells and ImSPEM cells.
C. 15 miRNAs that were both highly expressed in sorted chief cells (red) and downregulated in ImSPEM cells (yellow) compared with ImChief cells (blue). The read values for these miRNAs were over 500, and fold changes of expression between ImSPEM cells and ImChief cells were over 5. miRNA sequencing analyses detected 2 different let-7f-5p as upregulated miRNAs in chief cells. Top one was at chromosome X, and another was at chromosome 13 (see Table 1).

Table 1. miRNAs highly expressed in mouse chief cells

Accession	Chromosome	Strand	Start	End	Gene ID	Sample 1	Sample 2	Entrez ID
mmu-miR-148a-3p	chr6	–	51219828	51219849	MI0000550_1	157846.9654	154942.4573	387166
mmu-miR-375-3p	chr1	–	74947235	74947256	MI0000792_1	35248.20084	21476.74894	723900
mmu-let-7b-5p	chr15	+	85537755	85537776	MI0000558_1	25949.91154	27815.42445	387245
mmu-let-7c-5p	chr16	+	77599917	77599938	MI0000559_1	15987.66912	22193.04491	387246
mmu-let-7c-5p	chr15	+	85537046	85537067	MI0000560_1	14821.59409	20835.45521	723966
mmu-let-7f-5p	chrX	+	1.48E+08	1.48E+08	MI0000563_1	13039.97967	15870.56644	387253
mmu-miR-7a-5p	chr13	–	58494202	58494224	MI0000728_2	11223.58539	6231.293692	723902
mmu-miR-200b-3p	chr4	–	1.55E+08	1.55E+08	MI0000243_1	9422.302927	10591.6593	387243
mmu-let-7a-5p	chr13	–	48633608	48633629	MI0000556_2	8746.256843	12009.56271	387244
mmu-miR-7a-5p	chr7	+	86033181	86033203	MI0000729_1	8740.205588	4823.681713	723884
mmu-let-7a-5p	chr9	+	41344815	41344836	MI0000557_1	8363.615366	11563.89665	723965
mmu-let-7f-5p	chr13	–	48633258	48633279	MI0000562_2	8230.526464	11138.08047	387252
mmu-miR-192-5p	chr19	+	6264857	6264877	MI0000551_1	7084.120318	7057.18444	387187
mmu-miR-21-5p	chr11	–	86397622	86397643	MI0000569_2	5868.145795	7696.271615	387140
mmu-miR-26a-5p	chr10	+	1.26E+08	1.26E+08	MI0000706_1	5001.537708	3946.313897	723962
mmu-miR-26a-5p	chr9	+	1.19E+08	1.19E+08	MI0000573_1	5001.537708	3946.313897	387218
mmu-let-7i-5p	chr10	–	1.22E+08	1.22E+08	MI0000138_2	4517.566115	5195.810144	387251
mmu-miR-99a-5p	chr16	+	77599185	77599206	MI0000146_1	3504.250029	3589.631416	387229
mmu-miR-30d-5p	chr15	–	68172819	68172840	MI0000549_2	2757.120297	2825.520615	387228
mmu-miR-7b-5p	chr17	+	56382440	56382462	MI0000730_1	2657.301111	1373.046719	723883
mmu-miR-200a-3p	chr4	–	1.55E+08	1.55E+08	MI0000554_1	2465.225664	2397.499834	387242
mmu-miR-200c-3p	chr6	–	1.25E+08	1.25E+08	MI0000694_1	2239.877318	2418.092972	723944
mmu-miR-182-5p	chr6	–	30115962	30115986	MI0000224_2	2006.965359	1888.583689	387177
mmu-miR-1a-3p	chr18	–	10785483	10785504	MI0000652_1	1755.906123	63.24694981	723959
mmu-miR-125a-5p	chr17	+	17967781	17967804	MI0000151_1	1663.648576	1174.480463	387235
mmu-let-7g-5p	chr9	+	1.06E+08	1.06E+08	MI0000137_1	1585.004257	1562.052254	387249
mmu-miR-183-5p	chr6	–	30119711	30119732	MI0000225_2	1533.581369	2018.018941	387178
mmu-miR-151-3p	chr15	–	73085250	73085270	MI0000173_1	1308.233185	1660.600129	387169
mmu-miR-215-5p	chr1	+	1.87E+08	1.87E+08	MI0000974_1	1215.975967	3101.305644	387211
mmu-miR-127-3p	chr12	+	1.11E+08	1.11E+08	MI0000154_2	1188.753604	600.1103493	387146
mmu-miR-143-3p	chr18	–	61808853	61808873	MI0000257_1	1025.412731	771.4655906	387161
mmu-miR-378-3p	chr18	–	61557492	61557512	MI0000795_1	1020.875345	2281.30322	723889
mmu-miR-423-5p	chr11	–	76891624	76891646	MI0004637_2	1001.21424	1177.423	751519
mmu-miR-27b-3p	chr13	+	63402068	63402088	MI0000142_2	860.560016	781.7616481	387221
mmu-miR-30c-5p	chr1	+	23298553	23298575	MI0000548_1	852.9982668	620.7028672	723964
mmu-miR-30c-5p	chr4	–	1.2E+08	1.2E+08	MI0000547_2	848.4606843	617.0253704	387227
mmu-miR-92a-3p	chr14	+	1.15E+08	1.15E+08	MI0000719_2	739.5680038	1023.717545	751549
mmu-let-7e-5p	chr17	+	17967330	17967351	MI0000561_1	680.5837996	718.5145194	387248
mmu-let-7d-5p	chr13	–	48631447	48631468	MI0000405_2	603.4510756	628.792413	387247
mmu-miR-30a-5p	chr1	+	23279113	23279134	MI0000144_1	586.8142113	556.7203464	387225
mmu-miR-320-3p	chr14	+	70843364	70843385	MI0000704_2	580.7647177	527.3028558	723838
mmu-miR-25-3p	chr5	–	1.39E+08	1.39E+08	MI0000689_1	552.0292875	714.1023224	723926
mmu-miR-200a-5p	chr4	–	1.55E+08	1.55E+08	MI0000554_2	547.491972	686.8912993	387242

zymogen granules, although they do not express gastric intrinsic factor. In contrast, ImSPEM cells express SPEM-specific markers, such as *Tff2* and *He4* and some intestinalized markers, such as *Cftr* and *PigR*. We extracted total RNAs from ImChief cells and ImSPEM cells and performed miRNA sequencing. We detected 87 miRNAs downregulated ($p < 0.01$, with read values for ImChief cells >500 and fold-change >5) and 7 miRNAs upregulated ($p < 0.01$ with read values for ImSPEM cells >500 and fold-change >5) in ImSPEM cells compared with ImChief cells (Tables 2 and 3). From these two different sequencing studies, we identified 15 miRNAs that were both highly expressed in sorted chief cells and downregulated in ImSPEM cells compared with ImChief cells (Figure 4C), as candidate miRNAs related to SPEM development. This group of miRNAs included miR-148a-3p, miR-200 family members (miR-200a-3p, miR-200a-5p, miR-200b-3p and miR-200c-3p), miR-30 family members (miR-30a-5p and miR-30c-5p) and let-7 family members (let-7f-5p and let-7i-5p).

miR-148a expression in mouse stomach assessed by *in situ* hybridization.

Because it was by far the most highly expressed miRNA species in chief cells, we focused our subsequent studies on miR-148a. To examine the distribution of miR-148a expression, we performed *in situ* hybridization analyses for miR-148a (Figure 5). In normal stomach, miR-148a was strongly expressed in the bases of corpus glands, deep to GSII-positive mucous neck cells, and surface cells and mucous neck cells showed no or very low expression of miR-148a (Figure 5A). miR-148a expression was localized in the cytoplasm, especially in the basal side of cells. In contrast to the corpus, the antrum and the duodenum showed little or no expression of miR-148a. Importantly, dual immunostaining with *in situ* hybridization demonstrated that miR-148a-positive cells expressed the chief cell markers Mist1 and Gastric

Table 2. miRNAs downregulated in ImSPEM cells compared with ImChief cells

Feature	ImSPEM cells_1	ImSPEM cells_2	ImSPEM cells_3	ImChief cells_1	ImChief cells_2	ImChief cells_3	ImSPEM cells/ImChief cells
mmu-miR-141-5p	0	0	0	1005	1576	1593	0
mmu-miR-141-3p	60.5	75.5	84	147862	151753	220628.5	0.000423
mmu-miR-200c-3p	7	6	3	8326.5	13315	12489.5	0.000469
mmu-miR-205-5p	145	148	197	233099	355470	318724	0.00054
mmu-miR-205-3p	5	5	3	4571	5175	5850	0.000834
mmu-miR-203-3p	8	11	11	4932	6346	6065	0.00173
mmu-miR-672-5p	1	2	4	1015	1430	1390	0.001825
mmu-miR-676-3p	2	2	2	682	735	856	0.00264
mmu-miR-429-3p	60	69	73	18745.5	22299.5	23313.5	0.003139
mmu-miR-146a-5p	136.5	163.5	172.5	28169.5	67458.5	42172	0.003429
mmu-miR-200a-3p	42.5	40.5	46	9297	12749	13597.5	0.003619
mmu-miR-200b-3p	239	269	316	37915	48814.5	56526	0.005752
mmu-miR-135b-5p	6	16	17	1674.67	2275.83	2806.67	0.005772
mmu-miR-200a-5p	12	5	3	624	1067	745	0.00821
mmu-miR-183-5p	1153	1362	1308	109600	114757	173820	0.009601
mmu-miR-183-3p	11	14	13	1045	1147	1645	0.009904
mmu-miR-182-5p	15006	12308	14206	1002426	1136518	1453717	0.011557
mmu-miR-96-5p	98	112	92	6537	7080	10821	0.012358
mmu-miR-193b-3p	67	108	94	3006	2259	5077.5	0.026009
mmu-miR-31-3p	24	82	48	1569	1446	2632	0.027271
mmu-miR-31-5p	6738	5724	7552	182407	217916	244071	0.031059
mmu-miR-582-3p	32	21	48	844	905	1241	0.033779
mmu-miR-421-3p	167	192	226	4175	4981	5907	0.038837
mmu-miR-147-3p	26	18	28	427	604	599	0.044172
mmu-miR-222-3p	2279	1489	2261	32959	50742	47026	0.046119
mmu-miR-210-5p	39	46	64	684	1217	1212	0.047864
mmu-miR-27b-3p	58480	65172.5	74847.5	1248916	1245684	1584584	0.048662
mmu-miR-181b-5p	563	509.5	742.67	10536.83	12984.17	13485.67	0.04905
mmu-miR-181a-5p	7652	7487	8969	142888	140394	203123	0.049564
mmu-miR-148a-3p	8590.5	9828.5	9697.5	140196	181813	223713.5	0.051522
mmu-miR-148a-5p	67	66	78	1008	1140	1544	0.057151
mmu-miR-298-5p	770	630	794	10712	10690	15097	0.060111
mmu-miR-21a-3p	480	1124	901	7385	10894	16739	0.071535
mmu-miR-101b-3p	142.5	211	182	1863.5	2280	2870.5	0.076347
mmu-miR-27b-5p	82	85	100	965	1248	1267	0.076724
mmu-miR-126a-5p	212	406	383	3065	4248	5532	0.077929
mmu-miR-1843a-5p	85	103	117	1180	1189	1462	0.079614
mmu-miR-365-3p	64	129	103	1071	917	1658	0.081185
mmu-miR-221-3p	2572	2973	3118	27309	32974	39637	0.086699
mmu-miR-29b-3p	151.67	274	211	1543.33	2317	2887.33	0.094354
mmu-miR-30c-5p	2801	3116	3936	29133.67	30398.33	40878	0.098128
mmu-miR-92a-3p	5585	4445.33	5511.67	42970.67	47225.33	66885.67	0.098942
mmu-miR-194-5p	165	136	242	1465	2072	1948	0.098997
mmu-miR-425-5p	346	436	499	3521	4204	4789	0.102365
mmu-miR-19b-3p	301.5	369.5	309.5	2310.17	3555.5	3663.5	0.102895
mmu-miR-221-5p	607	297	339	3409	3600	5063	0.102966
mmu-miR-374b-5p	55	100	130	744	914	1025	0.106224
mmu-miR-126a-3p	53	49	76	387	561	665	0.110353
mmu-miR-17-5p	101	130	130	830	1150.83	1259.83	0.111397

Table 2. Continued

Feature	lmSPEM cells_1	lmSPEM cells_2	lmSPEM cells_3	lmChief cells_1	lmChief cells_2	lmChief cells_3	lmSPEM cells/lmChief cells
mmu-miR-328-3p	160	152.5	210.5	1513	1110.5	1946.5	0.114442
mmu-miR-130b-3p	119	112.5	176	629.5	1266.5	1656	0.114724
mmu-miR-19a-3p	57.5	63.5	55.5	363.83	552.5	615.5	0.115222
mmu-miR-484	1241	1134	1489	9205	9226	14465	0.117461
mmu-miR-20a-5p	84	113	84	570	774	887.33	0.125934
mmu-miR-23b-3p	1793.5	3092	2818.5	17506	18406.5	25082	0.126306
mmu-miR-30a-5p	22727.5	24771	26421.5	164380	193723.5	225365.3	0.126691
mmu-miR-30e-5p	10724.5	10780.5	11758.5	70581	89679	98109.33	0.128744
mmu-miR-192-5p	2938	2785	3313.5	20230	21444	27916.5	0.129852
mmu-let-7f-5p	22306.05	28289.77	35971.93	174340.2	270159	221880.1	0.129908
mmu-miR-210-3p	846	949	1217	6351	7870	8930	0.130102
mmu-miR-22-3p	107186	109978	146919	737758	925662	1022961	0.135529
mmu-miR-107-3p	182.5	186.33	225.67	1261.83	1418	1703.83	0.135617
mmu-let-7i-5p	7772	9401	12263.5	59123	79414.5	77297.5	0.136384
mmu-miR-191-5p	13618	16310	18084	97568	100312	151097	0.137579
mmu-miR-98-5p	514.27	1025.47	1211.27	4932.67	7444.4	7119.93	0.141099
mmu-miR-34b-5p	444.5	548	642	3035.5	4005.5	4381	0.143101
mmu-miR-93-5p	4297	4794	5926	31000	32748	40799	0.143639
mmu-let-7b-3p	63	87	108	539	443	811	0.143893
mmu-let-7j	980.5	966.5	1326	6196	8255.5	8213.5	0.144408
mmu-miR-99b-3p	104	119	123	625	822.5	854	0.150337
mmu-miR-30a-3p	357	445	506.5	2347.5	2619.5	3139.5	0.161414
mmu-miR-24-3p	3038	3982	3287	16617	22764	24253	0.161973
mmu-miR-27a-3p	4684	6406.5	7145.5	31267	36340	43419.5	0.164249
mmu-miR-34b-3p	347	405	567	2219	2505	3299	0.164402
mmu-miR-342-3p	179	159	162	899	732	1409	0.164474
mmu-miR-1839-5p	194	235	293	1243	1427	1642	0.16744
mmu-miR-130a-3p	2613	2714.5	3310	13909.5	17149.5	20256	0.168323
mmu-miR-140-3p	616	798	807	3466	4682	5039	0.168423
mmu-miR-29a-3p	5652.5	5820	6999	28115.5	38135.5	42291.83	0.170177
mmu-miR-450b-5p	310	290	330	1263	1804	2195	0.176739
mmu-miR-34c-5p	19682.5	20120	26912	100916.5	127993	144827	0.178507
mmu-miR-351-5p	2316	1802	1999	9210	9920	15121	0.178593
mmu-miR-34c-3p	126	327	317	1091	1488	1633	0.182811
mmu-miR-28a-3p	157	207	307	942	1264	1400	0.186079
mmu-miR-28a-5p	611	711	929	3248	4056	4324	0.193584
mmu-miR-186-5p	5336	5697	6401	23436	30215	36028	0.194404
mmu-let-7d-3p	387	589	647	2297	2030	3951	0.196062

Table 3. miRNAs upregulated in ImSPEM cells compared with ImChief cells

Feature	ImSPEM cells_1	ImSPEM cells_2	ImSPEM cells_3	ImChief cells_1	ImChief cells_2	ImChief cells_3	ImSPEM cells/ImChief cells
mmu-miR-10b-5p	255958.5	248754.5	263925	69.5	107.5	118.5	2601.144
mmu-miR-199a-5p	1767	1715	2536	6	8	18	188.0625
mmu-miR-199a-3p mmu-miR-199b-3p	2801	6977	7968	47	48	58	115.9869
mmu-miR-344d-3p	587	491	675	3	6	11	87.65
mmu-miR-10a-5p	60241.5	55707.5	59273	3125.5	3297.5	5008.5	15.328
mmu-miR-155-5p	887	1304	1593	164	199	235	6.327759
mmu-miR-181c-5p	561	590	657	213	267	328	2.237624

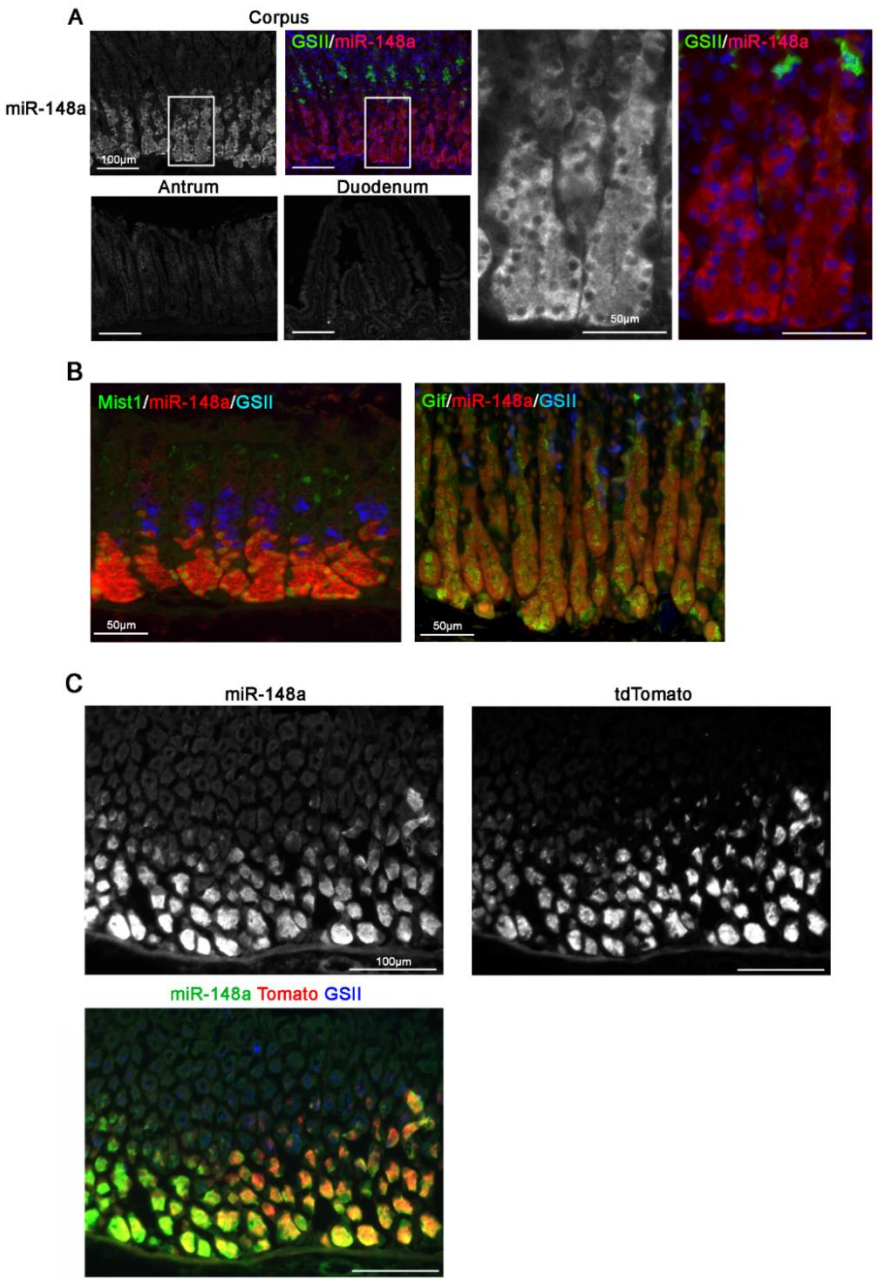

Figure 5. miR-148a expression in normal mouse stomach.
A. Fluorescence *in situ* hybridization for miR-148a (red) and immunofluorescence staining for GSII (green) and DAPI (blue). miR-148a was strongly expressed in the base of corpus glands deep to GSII-positive mucous neck cells. miR-148a expression was localized in the cytoplasm. No or little expression of miR-148a was seen in antrum and duodenum.
B. Fluorescence *in situ* hybridization for miR-148a (red) and immunofluorescence staining for GSII (blue) and Mist1 or GIF (green). miR-148a-positive cells expressed Mist1 and GIF.
C. Fluorescence *in situ* hybridization for miR-148a using Mist1CreERT2/+;R26RtdTomato/+ mice. miR-148a (green), tdTomato (red) and GSII (blue). miR-148a was expressed in tdTomato-positive chief cells.

intrinsic factor (GIF) (Figure 5B). Examination of Mist1$^{CreERT2/+}$;R26R$^{tdTomato/+}$ mice also showed that Mist1-positive chief cells have strong miR-148a expression (Figure 5C). These data suggest that miR-148a is strongly and specifically expressed in chief cells in the gastric corpus.

Next, to evaluate the alteration of expression of miR-148a during the development of SPEM, we examined *in situ* hybridization analyses in two mouse models of acute oxyntic atrophy (administration of either DMP-777 or L635). Compared with normal chief cells, miR-148a was downregulated in GSII-positive SPEM cells in mice after 10 days of DMP-777 treatment or 3 days of L635 treatment (Figure 6A). Importantly, miR-148a was downregulated in chief cells without GSII expression after 3 days of DMP-777 treatment or 1 day of L635 treatment. Fluorescence intensity was measured for quantitation, and miR-148a expression was decreased significantly in mice with 10 days of DMP-777 treatment or 3 days of L635 treatment (Figure 6B). We also examined miR-148a expression by *in situ* hybridization in mice infected with *Helicobacter felis* (*H. felis*), and mice infected with *H. felis* for 6 months and 12 months showed decreased level of miR-148a expression (Figure 6C, D). These findings suggest that the downregulation of miR-148a could be involved in the chief-cell transdifferentiation into SPEM cells.

miR-148a expression in human stomach assessed by *in situ* hybridization.

To assess whether the alteration in miR-148a expression was related to SPEM development in human, we performed *in situ* hybridization analyses for miR-148a using human stomach tissue (Figure 7). The human stomach tissue section shown in Figure 4 conveniently contained normal corpus glands and SPEM glands side-by-side, allowing for clear comparison of expression

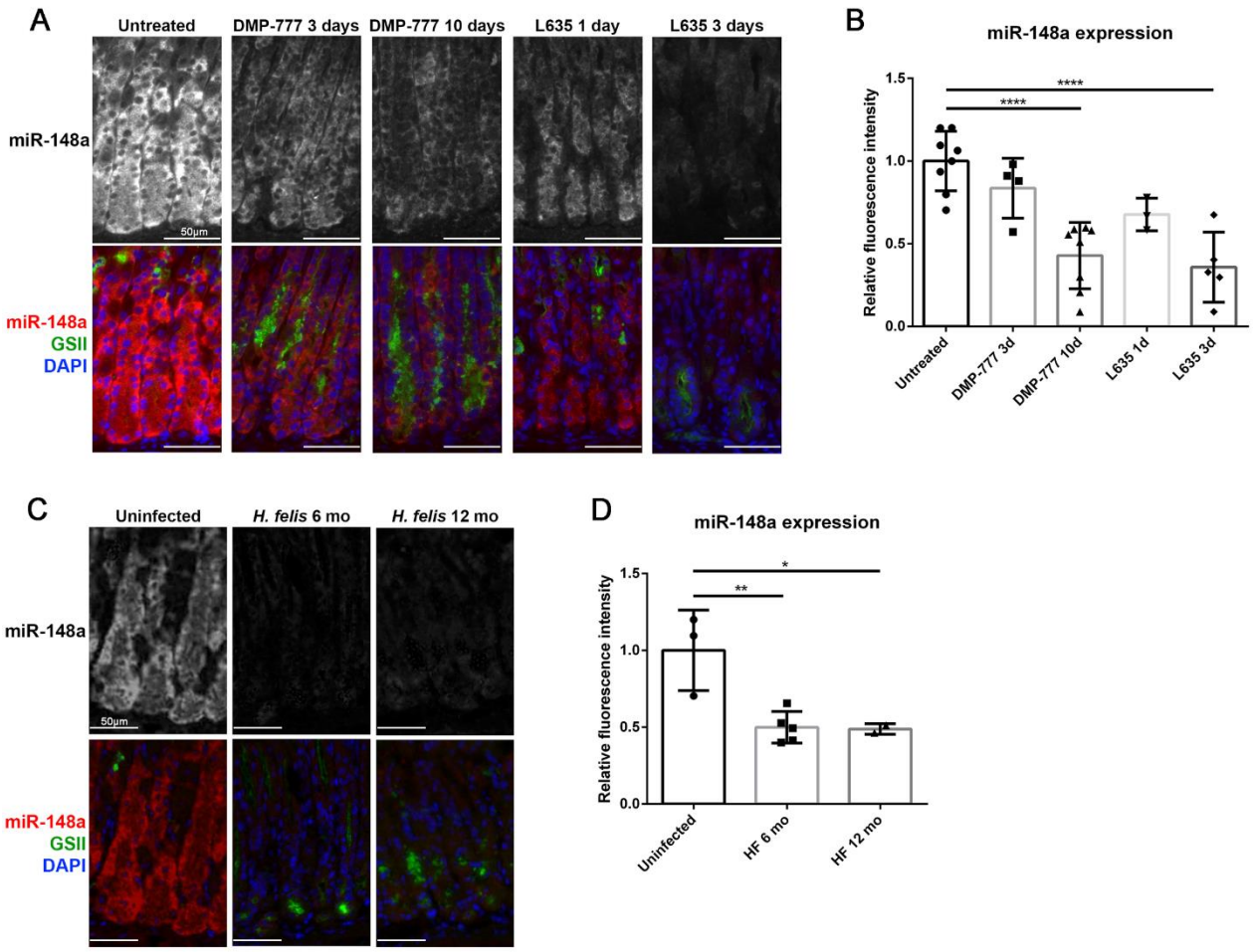

Figure 6. miR-148a expression during chief cell transdifferentiation into SPEM cells.
A. Fluorescence *in situ* hybridization for miR-148a (red) and immunofluorescence staining for GSII (green) and DAPI (blue). miR-148a was significantly downregulated in GSII-positive SPEM cells developed in mice after 10 days of DMP-777 treatment or 3 days of L635 treatment as well as in chief cells without GSII expression after 3 days DMP-777 treatment or 1 day L635 treatment, compared with normal chief cells.
B. Quantitation of relative miR-148a staining intensity in chief cells and transdifferentiating chief cells at the base of the gland. One-way ANOVA, p<0.0001. Bonferroni's multiple comparisons, ****$p < 0.0001$.
C. Fluorescence *in situ* hybridization for miR-148a (red) and immunofluorescence staining for GSII (green) and DAPI (blue). miR-148a was significantly decreased in GSII-positive SPEM cells developed in mice 6 months or 12 months after Helicobacter felis infection.
D. Quantitation of relative miR-148a staining intensity in chief cells and H. felis infection induced SPEM cells at the base of the gland. One-way ANOVA, p=0.0081. Bonferroni's multiple comparisons, *$p < 0.05$, **$p < 0.01$.

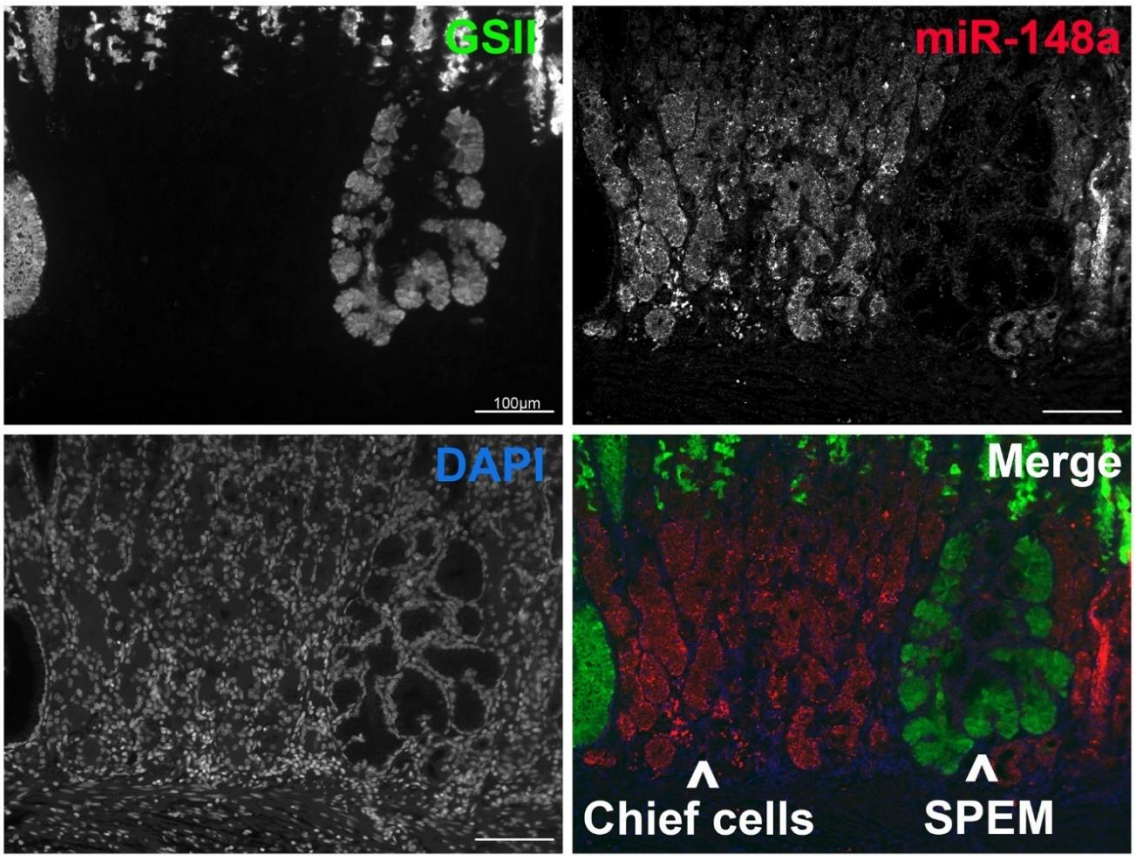

Figure 7. miR-148a expression in human stomach.
Fluorescence *in situ* hybridization for miR-148a (red) and immunofluorescence staining for GSII (green) and DAPI (blue). miR-148a was strongly expressed at the base of the normal glands below the GSII-positive mucous neck cells. The SPEM glands, marked with GSII-positive staining to the base of the glands, had no or little expression of miR-148a.

between them. The miR-148a was exclusively expressed in chief cells located at the base of the normal corpus glands below the GSII-positive mucous neck cells. The SPEM glands, marked with GSII-positive staining to the base of the glands, had no or very low expression of miR-148a. This finding confirmed the downregulation of miR-148a expression in SPEM in human stomach.

The involvement of miR-148a in the initiation of chief cell transdifferentiation.

ImChief cells and ImSPEM cells grow continuously at the permissive temperature of 33 ºC because of their expression of temperature-dependent T-antigen (Ts). However, at the non-permissive temperature (39 ºC), the temperature-sensitive T-antigen misfolds and thus no longer immortalizes the cells. Thus, ImChief cells and ImSPEM cells become more primary-like at the non-permissive temperature (Weis et al., 2014). To investigate the role of miR-148a in chief cell plasticity, we examined these cell lines incubated at the non-permissive temperature for 72 hours. First, to confirm the expression levels of miR-148a in ImChief cells and ImSPEM cells, the expression of miR-148a was detected by microRNA assay, and miR-148a expression in ImSPEM cells was significantly lower than in ImChief cells (Figure 8A).

To investigate whether downregulation of miR-148a is related to SPEM development, we examined the influence of inhibitors for miR-148a in ImChief cells. ImChief cells were transfected with miR-148a inhibitors and then incubated at 33 ºC overnight, followed by the incubation at 39 ºC for 72 hours. The expression of miR-148a was significantly downregulated in ImChief cells treated with the inhibitor (Figure 8B). Known chief cell and SPEM cell marker expression was examined by qRT-PCR, and ImChief cells treated with miR-148a inhibitor showed significant upregulation of the variant 9 splice isoform of *Cd44* (*Cd44v9*), an early

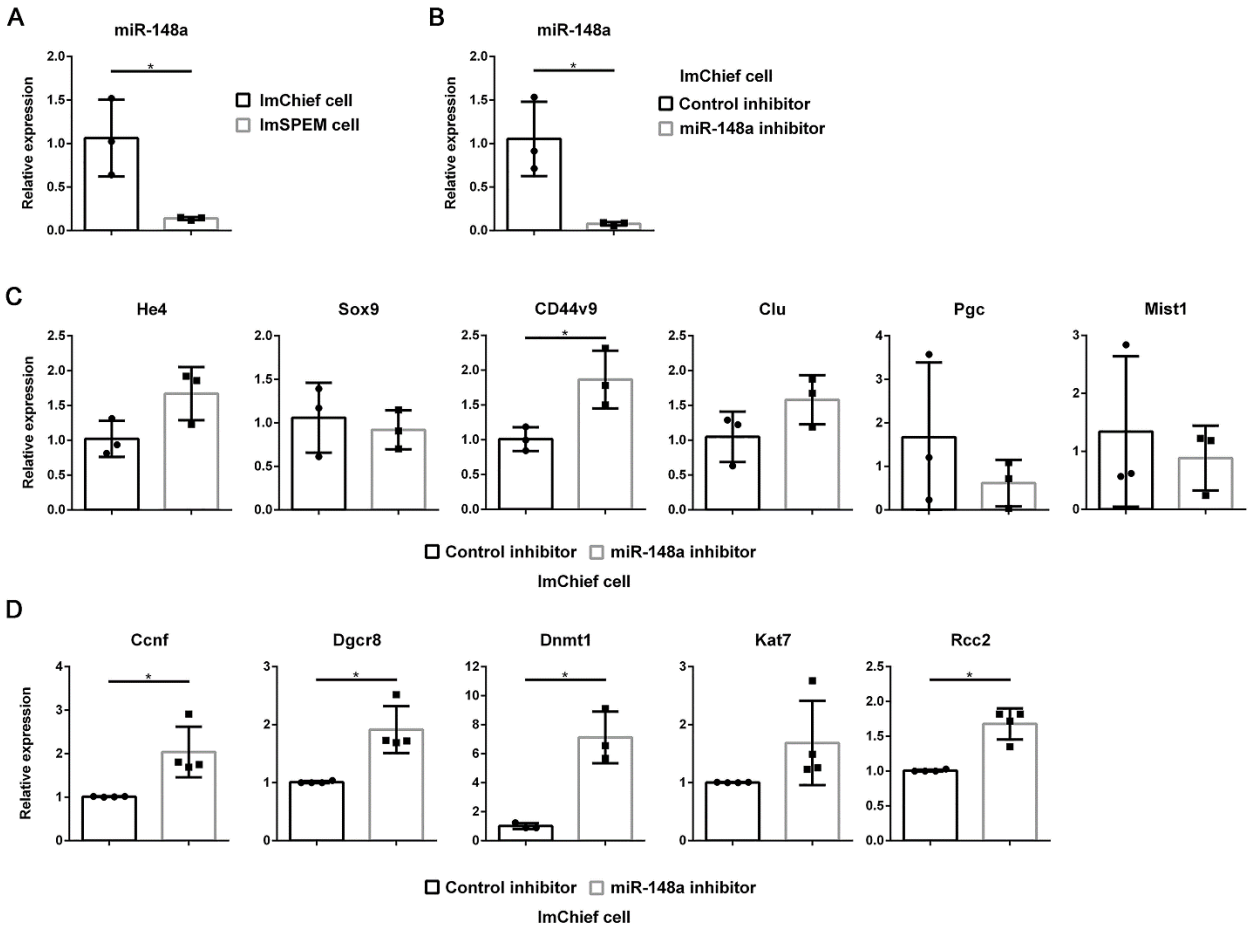

Figure 8. The involvement of miR-148a in the initiation of chief cell transdifferentiation.
A. The expression of miR-148a in ImChief cells and ImSPEM cells by microRNA assay. Mann-Whitney U test. *$p < 0.05$.
B. The expression of miR-148a by microRNA assay in ImChief cells treated with control inhibitor or miR-148a inhibitor. Mann-Whitney U test. *$p < 0.05$.
C. The expression of genes related with SPEM cells (He4, Sox9, Cd44v9 and Clu) or chief cells (Pgc and Mist1) in ImChief cells treated with control inhibitor or miR-148a inhibitor by qPCR. Mann-Whitney U test. *$p < 0.05$.
D. The expression of miR-148a target genes in ImChief cells treated with control inhibitor or miR-148a inhibitor by qPCR. Mann-Whitney U test. *$p < 0.05$.

marker of SPEM (Meyer et al., 2019; Wada et al., 2013), although *Tff2* expression was not detected (Figure 8C). The expression of *Sox9* and *Clusterin* (*Clu*), other SPEM-associated markers, were increased, but not significantly (Figure 8C). The expression of chief cell specific genes, such as *Mist1* and *Pgc,* was not significantly changed. These data suggest that downregulation of miR-148a could be involved in initiation of chief-cell transdifferentiation.

Dnmt1 upregulation in chief cells during chief cell transdifferentiation via downregulation of miR-148a.

We have previously examined genes related to the emergence of SPEM by investigating microarray assay for mRNA expression for RNA extracted from SPEM regions in Gastrin-deficient mice treated with DMP-777 for 1 day or 3 days (Nozaki et al., 2008). To investigate the direct linkage of changes in miRNA expression with the emergence of SPEM, we compared the candidate miR-148a target gene list with previous mRNA microarray data (Table 4). Interestingly, *Ccnf*, *Dgcr8*, *Dnmt1*, *Kat7* and *Rcc2* were identified as possible targets of miR-148a during the transdifferentiation process of chief cells into SPEM cells, all predicted by three different miRNA databases: microRNA.org, TargetScan and miRDB.

To confirm the miR-148a regulation of these possible target genes, mRNA expression was examined in ImChief cells transfected with control inhibitor or miR-148a inhibitor. As expected from miRNA database prediction, most of the candidate target genes showed upregulation of mRNA expression with miR-148a inhibition, including *Ccnf*, *Dgcr8*, *Dnmt1* and *Rcc2* (Figure 8D). Among the putative target genes, we focused on Dnmt1, one of the DNA methyltransferases that is essential for the maintenance of DNA methylation. Several studies have validated that miR-148a directly targets Dnmt1 3'-UTR in various cells, including gastric

Table 4. Candidate miRNAs and their targeted genes related to SPEM development

Candidate miRNAs (miRNA seq data)	Possible targeted genes upregulated in early stage of SPEM (Nozaki et al. Gastro 2008)
miR-148a	Ccnf Dgcr8 Dnmt1 Kat7 Rcc2
let-7f/7i	Limd2 Rdh10 Thoc1 Myo1f
miR-200b/200c	Rdh10 Dnajc5 Pou6f1 BC037034
miR-192	Ereg Thoc1
miR-200a	Csnk2a1 E2f3 Nme1 Sdf2 Sft2d2 Src
miR-182	Nup155 Rasa1
miR-183	(-)
miR-27b	Plekhh1 Nek6 Litaf Gpd1 Nfx1 Timm8a1
miR-30a/30c	Sdad1 Vat1 Xpo1 Arl6ip5 Mboat1 Poldip3

cancer cells, contributing to tumor progression (Gailhouste et al., 2013; Wu et al., 2016; Zhu et al., 2012). To confirm the expression of Dnmt1 in mouse stomach, we performed immunostaining analyses. In normal corpus, Dnmt1 was strongly expressed in isthmus cells and mucous neck cells (Figure 9A). Dnmt1-positive isthmus cells were positive for Ki67, but Dnmt1-positive mucous neck cells were negative for Ki67. In contrast, chief cells and parietal cells showed little or no detectable expression of Dnmt1. In mice with DMP-777 or L635 treatment, Dnmt1 was clearly upregulated in SPEM cells as well as in chief cells before SPEM development (Figure 9B, C), and 40~60% Dnmt1-positive cells were also proliferative (Figure 9B, D). These results suggest that the upregulation of Dnmt1 in chief cells via miR-148a downregulation could be involved in the initiation of chief-cell transdifferentiation.

miR-148a downregulation during the chief cell transdifferentiation process.

As described earlier, chief-cell transdifferentiation occurs through coordinated stepwise events, and the process of transdifferentiation can be arrested at different steps. Our group recently showed that inhibition of the cystine transporter, xCT, by sulfasalazine treatment or xCT knockout arrests chief-cell transdifferentiation process and prevents development of SPEM in mouse models of acute oxyntic atrophy (Meyer et al., 2019). It was also shown that xCT-deficiency blocks chief-cell transdifferentiation process at a distinct step, where the initiating step of Mist1 loss in chief cell reprogramming is not affected, but upregulation of CD44v9 and autophagy that occur during chief-cell transdifferentiation are blocked. To investigate where in this process miR-148a downregulation occurs, we utilized these mouse models of xCT-deficiency (Meyer et al., 2019). In mice treated with sulfasalazine only, miR-148a was expressed normally in chief cells, while co-treatment with sulfasalazine and 3 days of L635 resulted in loss

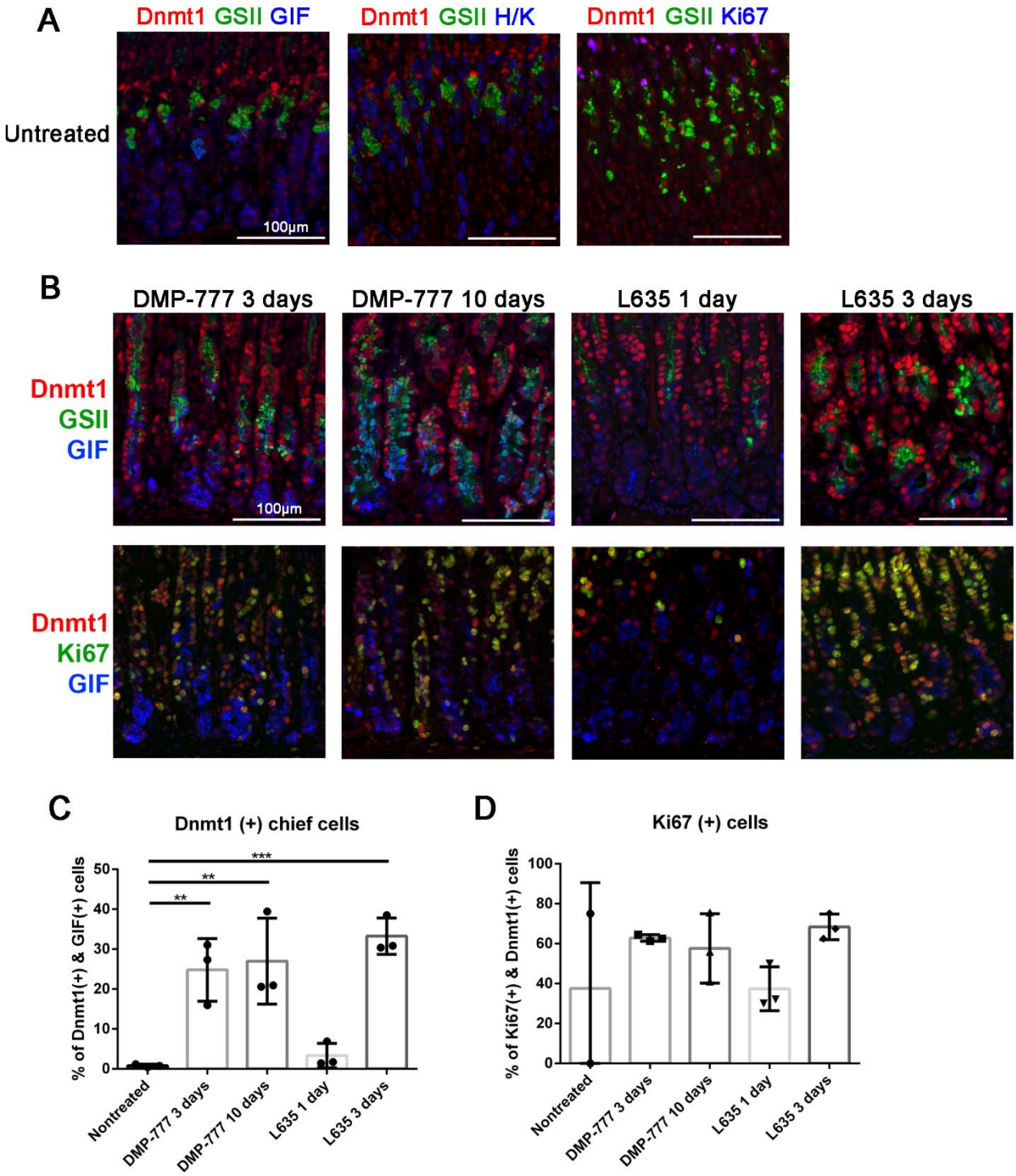
A
Dnmt1 GSII GIF
Dnmt1 GSII H/K
Dnmt1 GSII Ki67
Untreated
100μm
B
DMP-777 3 days
DMP-777 10 days
L635 1 day
L635 3 days
Dnmt1
GSII
GIF
100μm
Dnmt1
Ki67
GIF
C
Dnmt1 (+) chief cells
% of Dnmt1(+) & GIF(+) cells
***
**
**
Nontreated
DMP-777 3 days
DMP-777 10 days
L635 1 day
L635 3 days
D
Ki67 (+) cells
% of Ki67(+) & Dnmt1(+) cells
Nontreated
DMP-777 3 days
DMP-777 10 days
L635 1 day
L635 3 days

Figure 9. The upregulation of Dnmt1 in chief cells during chief cell transdifferentiation via the downregulation of miR-148a.

A. Immunofluorescence staining in the corpus of untreated mice. Left panel: GSII (green), Dnmt1 (red) and GIF (blue). Middle panel: GSII (green), Dnmt1 (red) and H/K-ATPase (blue). Right panel: GSII (green), Dnmt1 (red) and Ki67 (blue). Dnmt1 was strongly expressed in isthmus cells and neck cells. Dnmt1-positive isthmus cells were positive for Ki67, but Dnmt1-positive mucous neck cells were negative for Ki67.

B. Immunofluorescence staining in the corpus of mice treated by DMP-777 for 3 days or 10 days and L635 for 1 day or 3 days. Upper panel: GSII (green), Dnmt1 (red) and GIF (blue). Dnmt1 was upregulated in SPEM cells of mice treated with DMP-777 for 10 days or L635 for 3 days as well as in chief cells of mice treated with DMP-777 for 3 days or L635 for 1 day. Lower panel: Ki67 (green), Dnmt1 (red) and GIF (blue). Ki67 was expressed in Dnmt1-positive SPEM cells of mice treated with DMP-777 for 10 days or L635 for 3 days as well as in Dnmt1-positive chief cells of mice treated with DMP-777 for 3 days or L635 for 1 day.

C. Quantitation of Dnmt1-positive chief cells. Percent of GIF-positive chief cells per corpus glands that are Dnmt1-positive. One-way ANOVA, p=0.0003. Bonferroni's multiple comparisons, $**p < 0.01$, $***p < 0.001$.

D. Quantitation of Ki67 in Dnmt1-positive chief cells. Percent of Dnmt1-positive chief cells per corpus glands that are Ki67-positive.

of miR-148a (Figure 10A, B). In xCT KO mice, untreated stomach exhibited similar expression of miR-148a as in wild type mice, with expression in chief cells at the gland base, while 3 days of L635 treatment resulted in a significant downregulation of miR-148a expression (Figure 10C, D). These results suggest that, like Mist1, the loss of miR-148a cannot be rescued with xCT-deficiency, and miR-148a downregulation most likely occurs early in the initiating step of chief-cell transdifferentiation.

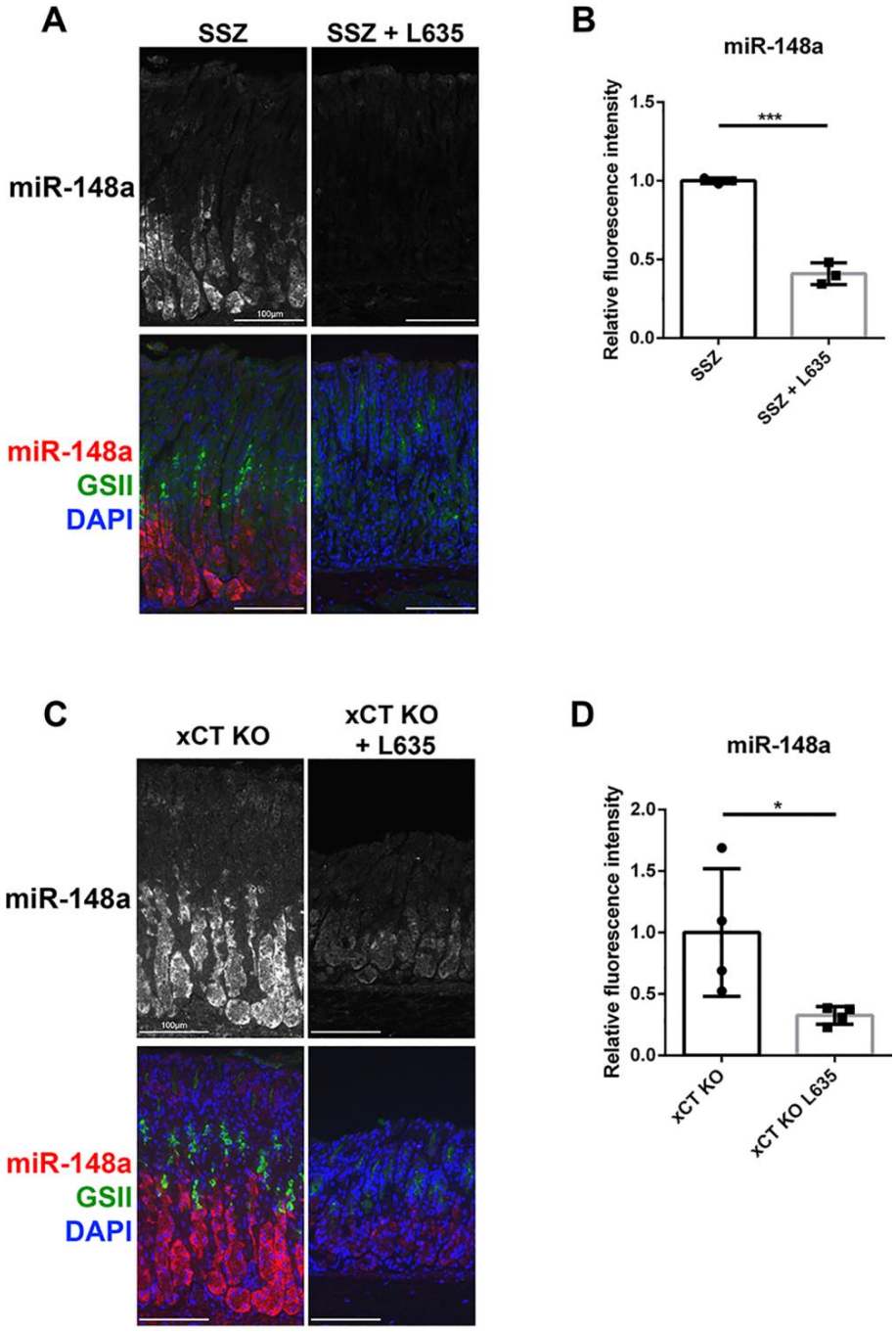

Figure 10. miR-148a downregulation during chief cell transdifferentiation process.
A. Fluorescence *in situ* hybridization for miR-148a (red) and immunofluorescence staining for GSII (green) and DAPI (blue). miR-148a was expressed in chief cells treated with xCT inhibitor, sulfasalazine, only. With 3 days of L635 co-treatment with sulfasalazine, miR-148a expression was lost.
B. Quantitation of relative miR-148a staining intensity. Mann-Whitney U test, $*p < 0.05$.
C. Fluorescence *in situ* hybridization for miR-148a (red) and immunofluorescence staining for GSII (green) and DAPI (blue). In xCT KO mice, miR-148a was expressed in chief cells. With 3 days of L635, miR-148a expression was decreased in xCT KO mice.
D. Quantitation of relative miR-148a staining intensity. Mann-Whitney U test, $*p < 0.05$.

Discussion

The gastric corpus mucosa contains six types of differentiated cells: parietal cells, chief cells, surface mucous cells, mucous neck cells, tuft cells and enteroendocrine cells. All cells originate from stem cells in the isthmus region, but mucous neck cells can function as an intermediate precursor for chief cells (Ramsey et al., 2007). The differentiation process from mucous neck cells into chief cells involves dynamic alterations, including granule changes from mucous to serous, the alteration of apical-basal cell shape organization and the expansion of rough endoplasmic reticulum (Karam & Leblond, 1993; Ramsey et al., 2007). MIST1 and its upstream gene, XBP1 are transcription factors that regulate the cellular architecture maturation in chief cells (Ramsey et al., 2007). In addition, parietal cell loss induces the transdifferentiation of chief cells into mucous cell metaplasia, designated SPEM (Nam et al., 2010). In this study, we have demonstrated the involvement of miR-148a in the process of transdifferentiation of chief cells into SPEM. *In situ* hybridization analyses showed that miR-148a was specifically expressed in normal chief cells compared to mucous neck cells. In addition, miR-148a was significantly downregulated in chief cells during SPEM development. Therefore, miR-148a could be involved in chief cell maturation and maintenance as well as plasticity.

The extremely high expression of several miRNAs in chief cells suggested that miRNAs could be also involved in chief cell maturation and maintenance in addition to chief cell plasticity. The report that XBP1 can directly induce the transcription of miR-148a supports this hypothesis (Cho et al., 2016). However, we did not find that miR-148a can increase chief cell factors in ImChief cells (data not shown). These results suggest that the downregulation of miR-148a might lead chief cells towards transdifferentiation into SPEM cells. To understand the role

of miRNAs on chief cell maturation, other experiments, such as the use of mouse models with the deletion of miR-148a specifically in chief cells will be needed.

To investigate chief-cell plasticity, we performed experiments using the ImChief cell line that we previously established (Weis et al., 2014). The ImChief cell line allows studies to be conducted in an *in vitro* model that resembles *in vivo* chief cells. The ImChief cell line also allows for the study of chief cell factors, that are difficult to study with gastric cancer cell lines and mouse models, although ImChief cells are not functionally fully mature (Weis et al., 2014). In this study, we also showed that ImChief cells can be transfected effectively with miRNA inhibitors. The list of miRNAs downregulated during chief-cell transdifferentiation included miR-148a, members of the miR-30, miR-200, and let-7 families. Among them, we examined the role of miR-148a in chief cell plasticity. A number of studies have shown that miR-148a is downregulated in human cancer tissues, including gastric cancer (Cao et al., 2017; Jiang et al., 2016; Liu et al., 2015; Peng et al., 2017; Zhu et al., 2012). These previous investigations have demonstrated that miR-148a downregulation could contribute to human gastric cancer progression by directly targeting MMP7, DNMT1, CCK-BR and ROCK1 (Li et al., 2017; Sakamoto et al., 2014; Yan et al., 2014; Yu et al., 2016; Zheng et al., 2011). This study suggests the role of miR-148a on the normal physiology of gastric chief cells.

DNA methylation is a major modulator of gene expression. In mammalian cells, methylation is catalyzed by DNA methyltransferases (DNMTs) that cooperatively establish tissue-specific methylation patterns. DNMT1 is responsible for the maintenance of DNA methylation during replication (Perdigoto et al., 2014). Previous reports demonstrated that aberrant DNA methylation is induced in human and Mongolian gerbil gastric mucosa by *H. pylori* infection (Maekita et al., 2006; Nakajima et al., 2009; Niwa et al., 2010), suggesting that

regulation of gene expression by DNA methylation could be related with the initiation of metaplasia and neoplasia development. However, the upregulation of DNMTs has not been observed in human or gerbil gastric mucosa with *H. pylori* infection (Nakajima et al., 2009; Niwa et al., 2010). In this report, we demonstrated that Dnmt1 is upregulated in chief cells during chief-cell transdifferentiation via the downregulation of miR-148a.

Previous studies have demonstrated that miR-148a directly targets the 3'-UTR of DNMT1 in various cancer cell lines (Gailhouste et al., 2013; Wu et al., 2016; Zhu et al., 2012). In contrast, overexpression of DNMT1 leads to hypermethylation of the promoter region of miR-148a in some cancer cell lines, including gastric cancer lines (Long et al., 2014; Zhu et al., 2012). Thus, the regulatory network between miRNAs and epigenetic pathways seems to be important to organize gene expression in cancer biology. In this study, Dnmt1 was upregulated in chief cells by the suppression of miR-148a especially at early stages of SPEM development. We have previously noted that transdifferentiating chief cells upregulate a number of proteins involved in unwinding DNA, consistent with a need to reprogram the cell transcriptome (Nozaki et al., 2008). The fact that transdifferentiating chief cells show Dnmt1 upregulation indicates that the induction of DNA methylation could be necessary for the transdifferentiation of chief cells. To identify methylated genes related to SPEM development, further detailed methylation analyses of chief cells and SPEM cells, such as a global methylation analysis are needed at different stages of transdifferentiation.

Interestingly, the downregulation of miR-148a correlated not only with its target gene, DNMT1, but also with the upregulation of CD44v9, an early SPEM cell marker, in chief cells. CD44v9 expression is observed in human gastric cancer tissues and has been implicated as a cancer stem cell marker (Go et al., 2016; Lau et al., 2014). Importantly, SPEM is also associated

with the upregulation of CD44s as well as CD44v9 (Bertaux-Skeirik et al., 2017; Wada et al., 2013), while CD44v9 is not expressed in any cells in the normal gastric corpus mucosa. CD44v9 functions by blocking the stress signaling induced by reactive oxygen species (ROS) via the interaction with the cystine transporter, xCT (Ishimoto et al., 2011; Meyer et al., 2019). Our recent report identified xCT as required for the SPEM development and chief cell reprogramming following injury, and showed that xCT-deficiency blocks the transdifferentiation process (Meyer et al., 2019). Targeting xCT arrested chief cell reprogramming at a specific step, where the transdifferentiation was initiated, marked by loss of Mist1, but upregulation of autophagy did not occur. Investigation of miR-148a expression at this early step in chief-cell transdifferentiation confirmed that miR-148a downregulation occurs early in the initiation of chief cell reprogramming.

Metaplasia is considered to be a precursor lesion for gastric cancer, however the mechanisms of how metaplasia develops in stomach are not fully elucidated. The mouse models of induced acute parietal cell loss, such as DMP-777, L635 and high-dose tamoxifen have shown that chief cells can give rise to SPEM cells via a transdifferentiation process (Leushacke et al., 2017; Nam et al., 2010; Willet et al., 2018). Recent analyses suggest that parietal cell loss alone is not sufficient to induce metaplasia (Burclaff et al., 2017) and another signaling process, such as the IL-33/IL-13 cytokine signaling network, is required for SPEM development (Petersen et al., 2018). The results from this study indicate that post-transcriptional regulation by miR-148a could be involved in the chief-cell transdifferentiation, by regulating DNMT1 expression and epigenetic change. Moreover, the miR-148a downregulation triggered in response to mucosal injury occurred very early in the chief-cell transdifferentiation process. miR-148a inhibition *in vitro* using ImChief cell lines also supported this notion, since miR-148a inhibition alone was

sufficient to induce upregulation of CD44v9 transcripts in chief cells. The rapid downregulation of miR-148a, especially from its such a high level of expression in normal chief cells, would be expected to result in a cascade of targeted events, and the early change in miR-148a expression suggests that miR-148a downregulation could play a crucial role in the initiation of chief cell reprogramming.

Materials and Methods

Mice

Eight-week-old C57BL/6J mice were used for all mouse experiments. For drug treatment experiments, three mice were used per group. DMP-777 and L635 treatment and dosage was conducted as previously described (Nam et al., 2010; Weis et al., 2013). Briefly, DMP-777 was dissolved in 1% methylcellulose and administered by oral gavage (350 mg/kg) once a day for 3 or 10 consecutive days. L635 was dissolved in deionized DNA and RNA-free water and administered by oral gavage (350 mg/kg) once a day for 1 or 3 consecutive days. Mist1$^{CreERT2/+}$ mice were crossed with R26R^{mTmG} or R26R^{tdTomato} mice, and 5 mg of Tamoxifen was administered to these mice subcutaneously on 3 every other day.

Archival sections of stomach from *H. felis* infected, sulfasalazine treated and xCT KO mice were obtained from previous study (Meyer et al., 2019; Weis et al., 2013). Regular mouse chow and water ad libitum were provided during experiments in a temperature-controlled room with 12-hour light-dark cycles. All treatment maintenance and care of animals in these studies followed protocols approved by the Institutional Animal Care and Use Committees of Vanderbilt University.

Cell Lines

Mouse chief-cell line (ImChief cell) and SPEM-cell line (ImSPEM cell) were established in a previous study (Weis et al., 2014). These cell lines were maintained in a 1:1 mixture of Ham's F-12 and Dulbecco's minimum essential medium containing 10% FBS, 8 µg/ml insulin/transferrin/selenium solution, 1 µg/ml hydrocortisone, 100 U/ml penicillin and streptomycin, 100 µg/ml MycoZap Plus-PR, 1 ng/ml EGF, 1 ng/ml bFGF, 10 ng/ml HGF, and

5 U/ml IFN-γ. For ongoing maintenance, these cells were incubated and passaged at the permissive temperature (33ºC). For analyses of experiments, cells were incubated at the non-permissive temperature (39ºC) for 72 hours.

Total RNA preparation from *in vivo* chief cells and chief cell or SPEM cell lines for miRNA sequencing

Mist1$^{CreERT2/+}$ mice were crossed with R26R^{mTmG} reporter mice, and 2 Mist1$^{CreERT2/+}$;R26R$^{mTmG/+}$ mice were used for chief cell isolation. Mice were sacrificed 10 days after Tamoxifen injection. The stomachs were removed and opened along the greater curvature. Stomachs were rinsed with ice cold phosphate buffered saline (PBS) without calcium and magnesium, and the antrums were removed with a razor blade and discarded. The corpus mucosa was separated from the serosa by dragging a cell scraper along the muscle layer. The corpus mucosa was minced with scissors and digested in the buffer containing advanced DMEM/F12, 5% FBS, 1 mg/ml collagenase type Ia and DNase I at 37ºC. Advanced DMEM/F12 supplemented with 10 μM Y-27632 and 1 mM DTT were added to stop the reaction. These cells were re-suspended in cold TrypLE Express supplemented with Y-27632 and incubated at 37ºC. After stopping reaction, cells were resuspended in Advanced DMEM/F12 with 1% FBS and DNase I supplemented with Y-27632. Before cell sorting, cells were incubated with 1.0 μg/ml 4’,6-diamidino-2-phenylindol (DAPI). Cells were sorted using a BD fluorescence-activated cell sorting (FACS) Aria III (BD Biosciences, San Jose, California) and initially segregated from debris using forward scatter (FSC) and side scatter (SSC) properties of the 488 nm laser. Single cells were selected using the voltage pulse geometries of the FSC diode and SSC photomultiplier tube detectors. Dead cells were excluded based on their DAPI staining. GFP-positive chief cells

were sorted directly into TRIzol (Invitrogen) using a 100 µm nozzle, followed by total RNA extraction according to the manufacturer's instructions.

Total RNA extraction from chief cell lines and SPEM cell lines for miRNA sequencing, ImChief cells and ImSPEM cells grown at the non-permissive temperature were collected from an 80% confluent T-75 dish. Cells were trypsinized, washed with PBS twice and pelleted. Total RNA was extracted using the miRVana miRNA Isolation Kit according to manufacturer's instructions (Sousa et al., 2016).

miRNA library preparation, sequencing, and data analysis

Total RNA from each sample was processed through an RNA library preparation protocol using NEBNext Small RNA Library Prep Set for Illumina (New England BioLabs Inc., Ipswich, MA, USA) according to manufacturer's protocol. Briefly, 3` adapters were ligated to total input RNA followed by hybridization of multiplex SR RT primers and ligation of multiplex 5` SR adapters. Reverse transcription (RT) was done using ProtoScript II RT for 1 hour at 50 °C. Immediately after RT reaction, PCR amplification was performed for 15 cycles using LongAmp Taq 2X master mix. Illumina indexed primers were added to uniquely barcode each sample. Post-PCR material was purified using QIAquick PCR purification kit (Qiagen Inc., Valencia, CA, USA). Size selection of small RNA was done using 3% agarose-free gel cassettes on Pippin prep instrument (Sage Science Inc., Beverly, MA, USA). Post-size selection concentration and quality of the libraries were assessed using Qubit 2.0 Fluorometer (Invitrogen, Carlsbad, California, USA) and DNA 1000 chip on Agilent 2100 Bioanalyzer (Applied Biosystems, Carlsbad, CA, USA), respectively. Accurate quantification for sequencing applications was performed using the qPCR-based KAPA Biosystems Library Quantification kit (Kapa

Biosystems, Inc., Woburn, MA, USA). Each library was diluted to a final concentration of 1.25 nM and pooled in equimolar ratios prior to clustering. Single End (SE) sequencing (50 bp) was performed to generate approximately 15 million reads per sample on an Illumina HiSeq2500 sequencer (Illumina, Inc., San Diego, CA, USA).

Post-processing of the sequencing reads from miRNA-seq experiments from each sample was performed as per the Genomic Services Laboratory unique in-house pipeline. Briefly, quality control checks on raw sequence data from each sample was performed using FastQC (Babraham Bioinformatics, London, UK). Raw reads were imported on a commercial data analysis platform AvadisNGS (Strand Scientifics, CA, USA). Adapter trimming was done to remove ligated adapter from 3' end of the sequenced reads with only one mismatch allowed, poorly aligned 3' ends were also trimmed. Sequences shorter than 15 nucleotides length were excluded from further analysis. Trimmed Reads with low qualities (base quality score less than 30, alignment score less than 95, mapping quality less than 40) were removed. Filtered reads were then used to extract and count the small RNA which was annotated with microRNAs from the miRBase release 20 database. The quantification operation carries out measurement at both the gene level and at the active region level. Active region quantification considers only reads whose 5' end matches the 5' end of the mature miRNA annotation. For comparison of ImChief and ImSPEM cells, samples were grouped as identifiers and the differential expression of miRNA was calculated on the basis of their fold change observed between different groups, p-value of differentially expressed miRNAs was estimated by implementing z-score calculations using Benjamini Hochberg FDR corrections of 0.05 (Benjamini & Hochberg, 1995).

Immunofluorescence staining

Mouse stomachs were fixed in 4% paraformaldehyde (Thermo Fisher Scientific, Waltham, MA) overnight and transferred into 70 % ethanol for paraffin embedding. Five-micrometer paraffin-embedded sections were used for all immunofluorescence staining. Sections were deparaffinized, rehydrated and submitted to antigen retrieval using Target Retrieval solution (Dako North America, Inc., Carpinteria, CA) in a pressure cooker. Blocking was performed using Protein Block Serum-Free (Dako North America, Inc.) for 1 hour 30 minutes at room temperature. The primary antibody incubation was performed in Antibody Diluent with Background Reducing Components (Dako North America, Inc.) overnight at 4ºC. Primary antibodies used were as follows: rat anti-Cd44v9 (1:25,000), goat anti-GIF (1:2000), rabbit anti-Mist1 (1:300), mouse anti-HK-ATPase (1:10,000), rat anti-Ki67 (1:50), rabbit anti-Dnmt1 (1:200). Fluorescent secondary antibodies (1:500) and Alexa-488 and 647-conjugated *Griffonia simplicifolia* lectin II (GSII) (1:2000) were incubated for 1 hour at room temperature. After incubation with DAPI for 5 minutes, slides were mounted with ProLong Gold Antifade Reagent (Invitrogen). Fluorescence imaging was analyzed using an Axio Imager 2 microscope (Carl Zeiss AG, Oberkochen, Germany) or a Versa S200 automated slide scanner (Leica Biosystems, Buffalo Grove, IL) in the Vanderbilt Digital Histology Shared Resource.

Fluorescence *in situ* hybridization for miR-148a

Stomachs of wild-type mice were fixed in 4% paraformaldehyde overnight and transferred into 70% ethanol for paraffin embedding. Five-micrometer paraffin-embedded sections were deparaffinized and rehydrated. Stomachs of $Mist1^{CreERT2/+}$;$R26R^{tdTomato/+}$ mice were fixed in 4% paraformaldehyde overnight and embedded in OCT compound. Ten µm sections

were cut from OCT-embedded blocks, mount them on SuperFrost Plus slides, let them air-dry for 15 minutes and then rinse them for 3 x 3 minutes. *In situ* hybridization process and TSA Plus fluorescence system were performed as the manufacturer's protocol from Exiqon. Briefly, incubation with Proteinase-K (2 µg/ml) was performed for 10 minutes at 37ºC. And then, blocking of endogenous peroxidase activity was performed using Peroxidase block (DAKO) for 10 minutes at room temperature. *In situ* hybridization was performed using locked nucleic acid (LNA) probes (25 nM) for 1 hour at 60ºC. After washing slides in SSC buffers, blocking was conducted using 1% sheep serum for 15 minutes at room temperature. Anti-DIG-POD antibody (1:400) was applied to slides and incubated for 1 hour at room temperature. To detect DIG, TSA Plus Cy5 substrate (1:200) was applied to slides and incubated for 10 minutes at room temperature. After incubation with Alexa-488 conjugated GSII (1:2000) for 30 minutes and DAPI for 5 minutes, slides were mounted with ProLong Gold Antifade Reagent (Invitrogen).

To examine the localization of miRNAs and proteins, a combination analysis with *in situ* hybridization for miRNAs and immunofluorescence staining for proteins was performed. Five-micrometer paraffin-embedded sections were deparaffinized, rehydrated and submitted to antigen retrieval using Target Retrieval solution (Dako North America, Inc.) in a pressure cooker. Blocking of endogenous peroxidase activity, *in situ* hybridization, protein blocking with sheep serum, incubation with anti-DIG-POD and incubation with TSA plus Cy5 were performed as noted above. After that, slides were blocked using Protein Block Serum-Free (Dako North America, Inc.) and incubated with primary and secondary antibodies as in the regular immunofluorescence staining method.

miRNA Transfection Experiments

ImChief cells were transfected with 100 nM miRNA inhibitors (miR-148a or Control inhibitor) using Lipofectamine 2000 reagent (Invitrogen) at 33ºC, incubated at 33ºC for 24 hours, and then cultured at 39ºC for 72 hours. Total RNA was extracted from ImChief cells or ImSPEM cells with TRIzol (Invitrogen) according to the manufacturer's instructions. For quantitative RT-PCR of mRNA, 1 μg of total RNA was treated with RQ1 RNase-free DNase (Promega) and then reverse-transcribed with Superscript III reverse transcriptase (Invitrogen). Quantitative real-time PCR was performed with SYBR Green using specific primers (Table 5) in triplicate using an ABI StepOnePlus Real-Time PCR System (Applied Biosystem). A set of PCR primers for TATA-box-binding protein (Tbp) gene was used as an endogenous control and reference for verification of sufficient cDNA in the reaction. Each sample was collected from at least three biological replicate experiments. The miRNA expression in cell lysates was analyzed using TaqMan MicroRNA assays according to the manufacturer's instructions. U6 was used as an endogenous control. Statistical significance (p <0.05) of the differences in the expression levels was determined with a Mann-Whitney U test.

Image Quantitation

For miR-148a expression, experimental groups contained 3–8 mice. Images were analyzed with CellProfiler, using total intensity divided by the area detected, and all graphs and statistics were completed in GraphPad Prism. The intensity and area were calculated by masking out all areas except the base of the gland. For quantification, > 100 glands of proximal stomach corpus were taken from each mouse at 20× objective. For acute and chronic mouse model of

SPEM, one-way ANOVA and Bonferroni's multiple comparisons test was used to calculate statistical

Table 5. List of qPCR primers used in Chapter II

Primer name	Sequence
Tbp F	CAAACCCAGAATTGTTCTCCTT
Tbp R	ATGTGGTCTTCCTGAATCCCT
He4 F	TGCCTGCCTGTCGCCTCTG
He4 R	TGTCCGCACAGTCCTTGTCCA
Sox9 F	CACGGAGCAGACGCACATCT
Sox9 R	TCTCGCTTCAGGTCAGCCTT
Cd44v9 F	GGAGATCAGGATGACTCCTTCT
Cd44v9 R	AGTCCTTGGATGAGTCTCGATC
Clu F	CCAGCCTTTCTTTGAGATGA
Clu R	CTCCTGGCACTTTTCACACT
Pgc F	TCTAACGGCGGGCAGATT
Pgc R	AGGTACTGGGCAGGCATGAC
Mist1 F	GCTGACCGCCACCATACTTAC
Mist1 R	TGTGTAGAGTAGCGTTGCAGG
Dnmt1 F	AGATGCCATCACCCAAAAAG
Dnmt1 R	TCATCGATGCTCACCTTCTG
Tff2 F	TGCTTTGATCTTGGATGCTG
Tff2 R	GGAAAAGCAGCAGTTTCGAC
Ccnf F	CACACCAGCCTGTCCATCTATG
Ccnf R	ACGAGGTCACTGTAGGAGAAGC
Dgcr8 F	GATGGTGTGACTTACGGATCTGG
Dgcr8 R	TAGGCTTCTCCTCAGAGGTCTG
Kat7 F	AGGAAAAGGTGGCTGAACTCAGG
Kat7 R	GTCAGGTTTTCCAAGAGAGGCTC
Rcc2 F	GTGGTTCGAGATGTAGCCTGTG
Rcc2 R	AGGCACCATCTCATCCTTCTGC

significance (p <0.05). For xCT-deficiency mouse model, the Mann-Whitney U test was used to determine statistical significance (p <0.05).

To perform the quantitation of the percentage of Dnmt1-positive cells or Ki67 and Dnmt1 double-positive cells in chief cells or SPEM cells, 30 corpus glands were analyzed for each sample. Three samples were analyzed per group (Untreated, DMP-777 treatment for 3 days, DMP-777 treatment for 10 days, L635 treatment for 1 day, and L635 treatment for 3 days). Chief cells were detected as GIF-positive cells. Counting was performed in slides digitally imaged with a Leica Versa 200 scanner (Vanderbilt Digital Histology Shared Resource) or in overlaid fluorescence images using Adobe Photoshop. One-way ANOVA and Bonferroni's multiple comparisons test was used to calculate statistical significance (p <0.05).

CHAPTER III

TELOCYTE RECRUITMENT DURING THE EMERGENCE OF A METAPLASTIC NICHE IN THE STOMACH

This chapter is adapted from a manuscript submitted to *Cellular and Molecular Gastroenterology and Hepatology*: **Sohn Y**, Flores Semyonov B, Wright CV, Kaestner KH, Choi E, Goldenring JR. Telocyte Recruitment During the Emergence of a Metaplastic Niche in the Stomach.

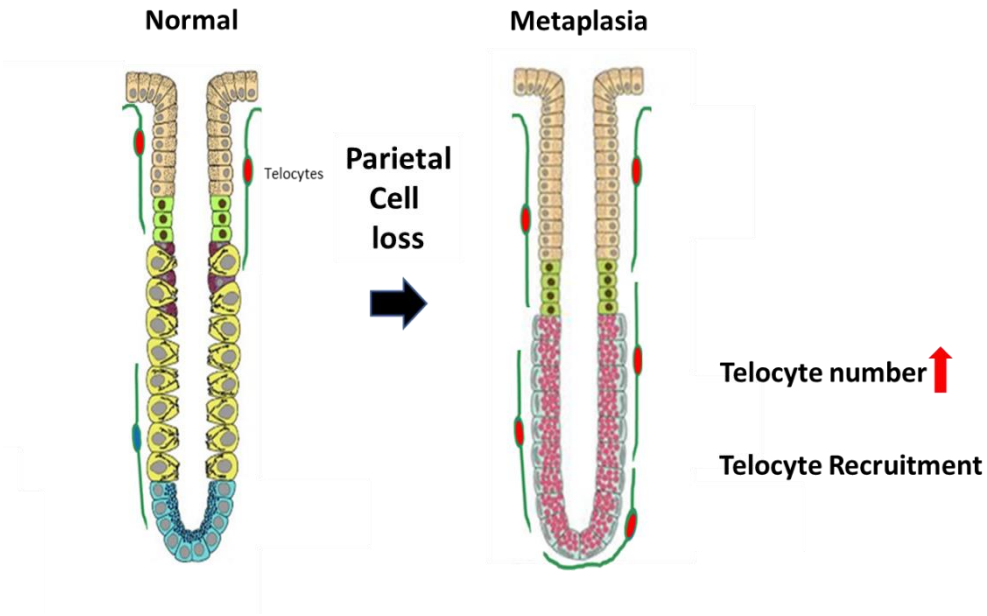

Figure 11. Recruitment of telocytes in metaplasia development in the stomach.
This graphical abstract illustrates the recruitment of telocytes in the stomach during metaplasia development, following the loss of parietal cells. It highlights the formation of a metaplastic cell niche at the base of the gland, accompanied by an increase in the number of telocytes.

Introduction

Telocytes are a relatively novel type of interstitial cell found in the connective tissues of various organs, including the reproductive system, urinary system, respiratory system, cardiovascular system, and gastrointestinal tract (Popescu & Faussone-Pellegrini, 2010; Rosa et al., 2021). Since their initial description in 2010 (Popescu & Faussone-Pellegrini, 2010), telocytes have attracted considerable interest due to their potential roles in tissue homeostasis and regeneration. Telocytes have distinct structural characteristics with small cell bodies and long, thin cytoplasmic extensions called telopodes. Over the years, several telocyte markers have been identified, revealing that telocytes exhibit immunophenotypic heterogeneity that varies depending on their specific anatomical location (Bei et al., 2015; Klein et al., 2022).

One intriguing aspect of telocytes is their potential role in tissue regeneration and repair. The mechanism by which telocytes contribute to tissue repair is not fully understood. However, it has been proposed that telocytes are involved in cell-to-cell communication, signal transmission, and maintaining tissue structure and function during wound healing (Wang et al., 2020). Telocytes are involved in liver tissue regeneration, as murine models of partial hepatectomy induce an increase in their numbers (Wang et al., 2014). Telocytes contribute to the formation of the extracellular matrix and the secretion of growth factors, cytokines, and chemokines, which are crucial in tissue repair (Albulescu et al., 2015; Cretoiu et al., 2016; Pomerleau et al., 2023). Studies investigating telocytes in the gastrointestinal tract have demonstrated that, in the small and large intestines, telocytes express the winged-helix transcription factor forkhead box l1 (FOXL1) and platelet-derived growth factor receptor alpha (PDGFRα) (Aoki et al., 2016). Intestinal FOXL1-positive subepithelial telocytes form a continuous plexus just beneath the epithelial cells, and express subsets of various Wnt signaling molecules and R-spondin3 in a location-dependent manner along crypt-villus axis (Aoki et al.,

2016; Shoshkes-Carmel et al., 2018). These intestinal telocytes function as a crucial component of the intestinal stem cell niche.

Metaplasia is defined as a conversion of one mature cell type to another mature cell type. In the gastrointestinal tract, metaplasia develops in response to physical or chemical damage to the mucosa. As a barrier separating the external and internal environments, the gastrointestinal mucosae promptly respond to mucosal damage by undergoing metaplasia, which serves to provide protection and facilitate tissue repair (Goldenring, 2018). Reparative metaplasia is beneficial following severe injury, but this normal cellular response can become problematic in the presence of persistent damage and chronic inflammation, subsequently increasing the risk of cancer development (Meyer & Goldenring, 2018).

In the stomach, metaplasia develops in the setting of acute or chronic gastritis. The gastric chief cells at the base of the oxyntic glands are characterized by expression of secretory zymogens. These cells differentiate from mucous neck cells without cell division and maintain their fully differentiated state under normal circumstances (Bredemeyer et al., 2009; Goldenring et al., 2011; J. K. Lennerz et al., 2010). When stomach acid-secreting parietal cells are lost, chief cells undergo transdifferentiation into a state of mucous-cell metaplasia, referred to as spasmolytic polypeptide-expressing metaplasia (SPEM), and under continued damage and inflammation, these cells become proliferative (Nam et al., 2010; Petersen et al., 2018). SPEM is considered a precursor lineage for the development of intestinal metaplasia (IM), and both of these metaplasias are possible precursor lesions for gastric cancer (Correa & Piazuelo, 2012; Schmidt et al., 1999). Earlier studies have highlighted the involvement of immune cells, including M2 macrophages and ILC2s, in the process of chief-cell transdifferentiation into

SPEM cells (Meyer et al., 2020; Petersen et al., 2014). Still, the contribution of telocytes during metaplasia development remains unexplored.

In this study, we aimed to investigate the involvement of telocytes in metaplasia development within the gastric context. Our investigations not only verified the presence of FOXL1+/PDGFRα+ double-positive telocytes in the stomach, but also uncovered their distributional dynamics in response to metaplastic transitions. In both acute injury models and genetically engineered mouse models, we observed an increase in telocyte abundance during metaplasia development, accompanied by a shift in distribution from the isthmus to the base of the gland. Importantly, this altered distribution correlated with expansion of the proliferative cell zone, suggesting a connection between the telocytes and the emerging metaplastic cell niche. This dynamic migration was demonstrated using a lineage tracing approach, highlighting the adaptability and responsiveness of these stromal cells. In addition, we demonstrated the presence of *Wnt5a* expression in PDGFRα-positive telocytes. These observations underscore the intricate interplay between stromal components and metaplastic changes and suggest potential molecular pathways through which telocytes could influence metaplasia development and maintenance.

Results

Telocytes in the stomach express FOXL1 and PDGFRα.

Leveraging the insights from prior research, our study aimed to extend the investigation of telocyte function to the stomach. While previous research has explored telocytes within the stomach's muscle layer (Rosa et al., 2021; Vannucchi et al., 2013), our objective was to investigate the potential interaction between telocytes and epithelial cells in the mouse stomach.

First, we evaluated the existence and characteristics of telocytes within the mouse stomach. Immunofluorescence staining was performed to investigate the expression of FOXL1 and PDGFRα in telocytes within the small intestine and stomach corpus, and FOXL1+/PDGFRα+ double-positive telocytes were observed in both the small intestine and stomach corpus (Figure 11A). As previously noted, in the small intestine, FOXL1+/PDGFRα+ double-positive telocytes were distributed throughout crypt and villi (Aoki et al., 2016; Shoshkes-Carmel et al., 2018), and in the stomach corpus, FOXL1+/PDGFRα+ double-positive telocytes were located towards the top of the gland. PDGFRα staining delineated the full extent of the telopodes, while FOXL1 staining labeled the nuclei of the telocytes. We further examined the spatial distribution of telocytes within the stromal context relative to epithelial cells. Immunofluorescence staining for p120 and PDGFRα demonstrated that PDGFRα-positive telocytes within the stroma were positioned in close proximity to epithelial cells (Figure 11B).

We next investigated the localization of FOXL1+/PDGFRα+ double-positive telocytes in relation to proliferative cells. Immunofluorescence staining for FOXL1, PDGFRα, and Ki67 demonstrated that these double-positive telocytes were positioned near proliferative progenitor cells in the isthmus of normal gastric glands (Figure 11C). In contrast, only single-positive PDGFRα-expressing fibroblasts were observed at the base of the gland, with a notable absence

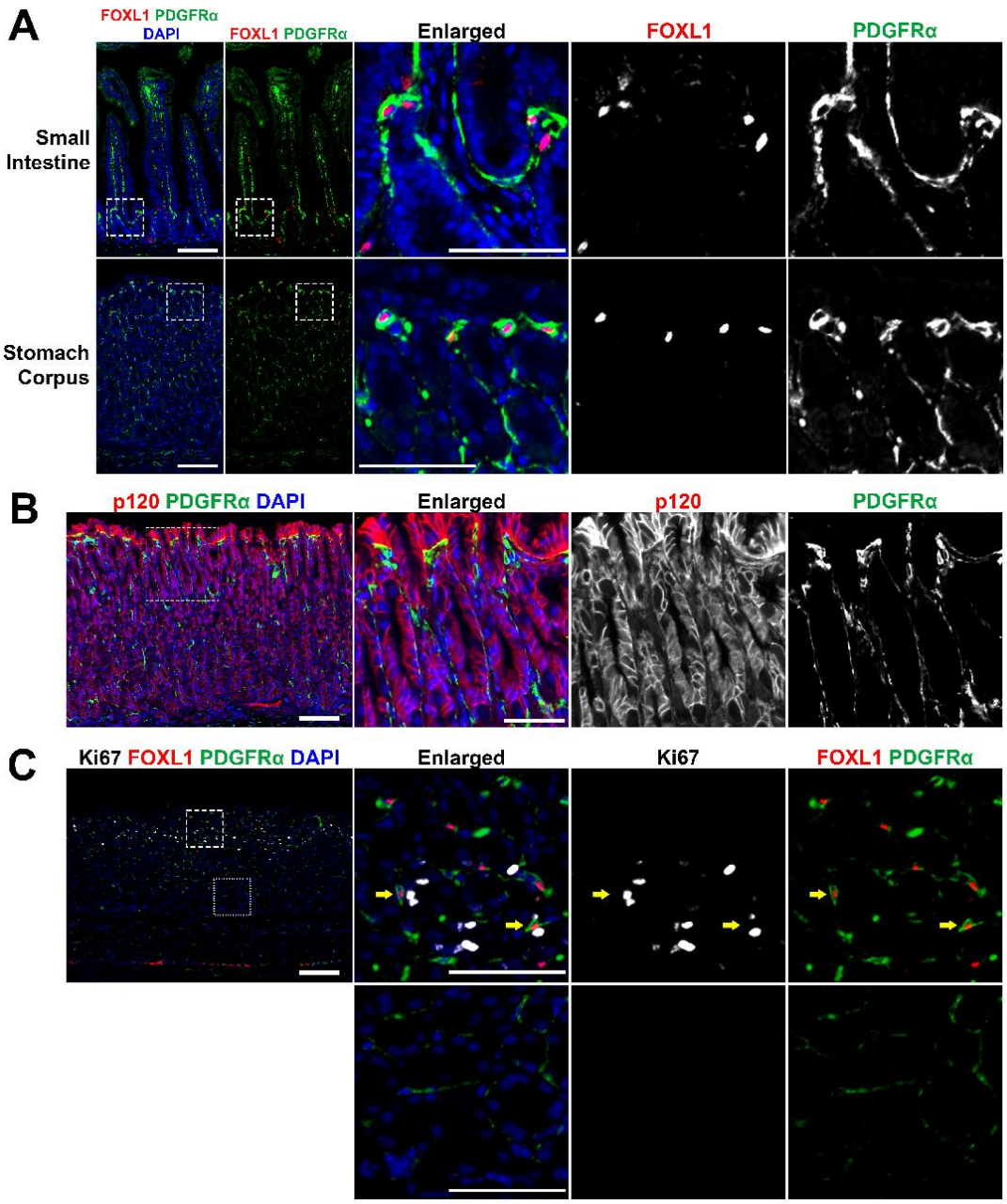

Figure 12. Telocytes in the stomach express FOXL1 and PDGFRα.
A) Immunofluorescence staining of FOXL1 (red), PDGFRα (green), and DAPI (blue) in the small intestine and stomach corpus. Telocytes co-expressing FOXL1 and PDGFRα are present in both tissues. PDGFRα staining reveals extended telopodes adjacent to epithelial cells, while FOXL1 staining marks telocyte nuclei. *Scale bar*: 100 μm and 50 μm for enlarged.
B) Immunofluorescence staining of p120 (red), PDGFRα (green), and DAPI (blue). Telocytes within the stroma are closely positioned to epithelial cells. *Scale bar*: 100 μm and 50 μm for enlarged.
C) IF staining of FOXL1 (red), PDGFRα (green), Ki67 (white), and DAPI (blue). FOXL1+/PDGFRα+ double-positive telocytes are found near the isthmus (dashed box), where proliferative progenitor cells are located. At the gland's base (dotted box), PDGFRα single-positive fibroblasts are present, without proliferative cells. *Scale bar*: 100 μm and 50 μm for enlarged.

of proliferative epithelial cells in this region. It is important to note that, while PDGFRα single-positive cells were distributed throughout the gland, telocytes characterized by the double-positive expression of FOXL1 and PDGFRα were exclusively found near the isthmus. Our findings demonstrated the presence of telocyte populations in both the normal intestine and stomach in association with proliferative progenitor zones.

FOXL1+/PDGFRα+ double-positive telocytes are increased during the metaplasia development in the stomach.

Metaplasia develops in the stomach in the setting of acid-secreting parietal cell loss. In humans, the loss of parietal cells occurs due to chronic *Helicobacter pylori* infection (Roth et al., 1999). However, the parietal cell loss triggered by *Helicobacter* infection is a gradual process that occurs over the course of years in humans and months in mice. To expedite the process of oxyntic atrophy and the development of metaplasia in the mouse stomach, we induced acute injury with drugs that specifically target parietal cells. These drugs, namely DMP-777 and L635, were utilized to induce metaplasia within a matter of days, facilitating the rapid observation of these cellular changes in the stomach (Nam et al., 2010; Nomura et al., 2005). Mice treated with DMP-777 develop SPEM cells within 10-14 days, and treatment with L635 induces SPEM cells within 3 days. Through the induction of stomach damage and the promotion of reparative metaplasia development, our study aimed to explore the potential role of telocytes in this process.

Immunofluorescence staining for FOXL1, PDGFRα, and GSII was conducted on stomach tissue obtained from mice treated with either DMP-777 or L635 to investigate the behavior of telocytes during metaplasia development (Figure 12A). In untreated stomach,

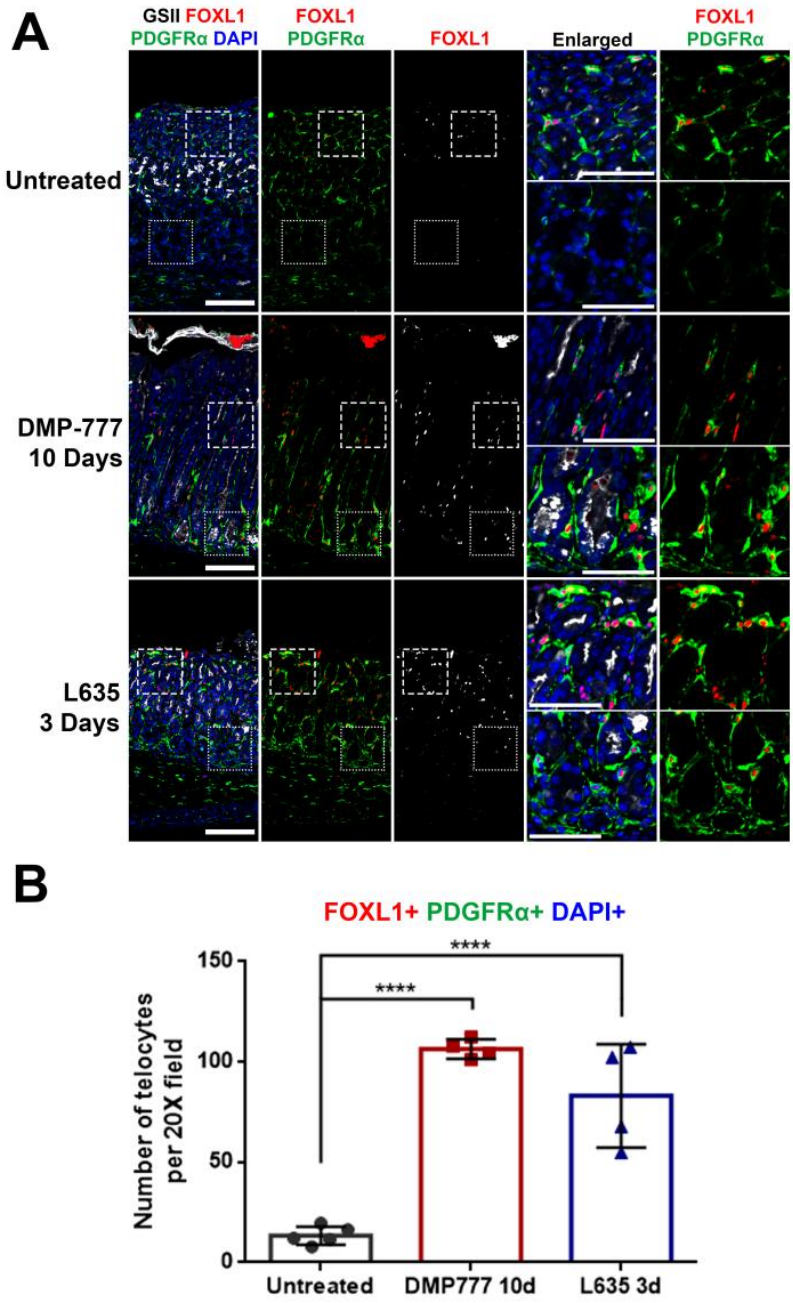

Figure 13. FOXL1+/PDGFRα+ double-positive telocytes are increased during the metaplasia development in the stomach.

A) Immunofluorescence staining of FOXL1 (*red*), PDGFRα (*green*) and DAPI (*blue*) in DMP-777 and L635-treated mouse stomach. In untreated mouse stomach, FOXL1+/PDGFRα+ double-positive telocytes are located near the isthmus. Following treatment with DMP-777 and L635, where metaplasia develops, there was an increase in the number of these telocytes. Also, telocytes spread throughout the gland, extending even to the base. *Scale bar*: 100 μm and 50 μm for enlarged.

B) Quantification of telocyte count. FOXL1+/PDGFRα+/DAPI+ telocyte count significantly increases in DMP-777 and L635-treated stomachs. Data presented as mean ± SD (n = 5 for Untreated and n = 4 for DMP-777 and L635). ****$p < .0001$. Tukey's multiple comparisons test; one-way ANOVA ($F (2, 10) = 49.96$, $p < 0.0001$).

FOXL1+/PDGFRα+ double-positive telocytes were primarily situated near the isthmus region. Upon treatment with DMP-777 and L635, which induced metaplasia characterized by GSII expression at the base of the gland, we observed a notable increase in the number of FOXL1+/PDGFRα+ double-positive telocytes. These telocytes were distributed extensively throughout the glands, including at their bases. The quantification demonstrated a significant increase in the number of FOXL1+/PDGFRα+/DAPI+ telocytes in the stomachs treated with either DMP-777 or L635, compared to the untreated stomach (Figure 12B). Along with the increase of FOXL1-positive telocytes, PDGFRα expression was globally increased within the stomachs treated with either DMP-777 or L635, particularly evident at the base of the gland. These results suggest that PDGFRα-positive stromal cells, including telocytes, formed a continuous subepithelial network that comprehensively enveloped the metaplastic glands.

Telocytes show altered distribution near the expanding proliferative zone in DMP-777-treated mouse stomach.

Earlier research demonstrated that the ablation of FOXL1+ mesenchymal cells in the intestine disrupted the proliferation of intestinal stem cells, demonstrating that FOXL1+ telocytes constitute an essential niche component for the proliferative epithelial stem cells (Aoki et al., 2016). Based on this observation, we hypothesized similar functions for telocytes in the stomach both during normal tissue homeostasis and in metaplasia. Upon inducing acute injury in the stomach and subsequent metaplasia via drug treatment, both isthmal progenitor cells and SPEM cells become proliferative, contributing to the expansion of the proliferative cell zone at the base of the gastric glands.

Examination of the mouse stomach treated with DMP-777, over varying durations from 1 day to 3 days and 10 days, revealed changes in the distribution of FOXL1+/PDGFRα+ double-positive telocytes, which closely correlated with the expanding proliferative cell zone. In untreated stomach tissue, only progenitor cells were positive for Ki67, concentrated in the upper region of the gland, specifically within the isthmus (Figure 13A). However, over the course of DMP-777 treatment, an expansion of the Ki67-positive proliferative cell zone was observed, gradually expanding towards the base of the gland, reaching its fullest extent after 10 days of DMP-777 treatment. Throughout this time, telocytes were consistently positioned in close proximity to the proliferating cell lineages.

In tandem with the expansion of proliferative cell zone, FOXL1+/PDGFRα+ double-positive telocytes appeared to undergo migration and expansion towards the base of the gland, aligning themselves adjacent to the proliferating epithelial cells (Figure 13A). Aligned with the gradual expansion of the proliferative cell zone during metaplasia development, there was a corresponding extension of FOXL1+/PDGFRα+ double-positive telocytes towards the mid-gland during the initial 1 and 3 days of DMP-777 treatment. By the end of the 10-day DMP-777 treatment, both proliferative SPEM cells and FOXL1+/PDGFRα+ double-positive telocytes were visibly present at the very base of the gland. These findings suggest a potential correlation between the expansion of the proliferative cell zone and the concurrent extension of the telocyte network during the process of metaplasia development.

To gain a more comprehensive understanding of the distributional changes of the FOXL1+/PDGFRα+ double-positive telocytes, we quantified their presence in three distinct regions along the height of the gland – the top, mid, and base (Figure 13B). The analysis revealed that with the increasing duration of DMP-777 treatment, there was a progressive

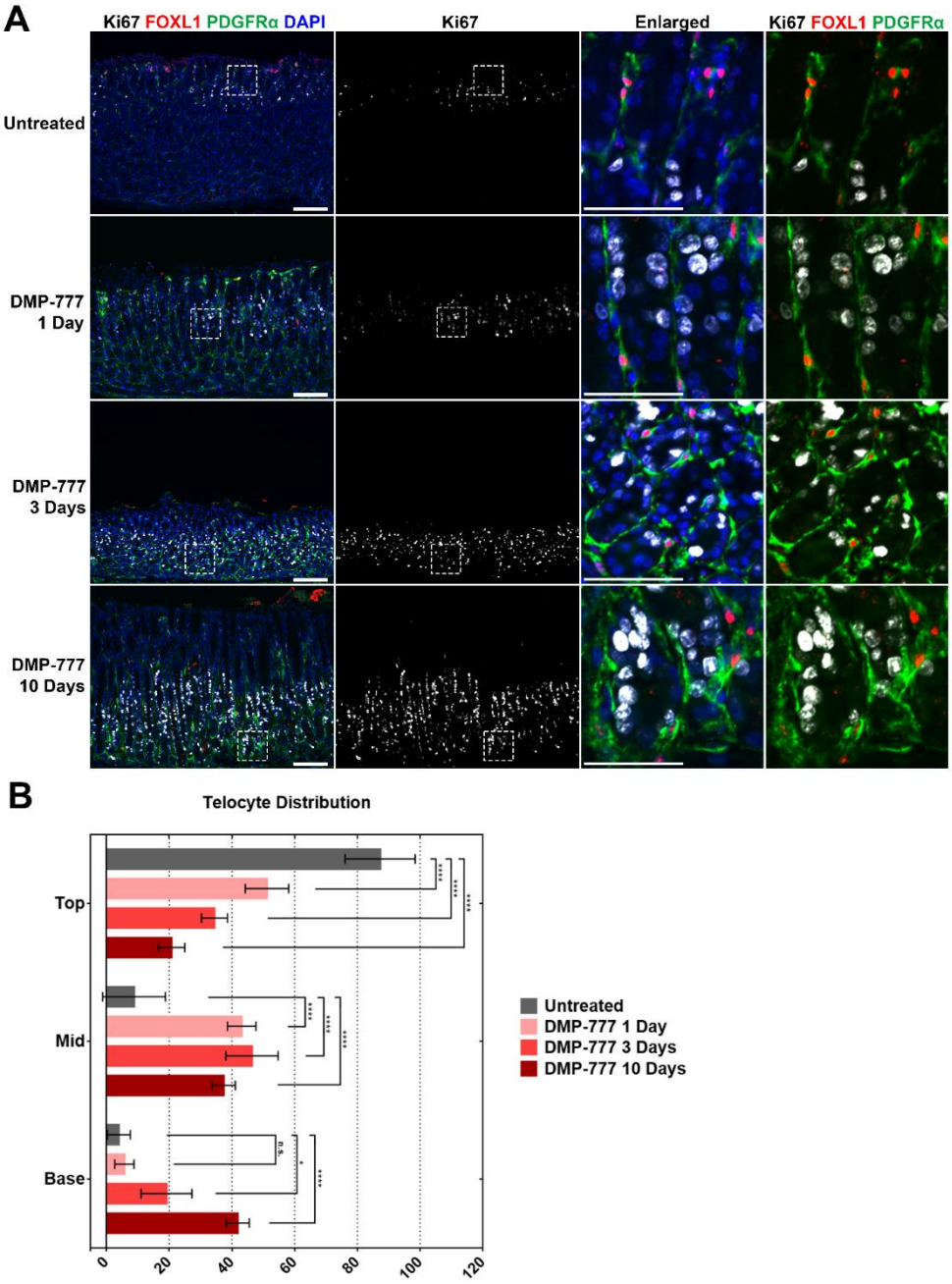

Figure 14. Telocytes show altered distribution near the expanding proliferative zone in DMP-777-treated mouse stomach.

A) Immunofluorescence staining of Ki67 (*white*), FOXL1 (*red*), PDGFRα (*green*) and DAPI (*blue*) on DMP-777-treated stomach tissue. As DMP-777 treatment duration increased, the proliferative cell zone expanded, and FOXL1+/PDGFRα+ telocytes extended toward the base. *Scale bar*: 100 μm and 50 μm for enlarged.

B) Quantification of telocyte distribution within the gland. Telocyte distribution within the gland was quantified in three positions along the gland's height (top, mid, and base). Extended DMP-777 treatment reduced top distribution but increased mid and base presence. Data presented as mean ± SD (n = 4, except for DMP-777 3 Days, n = 3). n.s. = not statistically significant; **p* < .05; *****p* < .0001. Tukey's multiple comparisons test; two-way ANOVA for interaction ($F(6, 22) = 44.22$, $p < 0.0001$).

reduction in the distribution of telocytes within the top region of the gland. Conversely, the distribution of telocytes in the mid and base regions exhibited a significant increase. After 3 days of DMP-777 treatment, a significant enhancement in telocyte distribution at the base region was observed, and this trend was even more pronounced after 10 days of DMP-777 treatment. This observation highlighted distributional shifts of telocytes that corresponded to the expanding proliferative cell zone.

L635 treatment promotes a shift in telocyte distribution corresponding with proliferative zone expansion.

To investigate the accelerated development of metaplasia within 3 days, we utilized another drug, L635. Immunofluorescence staining for Ki67, FOXL1 and PDGFRα was performed to assess the telocyte distribution in correlation with alterations in the proliferative cell zone. In untreated stomach tissue, immunofluorescence staining revealed the localization of Ki67-positive progenitor cells in the isthmus, and FOXL1+/PDGFRα+ double-positive telocytes were also observed in close proximity to the proliferative cells. (Figure 14A). Following L635 treatment, there was an expansion of the Ki67-positive proliferative cell zone, which coincided with the extension of FOXL1+/PDGFRα+ double-positive telocytes towards the gland's base.

To further understand the distributional changes of FOXL1+/PDGFRα+ double-positive telocytes, a quantitative analysis for telocyte distribution was conducted (Figure 14B). The results demonstrated a progressive decrease in telocyte distribution at the top region with increasing duration of L635 treatment, accompanied by a concurrent increase in their distribution at the mid and base regions. Particularly, after 3 days of L635 treatment, a significant increase in

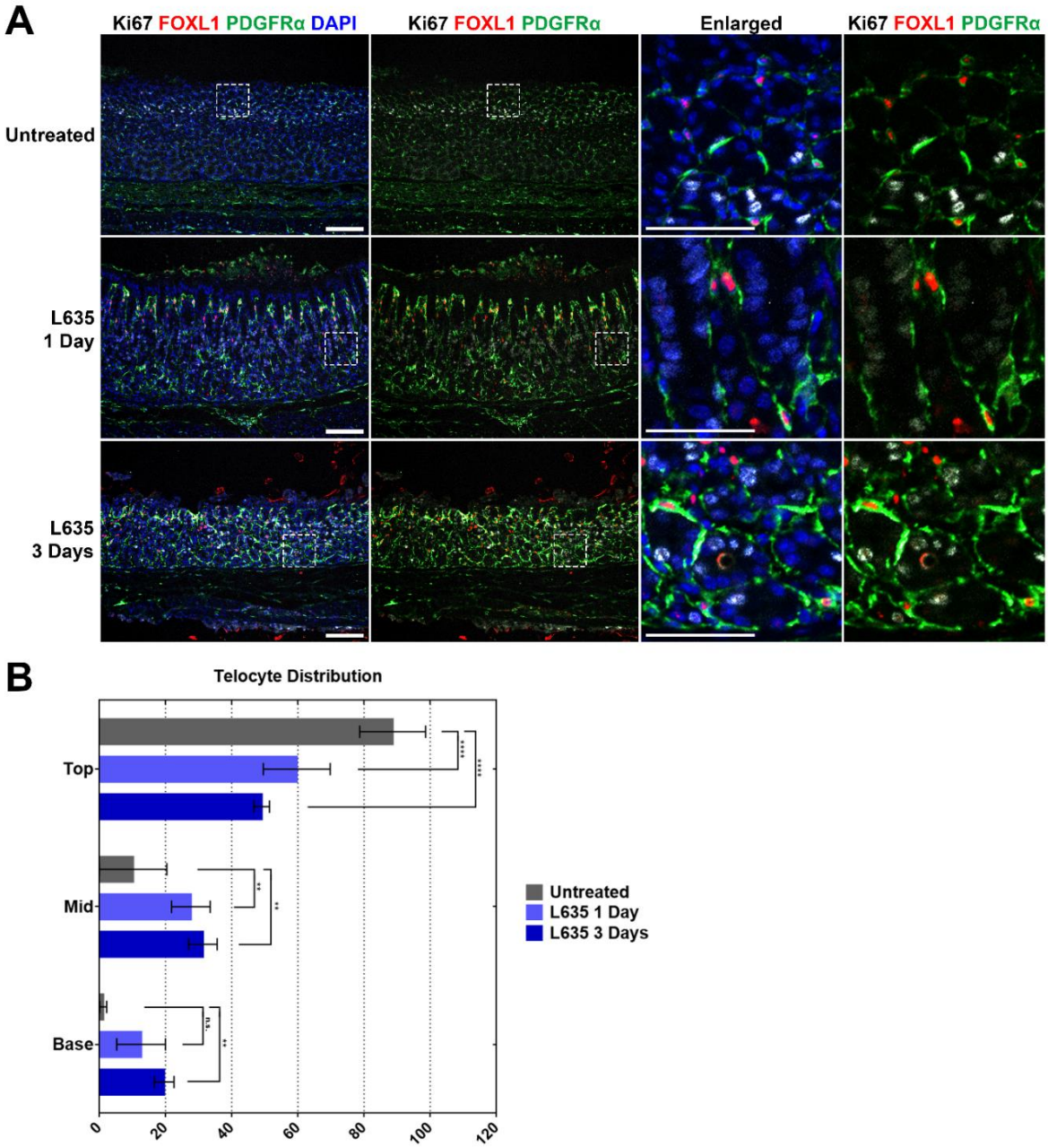

Figure 15. L635 treatment promotes a shift in telocyte distribution corresponding with proliferative zone expansion.

A) Immunofluorescence staining of FOXL1 (*red*), PDGFRα (*green*), Ki67 (*white*) and DAPI (*blue*) on L635-treated mouse stomach tissue. In untreated stomachs, Ki67-positive zone and FOXL1+/PDGFRα+ telocytes were at the upper region. With L635 treatment, the progenitor zone expanded, accompanied by telocytes extending towards the gland's base. *Scale bar*: 100 μm and 50 μm for enlarged.

B) Quantification of telocyte distribution within the gland. Telocyte distribution within the gland was quantified in three positions along the gland's height (top, mid, and base). During L635 treatment (1 to 3 days), telocyte distribution shifted: diminished presence at the top but increased prevalence in the mid and base areas. Data presented as mean ± SD (n = 4, except for Untreated, n = 3). n.s. = not statistically significant; $^{**}p < .01$; $^{****}p < .0001$. Tukey's multiple comparisons test; two-way ANOVA for interaction ($F(4, 16) = 15.57$, $p < 0.0001$).

telocyte distribution at the base region was observed. These observations highlight distributional shifts of telocytes that parallel the changes in the proliferative cell zone during L635 treatment.

In summary, our findings suggest that FOXL1+/PDGFRα+ double-positive telocytes display an altered distribution pattern near the proliferative cell zone in response to acute injury induced by drug treatments. The correlation between the expansion of the proliferative cell zone and the concurrent extension of the telocyte network highlights a potential interaction between these factors during the metaplasia development.

Telocytes exhibit a consistent proximity to the proliferative cell zone during recovery.

Earlier research has already demonstrated that discontinuing DMP-777 treatment results in the reversal of the acute drug-induced injury, leading to the recovery of changes induced by DMP-777 within 14 days after the cessation of treatment (Nomura et al., 2005). By utilizing immunofluorescence staining for Ki67, FOXL1, and PDGFRα, we investigated the behavior of telocytes in mouse stomach tissue that had undergone recovery from DMP-777-induced injury.

Upon DMP-777 10 days treatment, the stomach exhibited an expanded proliferative cell zone as well as extended telocyte network, as shown above (Figure 15A). Nevertheless, after 14 days of recovery, FOXL1+/PDGFRα+ double-positive telocytes reverted to their normal distribution, exclusively located at the top of the gland. This reversion paralleled the restoration of the normal proliferative cell zone, marked by the presence of progenitor cells primarily situated in the isthmus.

To further investigate telocyte distribution, quantitative analysis was conducted (Figure 15B). Treatment with DMP-777 induced a shift in telocyte distribution, resulting in an increased presence of telocytes in the mid and base regions of the gastric gland. However, following

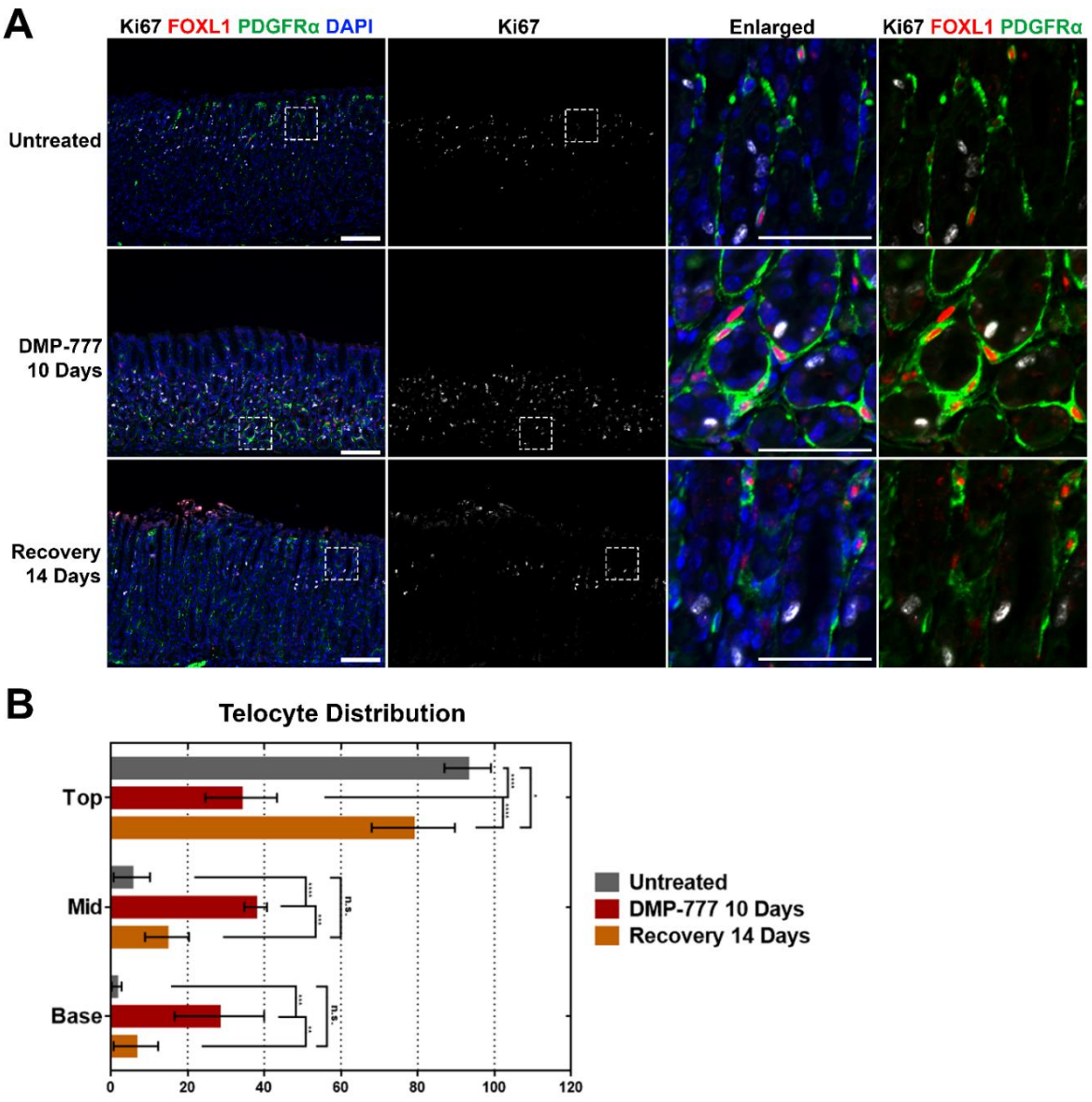

Figure 16. Telocytes exhibit a consistent proximity to the proliferative cell zone during recovery.
A) Immunofluorescence staining of Ki67 (*white*), FOXL1 (*red*), PDGFRα (*green*), and DAPI (*blue*) on recovered mouse stomach tissue following DMP-777 treatment. The injury-induced changes, including the expansion of the proliferative zone and telocyte distribution, were restored after a 14-day recovery period, with FOXL1+/PDGFRα+ double-positive telocytes reverting to their normal top-of-gland position. *Scale bar*: 100 μm and 50 μm for enlarged.
B) Quantification of telocyte distribution within the gland. DMP-777 treatment altered telocyte distribution, increasing their presence at the mid and base regions. Post-recovery, telocyte distribution mirrored the untreated state, predominantly at the top of the gland. Data presented as mean ± SD (n = 3, except for Recovery 14 Days, n = 5). n.s. = not statistically significant; *$p < .05$; **$p < .01$; ***$p < .001$; ****$p < .0001$. Tukey's multiple comparisons test; two-way ANOVA for interaction ($F(4, 16) = 26.77$, $p < 0.0001$).

recovery, the distribution of telocytes reflected that of the untreated stomach, where the majority of telocytes were localized at the top of the gland.

Our findings demonstrate that FOXL1+/PDGFRα+ double-positive telocytes consistently maintain their proximity to the proliferative cell zone during both the injury caused by DMP-777 and the subsequent recovery phase. Notably, telocytes restored their network back to their normal distribution after 14 days of recovery period, suggesting their prompt responsiveness to the changes in proliferation throughout both the injury and recovery phases. The shift in telocyte distribution and its subsequent restoration during recovery indicate a dynamic crosstalk between telocytes and the proliferative epithelial cells during injury and healing processes.

Telocytes are increased during Kras-driven metaplasia development in the stomach.

In addition to the drug-induced acute injury mouse model, we further explored telocyte contributions using a genetically engineered mouse model known as Mist1-Kras mice. In these mice, the administration of tamoxifen triggers the expression of a constitutively active Kras allele (G12D) in Mist1-expressing chief cells, leading to the onset of metaplasia within one month (Choi et al., 2016). This model offers a distinct mode of metaplasia development compared to acute injury, simulating the gradual changes driven by genetic modifications in chief cells.

Utilizing immunofluorescence staining, we examined the changes in the telocyte network in Mist1-Kras mouse stomach tissue during metaplasia development driven by active Kras expression in chief cells. In the wild-type (WT) control stomach, FOXL1+/PDGFRα+ double-positive telocytes were located near the proliferative progenitor cells at the top of the gland as noted before (Figure 16A). In contrast, in the Mist1-Kras 1 month stomach, which showed

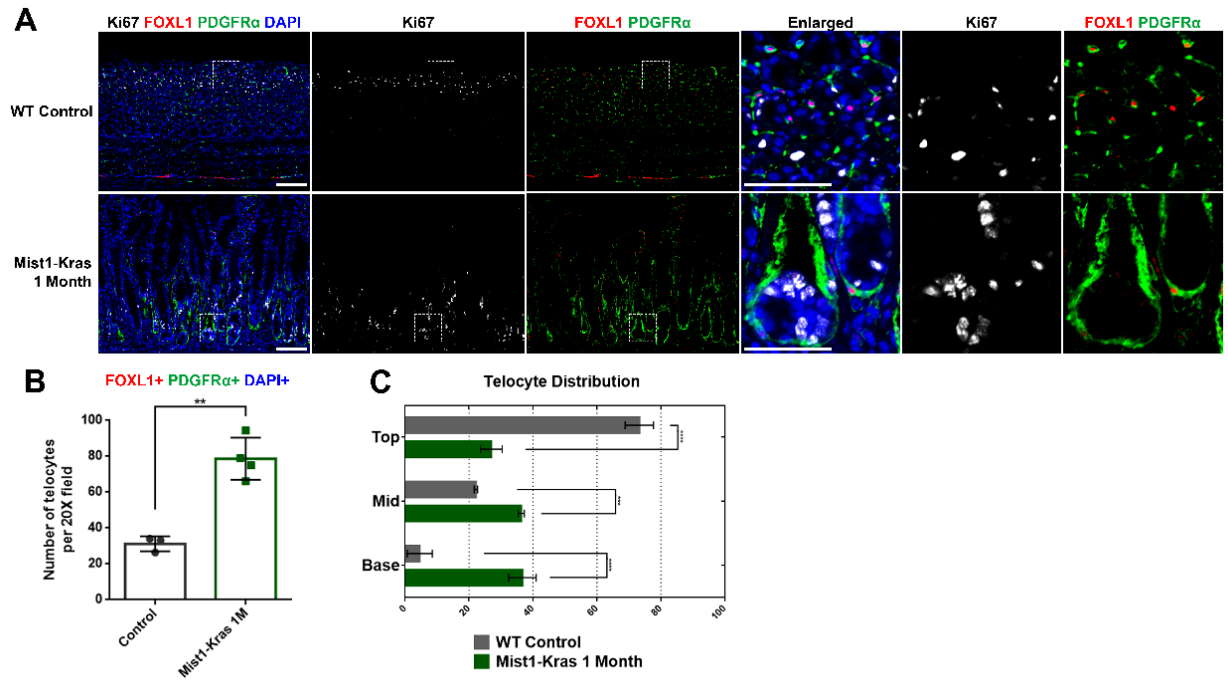

Figure 17. Telocyte numbers are increased during Kras-driven metaplasia development in the stomach.

A) Immunofluorescence staining of Ki67 (*white*), FOXL1 (*red*), PDGFRα (*green*), and DAPI (*blue*) on Mist1-Kras mouse stomach tissue. In the WT control, telocytes are situated near the gland's top with proliferative progenitor cells. However, in Mist1-Kras 1 Month stomach, these telocytes are detected at the base where proliferative cells accumulate. *Scale bar*: 100 µm and 50 µm for enlarged.

B) Quantification of telocyte count. The number of FOXL1+ PDGFRα+ DAPI+ telocytes significantly increased in Mist1-Kras metaplastic stomach. Data presented as mean ± SD (n = 3 for Untreated and n = 4 for Mist1-Kras 1 Month). **P < .01. Unpaired t-test.

C) Quantification telocyte distribution within the gland. Mist1-Kras metaplastic stomach exhibited a redistribution of telocytes, with reduced presence at the top and enhanced distribution at the mid and base regions. Data presented as mean ± SD (n = 3 for Untreated and n = 4 for Mist1-Kras 1 Month). ***p < .001; ****p < .0001. Sidak's multiple comparisons test; two-way ANOVA for interaction (F (2, 10) = 177.4, p < 0.0001).

prominent metaplasia development, a notable shift occurred in the FOXL1+/PDGFRα+ double-positive telocytes. These telocytes were observed at the base of the gland, where proliferative metaplastic cells were also found. Quantitative analysis demonstrated a significant increase in the count of FOXL1+/PDGFRα+/DAPI+ telocytes in the Mist1-Kras metaplastic stomach (Figure 16B). Moreover, the quantitative analysis for telocyte distribution within the gland revealed a distinct redistribution pattern in the Mist1-Kras metaplastic stomach (Figure 16C). This shift was marked by a decrease in telocyte distribution at the top of the gland and a concurrent increase in their abundance at the mid and base regions. In summary, our findings from Mist1-Kras mouse stomach tissue during metaplasia development demonstrated a pattern analogous to what was observed with telocytes during acute injury. These telocytes displayed a shift in distribution in response to the genetic activation of Kras, which in turn induced metaplasia and led to changes in the proliferative zone. Again, these findings suggest the potential for interactions between telocytes and the evolving metaplastic cell niche.

Telocytes are found at the base of the gland only when metaplasia develops.

To investigate whether the observed telocyte relocation during metaplasia was solely attributed to mucosal injury or potentially associated with the establishment of a metaplastic cell niche, we employed a mouse model deficient in the IL-33 receptor (ST2), known as the ST2KO mouse model, wherein metaplasia development is interrupted. In the ST2KO mouse treated with L635, chief-cell transdifferentiation was stalled, preventing the emergence of proliferative metaplasia, even in the context of parietal cell loss (Petersen et al., 2018). Furthermore, the administration of recombinant IL-13 to ST2KO mice alongside L635 treatment resulted in the re-established of metaplasia in the absence of IL-33 signaling (Petersen et al., 2018). This model

provided a unique opportunity to dissect the relationship between mucosal injury, cellular responses, and the subsequent metaplasia development.

Utilizing immunofluorescence staining for GSII, FOXL1, and PDGFRα, we examined the metaplasia development and telocyte distribution in the ST2KO mouse model (Figure 17A). As previously described, untreated stomachs predominantly displayed telocytes at the upper region, while telocyte extension towards the base of the gland was observed in L635-treated stomach. In untreated ST2KO stomach, the telocyte phenotype closely resembled that observed in the untreated WT stomach, with telocytes concentrated on the top region of the gland. In L635-treated ST2KO stomach, consistent with previous reports, metaplasia characterized by GSII expression at the gland's base did not manifest. Furthermore, FOXL1+/PDGFRα+ double-positive telocytes were absent from the gland base in this context. Nevertheless, upon supplementation with recombinant IL-13, metaplasia emerged at the base of the gland, coinciding with the appearance of telocytes in this region.

To quantitatively assess the changes, a telocyte distribution analysis was conducted in ST2KO mouse models (Figure 17B). In ST2KO stomach treated with L635, the distribution of telocytes remained unchanged. However, a significant shift in telocyte distribution was evident when ST2KO stomach received both L635 and recombinant IL-13. This redistribution was characterized by a decrease in telocytes in the top region and a simultaneous increase in their presence at the base region, replicating the changes observed during metaplasia development in L635-treated WT stomach.

These findings shed light on the complex interplay among mucosal injury, the establishment of a metaplastic cell niche, and the recruitment of telocytes during metaplasia development. Notably, the shift in telocyte distribution was specifically associated with the

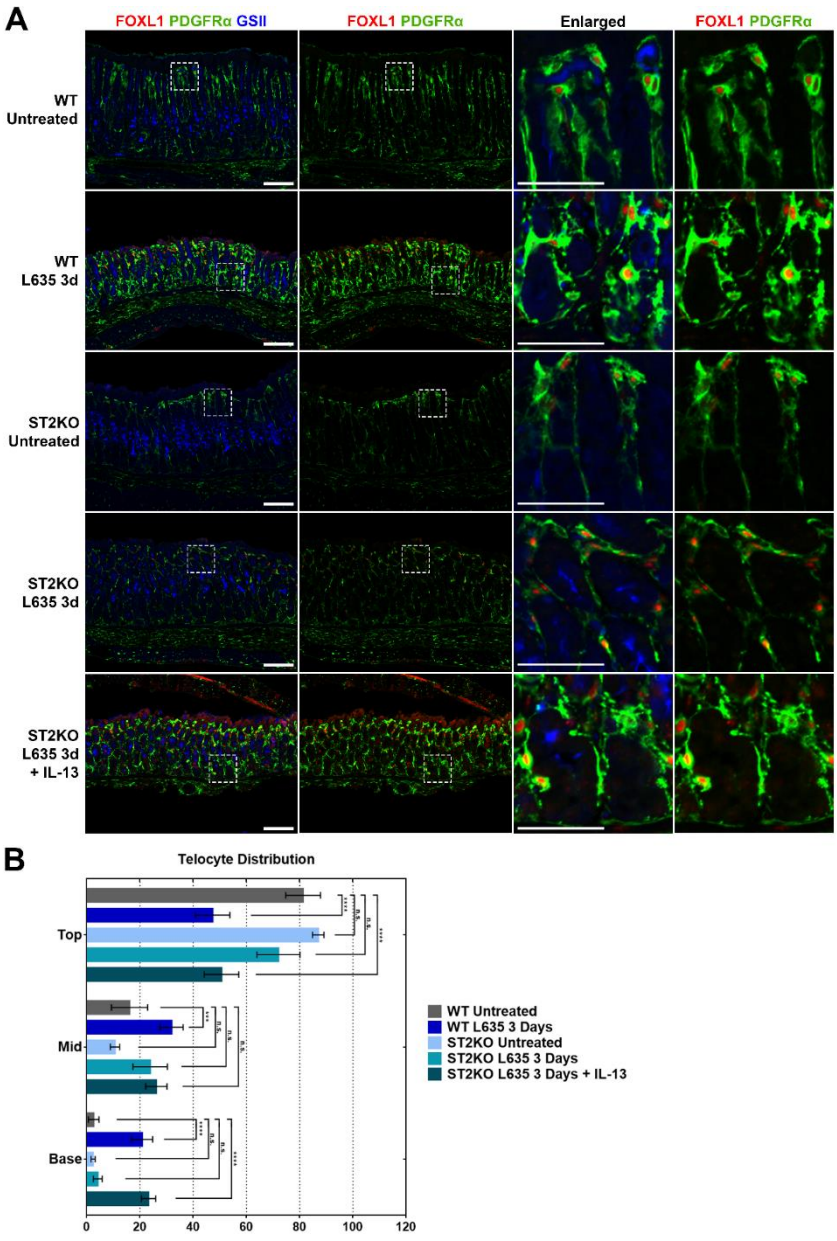

Figure 18. Telocytes are only found at the base of the gland when metaplasia develops in that region.

A) Immunofluorescence staining of FOXL1 (*red*), PDGFRα (*green*), and GSII (*blue*) on the ST2KO mouse model. Inhibition of metaplasia development in the ST2KO stomach was observed. L635 treatment on the ST2KO stomach prevented metaplasia and resulted in the absence of telocytes at the base. However, supplementation with recombinant IL-13 induced metaplasia and concurrent telocyte presence. The untreated ST2KO stomach exhibited telocyte distribution similar to the untreated WT stomach. *Scale bar*: 100 µm and 50 µm for enlarged.

B) Quantification of Telocyte Distribution. Administration of L635 in ST2KO mice preserved unchanged telocyte distribution. However, a significant shift in telocyte distribution occurred with combined L635 and recombinant IL-13 treatment in ST2KO mice, reducing top-localized telocytes and increasing base-localized telocytes. Data presented as mean ± SD (n = 4 for WT and n = 3 for ST2KO). n.s. = not statistically significant; ***$p < .001$; ****$p < .0001$. Tukey's multiple comparisons test; two-way ANOVA for interaction ($F (8, 24) = 23.62$, $p < 0.0001$).

presence of metaplastic cells at the base, suggesting that telocyte relocation is closely tied to the establishment of a metaplastic cell niche.

Telocytes are actively recruited during metaplasia development.

To investigate the recruitment of telocytes during the development of metaplasia in the stomach, we utilized the previously described inducible *Foxl1*-dependent lineage tracing model (Shoshkes-Carmel et al., 2018). Specifically, *Foxl1-CreERT2* mice were crossed with *R26R-tdTomato* mice. Using this inducible Cre model, we selectively labeled *Foxl1*-expressing telocytes with tdTomato and subsequently traced their behavior following mucosal damage induced by L635. Our aim was to discern whether telocytes located near the more basal proliferative cell zone in metaplastic glands originated from existing telocytes situated near the isthmus in normal glands. We performed immunofluorescence staining for FOXL1, PDGFRα, and RFP to detect the tdTomato-labeled telocytes in *Foxl1-CreERT2;R26R-tdTomato* mouse stomach tissue. We observed tdTomato-labeled FOXL1+/PDGFRα+ double-positive telocytes at the top of the gland in stomach tissue treated only with tamoxifen, in agreement with our findings with endogenous FOXL1 immunostaining (Figure 18A). In contrast, we observed the extension of tdTomato-labeled Foxl1-expressing telocytes toward the base of the gland in Foxl1-CreERT2;R26R-tdTomato mice treated with L635. This visual evidence highlighted the recruitment of Foxl1-expressing telocytes to the metaplastic niche during metaplasia development in response to injury.

For a more comprehensive understanding of the distribution and network of these labeled telocytes, we employed three-dimensional whole mount imaging coupled with tissue clearing techniques. Subsequently, three-dimensional imaging was performed using confocal microscopy

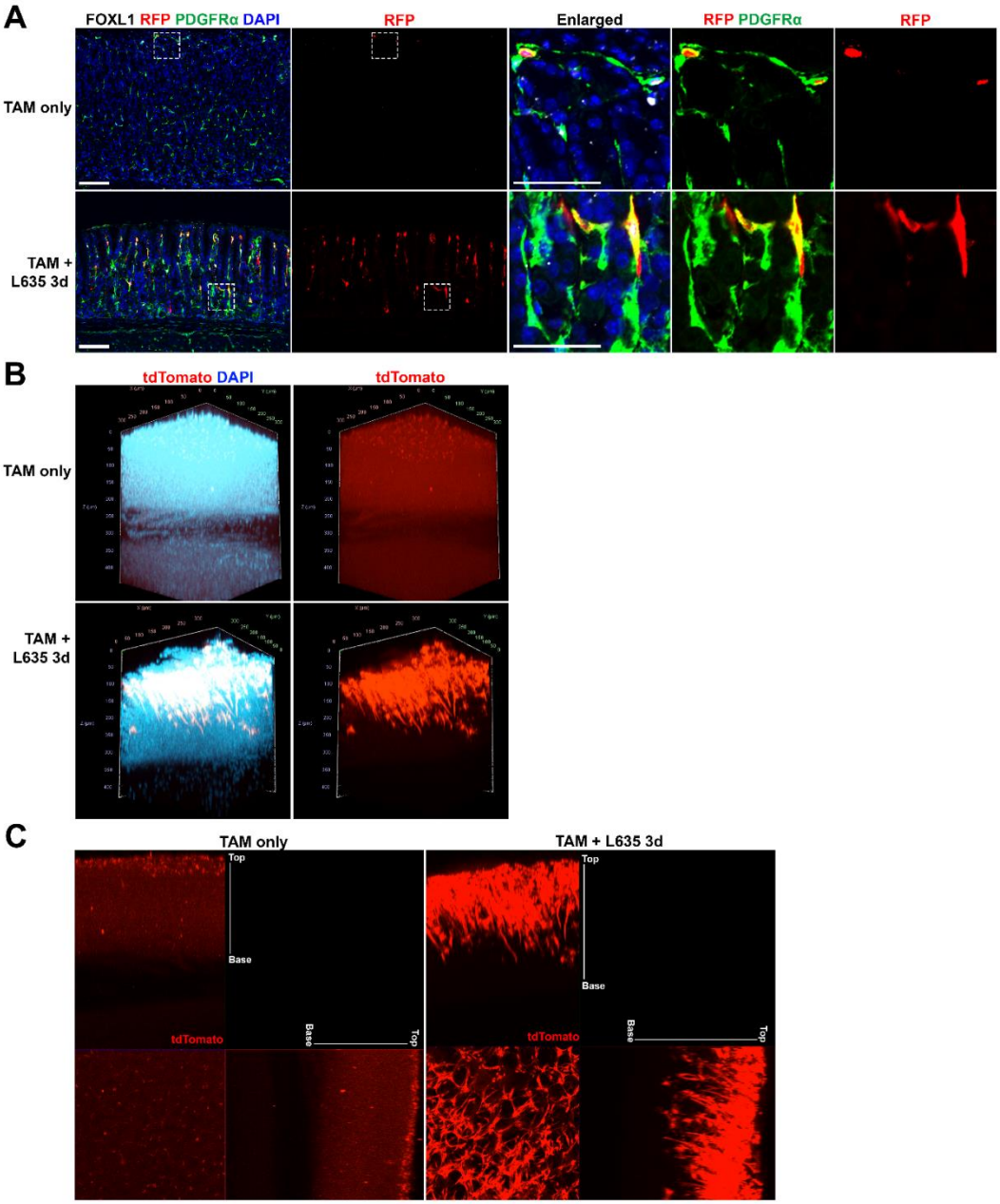

Figure 19. Telocytes are actively recruited during metaplasia development.
A) Immunofluorescence staining of RFP (*red*), FOXL1 (*white*), PDGFRα (*green*) and DAPI (*blue*) on L635-treated *Foxl1-CreERT2*;*R26R-tdTomato* mouse stomach tissue. The use of RFP antibody to detect the tdTomato expression revealed an extension of labeled Foxl1-expressing telocytes toward the base of the gland, specifically in L635-treated stomach tissue. *Scale bar*: 100 μm and 50 μm for enlarged.
B) 3D whole mount image of *Foxl1-CreERT2*;*R26R-tdTomato* mouse stomach tissue after tissue clearing. Endogenous tdTomato (*red*) and DAPI (*cyan*) were observed under a confocal microscope. While untreated stomachs mainly exhibited tdTomato-labeled telocytes at the upper part of the gland, L635 treatment showed these telocytes expanded with longer telopodes reaching the gland's mid and base sections.
C) Orthogonal views obtained from different planes (x/y, x/z and y/z) using Maximum Intensity Projection (MIP). Endogenous tdTomato (*red*) signal showed telocytes in the L635-treated stomach extending further to the gland base, contrasting with the TAM-only control.

to capture the endogenous tdTomato fluorescence. The result recapitulated the distribution pattern observed in immunofluorescence staining conducted on two-dimensional tissue sections (Figure 18B). In the context of tamoxifen-only treated stomach, the tdTomato-labeled telocytes were predominantly situated towards the upper region of the gland. However, in L635-treated stomachs, a distinct expansion of these telocytes was evident as they extended their network towards the gland's base. These telocytes exhibited elongated telopodes that projected towards the mid and base of the gland, illustrating a pronounced shift in their distribution associated with metaplasia development. We also captured orthogonal views from different planes (x/y, x/z, and y/z) to obtain additional perspectives on the altered telocyte distribution (Figure 18C). By utilizing Maximum Intensity Projections on orthogonal views, we enhanced the visualization of the endogenous tdTomato single-channel image. This visualization revealed that telocytes labeled by tdTomato exhibited significant elongation towards the base of the gland in the L635-treated stomach, in contrast to the tamoxifen-only control. These findings collectively highlighted the dynamic recruitment and redistribution of *Foxl1*-expressing telocytes during the course of metaplasia development in response to mucosal injury.

Wnt5a **expression co-localizes with PDGFRα-positive telocytes.**

To gain further insights into the molecular mechanisms underlying the potential role of telocytes in metaplasia development, we directed our focus to *Wnt5a*, a Wnt ligand expressed in intestinal telocytes (Shoshkes-Carmel et al., 2018). Using RNAscope fluorescence *in situ* hybridization (FISH), we assessed *Wnt5a* expression while concurrently performing immunofluorescence staining for PDGFRα on stomach sections from Mist1-Kras mice 1 month after induction.

In the WT control stomach, *Wnt5a* expression, detected by the RNAscope FISH, displayed a distinct enrichment within the PDGFRα-positive cell population, predominantly located at the upper part of the gland (Figure 19). This specific pattern of *Wnt5a* localization aligned with the distribution of telocytes observed in the same region. In contrast, in the context of metaplastic Mist1-Kras 1-month induced stomach, the expression of *Wnt5a* extended more broadly throughout the gland, encompassing PDGFRα-positive cells which reached from the top to the base of the metaplastic glands. This shift in *Wnt5a* expression in PDGFRα-positive cells reflected the expanded distribution of telocytes to the base of the gland in metaplastic regions. These findings suggest that similar to their counterparts in the intestine, telocytes within the stomach express *Wnt5a*. Furthermore, the extended presence of *Wnt5a* in the metaplastic stomach suggests that telocytes may contribute to the metaplastic cell niche, potentially facilitating or maintaining metaplastic changes via *Wnt5a*-mediated pathways.

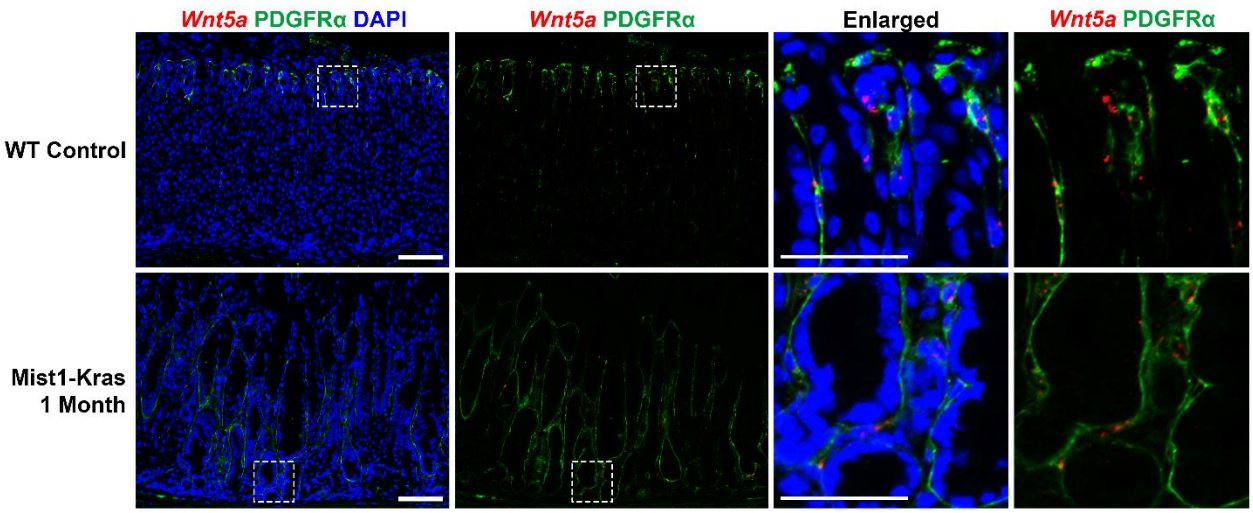

Figure 20. *Wnt5a* expression co-localizes with PDGFRα-positive telocytes and reflects the telocyte distribution shift in metaplasia.
RNAscope fluorescence *in situ* hybridization (FISH) of *Wnt5a* (*red*) and Immunofluorescence staining of PDGFRα (*green*) and DAPI (*blue*) on Mist1-Kras 1 Month mouse stomach. *Wnt5a* expression, detected by RNAscope, exhibited co-localization with PDGFRα-positive cells located towards the upper region of the WT control stomach, where telocytes were observed. In the metaplastic Mist1-Kras 1 Month stomach, *Wnt5a* expression extended throughout the gland in PDGFRα-positive cells, encompassing the base of the gland. *Scale bar*: 100 μm and 50 μm for enlarged.

Discussion

The results presented in this study shed light on the role of telocytes in the stomach, especially concerning their response to mucosal injury and metaplasia development. By elucidating their recruitment, migration, and potential signaling contributions, we contribute to the growing understanding of the complex microenvironmental interactions that drive tissue adaptation and disease progression. Telocytes, characterized by the co-expression of FOXL1 and PDGFRα markers, are found in both the small intestine and the stomach. Within the stomach, FOXL1+/PDGFRα+ double-positive telocytes are predominantly located near the isthmus region where proliferative progenitor cells reside, maintaining an optimal position to function as a component of the isthmal progenitor niche, providing necessary factors to the proliferative cells.

A significant aspect of this study is that the population of FOXL1+/PDGFRα+ double-positive telocytes increases during the development of metaplasia. This phenomenon is evident in both drug-induced and genetically induced active Kras-driven metaplasia. However, telocytes did not extend toward the base of the gland in ST2KO mouse models treated with L635, where metaplasia development was arrested (Petersen et al., 2018), even though prominent loss of parietal cells was present. The telocytes redistributed in the ST2KO mice upon supplementation with IL-13, which re-established development of metaplasia. This indicates that telocyte relocation is not a generic response to mucosal injury, but may specifically function to support the establishment of a metaplastic cell niche.

The observed increase in the number of telocytes and the expansion of the telocyte network during metaplasia development in the stomach are consistent with previous reports on the involvement of telocytes in tissue regeneration and repair in other organs, including the liver and skin (Wang et al., 2014; Wang et al., 2020). Beyond simple numerical increases, these

telocytes also extend their network within the metaplastic gland shifting from their initial position in the isthmus to span the entire gland down to its base. Intriguingly, this altered distribution of telocytes coincides with the expansion of the proliferative cell zone in the stomach gland during metaplasia. The utilization of the *Foxl1-CreERT2;R26R-tdTomato* mouse model for lineage tracing provides insights into the elongation and migratory dynamics of the telocytes. The lineage labeling in the mice demonstrated the trajectory of labeled telocytes from their initial position in the upper glandular region to the proliferative cell zone at the gland base. Therefore, these findings suggest that the recruitment of telocytes to the metaplastic cell niche predominantly originates from pre-existing telocyte populations situated in the isthmus. Also, telocytes may play a role in facilitating or responding to the emerging metaplastic cell niche.

A noteworthy observation regarding this alteration in telocyte distribution during metaplasia is its resemblance to PDGFRα+ cells in the human stomach. Recent investigations from our group identified a population of PDGFRα+ telocyte-like cells in the human stomach and established their involvement in gastric carcinogenesis (Lee et al., 2023). Similar to telocytes, PDGFRα+ stromal cells in the human stomach were predominantly located in the isthmus region of the normal stomach corpus, and expansion of these cells was observed in close proximity to the epithelium at the bases of metaplastic and dysplastic glands (Lee et al., 2023). The consistent distribution pattern of PDGFRα+ cells across both human and mouse stomach tissues underscores the potential translational implications of insights gained from mouse models for understanding human pathology. Presently no antibody reagents are available for immunostaining for FOXL1 in human fixed tissue samples.

These investigations also support the potential role of *Wnt5a* expression in gastric telocytes. Telocytes within the stomach may contribute to the establishment of a supportive

microenvironment for proliferative cells, potentially through secreted factors. Notably, the single-cell transcriptomic analysis of cells from human stomachs with metaplasia identified *WNT5A* expression in the PDGFRα+ telocyte-like cells in human stomach (Lee et al., 2023). In mouse stomach, *Wnt5a* expression co-localized with PDGFRα-positive telocytes and reflects the shift in telocyte distribution seen during metaplasia. Given the recognized significance of Wnt signaling pathways in tissue development and homeostasis, the observed correlation between *Wnt5a* expression and telocyte distribution suggests a possible influence on metaplasia development via Wnt-mediated pathways. This insight emphasizes the need for further investigation into mechanistic implications and potential roles of *Wnt5a* in maintaining gastric tissue homeostasis and driving metaplasia development.

In conclusion, the findings of this study contribute to our understanding of telocyte biology in the stomach, particularly the roles of telocytes during mucosal injury and metaplasia development. These results serve as a foundation for future investigations, presenting a potential avenue to explore the functional significance of telocytes within the gastric mucosa. Further study of telocyte and fibroblast influences on mucosal lineage differentiation and maintenance could support the development of interventions targeting the progression of metaplasia-associated gastric carcinogenesis.

Materials and Methods

Mice

Approximately 8 weeks C57BL/6J mice were used for mouse experiments. For drug treatment experiments, DMP-777 was dissolved in 1% methylcellulose and administered through oral gavage (350 mg/kg) once a day for up to 10 consecutive days. L635 was dissolved in deionized DNA and RNA-free water and administered through oral gavage (350 mg/kg) once a day for up to 3 consecutive days. Archival sections of stomach from Mist1-Kras mice and ST2 knockout mice were obtained from previous studies (Choi et al., 2016; Petersen et al., 2018). The generation of *Foxl1-CreERT2* mice has been described previously (Shoshkes-Carmel et al., 2018). For lineage-tracing experiments of *Foxl1*-expressing cells, *Foxl1-CreERT2* mice were crossed with *R26R-tdTomato* mice, and 5 mg tamoxifen was administered to these mice subcutaneously daily for a total of 3 doses. L635 was then administered 7 days post-tamoxifen injection, for 3 consecutive days. Regular mouse chow and water *ad libitum* were provided during experiments in a temperature-controlled room with 12-hour light-dark cycles. All treatment maintenance and care of animals in these studies followed protocols approved by the Institutional Animal Care and Use Committees of Vanderbilt University.

Immunofluorescence Staining

Mouse stomachs were fixed in 4% paraformaldehyde overnight and transferred into 70% ethanol for paraffin embedding. Five-micrometer paraffin-embedded sections were used for all immunofluorescence staining. Sections were deparaffinized, rehydrated, and submitted to antigen retrieval using Target Retrieval solution (Dako North America, Inc) in a pressure cooker. Blocking was performed by using Protein Block Serum-Free (Dako North America, Inc) for 90

minutes at room temperature. The primary antibody incubation was performed in Antibody Diluent with Background Reducing Components (Dako North America, Inc) overnight at 4°C. Primary antibodies used were as follows: goat anti-PDGFRα (1:500; R&D systems), guinea pig anti-FOXL1 (1:1500), rat anti-Ki67 (1:200; BioLegend) and rabbit anti-Ki67 (1:1000; Cell Signaling). Fluorescent second antibodies (1:500; Jackson ImmunoResearch) and Alexa-488 and 647-conjugated GSII (1:2000) were incubated for 1 hour at room temperature. FOXL1 staining required the use of amplification of signal using tyramide (TSA systems; PerkinElmer). After incubation with DAPI for 5 minutes, slides were mounted with ProLong Gold Antifade Reagent (Invitrogen). Fluorescence imaging was analyzed by using an Axio Imager 2 microscope (Carl Zeiss AG).

Immunofluorescence Quantitation

Experimental groups contained 3–5 mice. Images were analyzed using CellProfiler (Cambridge, MA) to quantify objects and verified manually (nuclei, cells). At least 4 representative images (>100 glands) of proximal stomach corpus were taken from each mouse at 20x objective for quantification. Quantification of telocyte distribution within the gland was conducted by assessing their presence in three distinct positions along the gland's height, namely the top, middle, and base. All graphs and statistics were generated using GraphPad Prism. Significance was determined through various methods including unpaired t-test, one-way ANOVA with Tukey's multiple comparisons test, or two-way ANOVA with Tukey's multiple comparisons test and Sidak's multiple comparisons test; n.s. = not statistically significant; *$p < .05$; **$p < .01$; ***$p < .001$; ****$p < .0001$.

Tissue Clearing

Tissue clearings using CUBIC protocol was performed as previously described (Yum et al., 2021). Briefly, fixed tissue was dissected into small fragments and incubated in 5 ml CUBIC R1a solution (10% urea, 5% Quadrol, 10% Triton X-100 and 25mM NaCl in distilled water) for 2 days at 37°C with shaking. The tissues were then incubated in 5 ml Blocking and Permeabilization solution (5% DMSO, 0.5% Triton X-100 and 2% normal donkey serum (NDS) in PBS) overnight at 4°C. The tissues were washed 6 times with 0.2 µg/ml DAPI in PBS over a 24-h period at 4°C. The tissues were then incubated in 5 ml CUBIC R2 solution (50% sucrose, 25% urea, 10% triethanolamine, and 0.1% Triton X-100 in distilled water) for 2 days at RT with shaking. The tissues were transferred into 500 µl RapiClear 1.52 (Sunjin Lab) to match the refractive index and incubated overnight at 4°C. The tissues were then mounted on Glass Bottom Culture Dish (MatTek Corporation) with RapiClear 1.52. The tissues were imaged using ZEISS LSM 980 with Airyscan 2 in the Vanderbilt Cell Imaging Shared Resource Core.

RNAscope – fluorescence *in situ* hybridization

Stomachs from both wild-type and Mist1-Kras mice, fixed in 10% neutral buffered formalin, were used. RNAscope fluorescence *in situ* hybridization (FISH) was performed using the RNAscope LS Multiplex Fluorescent Reagent Kit (322800, Advanced Cell Diagnostics) according to manufacturer's protocol using a Bond RX Autostainer (Vanderbilt Translational Pathology Shared Resource), except for the addition of immunofluorescence detection of PDGFRα. Briefly, sections were deparaffinized, treated with heat target retrieval and protease, followed by a series of hybridizations with the target-specific probes (316798, *Wnt5a*) and amplifiers. After probe detection with OPAL520 dye, sections were washed with PBS, blocked

using Protein Block Serum-Free (Dako North America, Inc), and incubated with goat anti-PDGFRα (1:500; R&D systems) primary antibody overnight at 4°C. After washing with PBS, sections were stained with fluorescent second antibodies for 1 hour at room temperature. Sections were washed in PBS, incubated with DAPI for 5 minutes, and slides were mounted with ProLong Gold Antifade Reagent. Fluorescence imaging was analyzed by using an Axio Imager 2 microscope (Carl Zeiss AG).

CHAPTER IV

CONCLUSIONS AND FUTURE DIRECTIONS

Conclusions

This thesis has aimed to elucidate the mechanisms and primary contributors to metaplasia development in the gastric mucosa. Gastric cancer constitutes a significant global health challenge, ranking as one of the predominant causes of cancer-related mortality. The progression toward gastric carcinogenesis, characterized by the development of metaplasia and dysplasia, is frequently precipitated by chronic inflammation and oxyntic atrophy, conditions typically induced by *Helicobacter pylori* infection. These conditions foster an environment conducive to metaplastic changes, thereby elevating the risk of cancer. Unraveling the mechanisms underlying gastric metaplasia is critical for improving disease surveillance and therapy.

Following oxyntic atrophy, metaplasia development is characterized by the transdifferentiation of chief cells into SPEM cells. This highly regulated process involves dismantling the chief cell's secretory architecture and initiating transcriptional changes to upregulate metaplastic genes. Previous studies have shed light on various aspects of this transdifferentiation; however, this study has identified a new key player: miR-148a.

Chapter 2 of this thesis presents findings from mouse models with acute parietal cell loss, demonstrating that microRNA (miRNA) alterations are integral to stomach metaplasia development. miR-148a emerges as the most abundantly expressed miRNA in chief cells, with levels more than 10-fold higher than other miRNAs. As metaplasia develops following acute oxyntic atrophy, miR-148a expression significantly decreases. This decrease is mirrored in human tissues where metaplastic cells exhibit much lower levels of miR-148a compared to

normal chief cells. The suppression of miR-148a leads to the upregulation of CD44v9, an early SPEM marker, and its target gene, Dnmt1. The high miR-148a levels in gastric chief cells and their rapid decrease post-injury suggest that miR-148a may initiate chief-cell transdifferentiation, contributing to metaplasia development.

Beyond the chief-cell transdifferentiation within epithelial cells, microenvironmental factors play a pivotal role in the development of metaplasia. Previous studies have focused extensively on immune cell involvement, particularly since *Helicobacter* infection and chronic inflammation are primary causes of metaplasia in humans (Nam et al., 2010). Immune cells such as M2 macrophages and type 2 innate lymphoid cells (ILC2s) have been recognized as critical components of the immune microenvironment, influencing both chief-cell transdifferentiation and the progression of metaplasia in the stomach (Busada et al., 2019; Meyer et al., 2020; Petersen et al., 2014). Furthermore, recent studies have shed light on the role of fibroblasts, another vital stromal element, in the progression of metaplasia to dysplasia (Lee et al., 2023). This thesis introduces a novel element in the stromal compartment, previously unexplored in this context: telocytes.

Chapter 3 investigates the role of telocytes in the stomach, particularly their involvement in metaplasia development and the evolution of a gastric metaplastic niche. Telocytes in the stomach express FOXL1 and PDGFRα, markers consistent with telocytes in other parts of the gastrointestinal tract. In the normal stomach, telocytes are strategically located near the proliferating progenitor cells at the gland's isthmus. Upon metaplasia induction, either through acute injury or KRAS-induced models, an increase in telocyte abundance was observed, along with a distribution shift from the isthmus to the gland base. This shift correlates with an expanded proliferative cell zone, suggesting a connection between telocyte recruitment and the

emerging metaplastic cell niche. One potential function of telocytes in this niche could be through the expression of WNT molecules, such as *Wnt5a*. The intricate interplay observed between telocytes and epithelial cells in developing metaplasia underscores the importance of telocytes in tissue adaptation and repair processes.

In summary, this thesis presents a comprehensive exploration of the intricate interplay of intrinsic and extrinsic factors involved in gastric metaplasia development. It highlights the critical role of chief-cell transdifferentiation in response to chronic inflammation and oxyntic atrophy. The discovery of miR-148a's significant role in initiating the transdifferentiation process, as well as the novel insights into the involvement of telocytes in shaping the metaplastic microenvironment, represent important advancements in our understanding of gastric carcinogenesis. These findings not only deepen our comprehension of the cellular and molecular dynamics at play but also open new avenues for potential therapeutic interventions aimed at preventing or halting the progression of gastric cancer at its earliest stages. This research underscores the importance of a multifaceted approach, considering both epithelial and stromal components, to fully grasp the complexity of gastric metaplasia and its transition to malignancy.

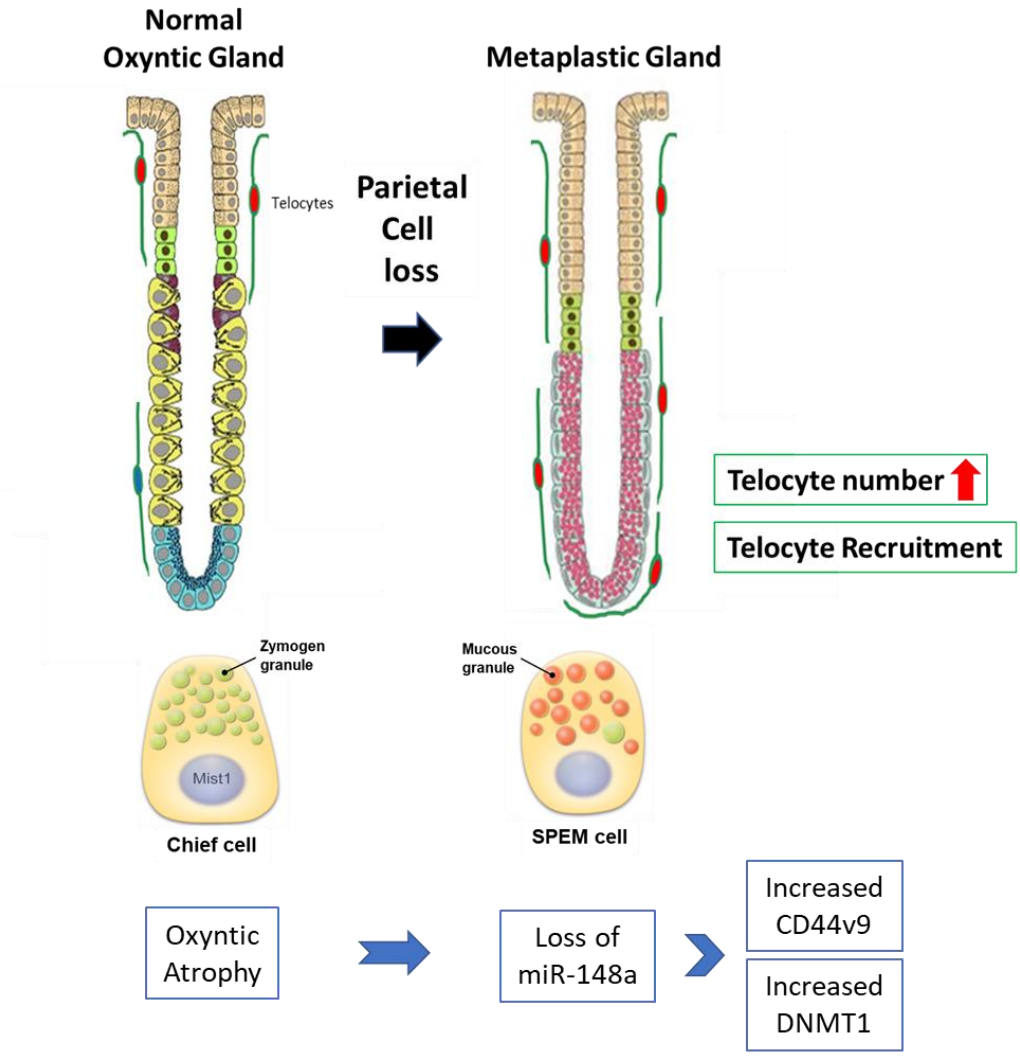

Figure 21. Major discoveries of the thesis.
This figure captures the key findings of the study, illustrating the intrinsic and extrinsic factors involved in the development of gastric metaplasia. It highlights the transdifferentiation of chief cells into SPEM (spasmolytic polypeptide-expressing metaplasia) cells, a transformation characterized by the loss of miR-148a. Additionally, the figure illustrates the role of telocytes, highlighting their recruitment and involvement during the development of metaplasia.

Future Directions

The research outlined in this thesis has laid the groundwork for a deeper understanding of the mechanisms and key players involved in the development of gastric metaplasia. Building on these findings, future research should explore two critical areas of interest that promise to further unravel the complex dynamics of metaplasia development:

1) miR-148a Downregulation in Chief Cell Transdifferentiation:

Our research has identified miR-148a as the primary microRNA (miRNA) in chief cells, with its rapid downregulation marking the onset of transdifferentiation. This pivotal finding propels further inquiries into the extensive consequences of this decrease on the gene and protein expression landscapes within chief cells. The role of miR-148a in initiating a cascade of gene-expression changes during the transdifferentiation of chief cells into SPEM cells is a compelling area for further investigation. Future studies should aim to delineate the comprehensive downstream effects of miR-148a downregulation, exploring how this alters the cellular behavior and protein expression profile of chief cells. Investigating the potential therapeutic implications of modulating miR-148a expression could provide new strategies for controlling or reversing metaplastic changes in the gastric mucosa.

Septin 9 as a Novel miR-148a Target

MicroRNAs (miRNAs) are noncoding RNAs that regulate gene expression, through the degradation mRNAs or by inhibiting protein translation. While traditional research has largely focused on their role in degrading target mRNAs, recent developments in the field suggest that miRNAs can also act as inhibitors of transcript translation (Gu & Kay, 2010; Naeli et al., 2023).

This can occur through mechanisms such as direct interference with transcript interactions at the ribosome or by inhibiting translation elongation (Eulalio et al., 2008; Ricci et al., 2013). These insights have led to a growing interest that high expression levels of certain miRNAs might be more closely associated with the repression of translation rather than the direct degradation of mRNAs.

In chief cells, miR-148a stands out as the most abundantly expressed miRNA, with expression levels exceeding other miRNAs by over 10-fold. Considering the extensive role of miRNA in post-transcriptional regulation, the predominant presence of miR-148a suggests its significant influence on chief cell's transcriptome and proteome. To understand the consequences of miR-148a inhibition in chief cells, we conducted extensive transcriptome and proteome analyses. Our aim was to explore how miR-148a depletion affects the expression of various transcripts and proteins, particularly those involved in transdifferentiation.

For analysis, ImChief cells were treated with a miR-148a inhibitor and a non-specific control. We employed parallel approaches for our study: bulk RNA sequencing for transcriptomic analysis and mass spectrometry for proteomic analysis. This dual method allowed us to accurately identify specific miR-148a targets that are pivotal in the transdifferentiation process of chief cells. The findings from this study lay the groundwork for future validation studies, which are essential to fully understand the role of these regulators in the distinct stages of chief-cell transdifferentiation.

Our proteomic analysis has identified Septin 9 (SEPT9) as a novel target of miR-148a. SEPT9 is a cytoskeletal GTPase that plays a multifaceted role in various biological processes, including cytokinesis, vesicle trafficking, membrane reconstruction, cell migration, and apoptosis (Sun et al., 2020). This diverse functionality positions SEPT9 as a critical player in cellular

dynamics and integrity. In a comparative study, SEPT9 emerged as an upregulated gene in human SPEM cells compared to normal chief cells, as identified through microarray analysis of microdissected cell lineages in the human stomach (Lee et al., 2010). The consistent elevation of SEPT9 levels in SPEM cells across various studies, including our miR-148a inhibition experiment, not only validates our findings but also suggests a significant role for SEPT9 in chief-cell transdifferentiation.

Furthermore, other studies have highlighted roles of SEPT9, which is relevant for chief-cell transdifferentiation process. Under conditions of oxidative stress, marked by increased levels of reactive oxygen species, SEPT9 has been observed to exhibit enhanced localization to lysosomes (Kesisova et al., 2021). This response likely reflects an adaptive mechanism for lysosomal transport, enabling cells to cope with oxidative damage. Such a mechanism is particularly relevant in the context of gastric mucosal injury, where oxidative stress is a known characteristic in cellular response and metaplasia. Moreover, SEPT9 has been implicated in the stability of the plasma membrane, notably reducing the degradation of ubiquitin-independent EGFR (Diesenberg et al., 2015). This role further underscores SEPT9's importance in maintaining cellular structures and signaling pathways, which are vital for cell survival and adaptation in changing environments. These findings collectively highlight SEPT9's multifaceted roles and its potential significance in chief-cell transdifferentiation. Future investigations should explore to deepen our understanding of SEPT9's functions in chief-cell transdifferentiation.

miR-148a Knockout Study

In this thesis, we investigated the role of miR-148a in chief-cell transdifferentiation through targeted miR-148a knockdown approach *in vitro*. Building on these findings, for our

future studies, we plan to focus on knocking out miR-148a in chief cells *in vivo*. This will be accomplished using the miR-148a$^{flox/flox}$ mouse strain, in combination with the previously described Gif-rtTA;TetO-Cre transgenic mouse model (Caldwell et al., 2022). This model is uniquely advantageous due to its utilization of the chief cell-specific gastric intrinsic factor (GIF) locus, Gif-rtTA. It employs a tetracycline-inducible rtTA system that consequently triggers the expression of Cre recombinase under a tetracycline-responsive promoter. By using the Gif-rtTA;TetO-Cre;miR-148a$^{flox/flox}$ mice, our objective was to achieve a specific knockout of miR-148a in chief cells, which would provide insights into its role in their transdifferentiation.

Our hypothesis is that by simulating the downregulation of miR-148a, chief cells would initiate the transdifferentiation process even without mucosal damage. We expect this knockout would trigger a cascade of post-transcriptional changes in chief cells, driving transdifferentiation typically observed during oxyntic atrophy. Based on our *in vitro* observations, where miR-148a inhibition led to the upregulation of CD44v9, we expect the chief cells to begin transdifferentiation, evidenced by the upregulation of SPEM cell markers and downregulation of chief cell markers.

The optimal outcome would be for miR-148a KO to independently drive chief-cell transdifferentiation. However, if this does not occur, we will explore whether miR-148a KO predisposes chief cells to accelerated transdifferentiation. Prior research have shown miR-148a-deficient mice to be more susceptible to colitis and colitis-associated tumorigenesis, indicating miR-148a's role as an indirect tumor suppressor by modulating colitis and tumorigenesis through the suppression of NF-κB and STAT3 signaling pathways (Zhu et al., 2017). If miR-148a KO alone does not visibly induce transdifferentiation, we plan to administer parietal cell toxic drugs, such as DMP-777 or L635. This will help us determine if miR-148a deficiency influences the

timing of SPEM development in mice. In wild-type mice, SPEM develops within 10 days post-DMP-777 treatment and 3 days post-L635 treatment (Nam et al., 2010). We hypothesize that miR-148a KO could accelerate SPEM development, potentially shortening the transdifferentiation process to 5- or 3-days post DMP-777 treatment. The outcomes of this research could provide insights into the intricate processes of chief-cell transdifferentiation.

miR-148a Expression during KRAS-induced Gastric Carcinogenesis

Although numerous studies have documented the downregulation of miR-148a in gastric cancer compared to normal tissues, its expression across the entire carcinogenesis pathway, from metaplasia development through dysplasia progression, remains understudied. Given our findings that miR-148a downregulation is one of the initial changes during chief-cell transdifferentiation into the metaplastic lineage, it is interesting to consider whether the expression of miR-148a remains consistently suppressed during carcinogenesis or exhibits fluctuations. For instance, in the esophagus, miR-148a levels are higher in Barrett's esophagus (BE) compared to normal esophageal mucosa, but decrease significantly in esophageal adenocarcinoma relative to BE (Slaby et al., 2015). Such patterns suggest that miR-148a expression might vary as the disease progresses. Thus, examining the expression patterns of miR-148a at each stage of the carcinogenesis pathway could offer valuable insights.

Previous studies have established a correlation between reduced miR-148a expression in gastric cancer and poor patient outcomes, including lower overall survival rates and a propensity for lymph node metastasis (Liu et al., 2015; Qiu et al., 2017; Tseng et al., 2011; Zheng et al., 2011). It's important to note that lymph node metastasis is a common and prognostically significant form of metastasis in gastric cancer, often necessitating regional lymph node resection

in therapeutic protocols (Banan et al., 2020; Kinami et al., 2021; Lee et al., 2012). These findings highlight the potential impact of understanding miR-148a expression patterns in gastric carcinogenesis in a more comprehensive manner. Given miR-148a's role as a tumor suppressor, assessing its expression levels in a mouse model of gastric carcinogenesis could be highly informative.

To study these stages, we propose employing the KRAS-activated genetically engineered mouse model previously mentioned in this thesis (Choi et al., 2016). This KRAS model accurately elicits the full spectrum of gastric carcinogenesis, from normal tissue through to pyloric metaplasia, intestinal metaplasia, and dysplasia. The objective for this proposed study is to investigate the expression patterns of miR-148a at each stage of this progression. This will not only enhance our understanding of chief cell biology and transdifferentiation nuances but also shed light on the role of miR-148a in the broader context of gastric cancer development. We aim to determine whether miR-148a expression is consistently downregulated or exhibits fluctuations throughout the stages of gastric carcinogenesis.

In conclusion, the exploration of miR-148a's role in chief-cell transdifferentiation has provided essential insights into the process of gastric metaplasia. Our research has not only identified the crucial downregulation of miR-148a at the onset of transdifferentiation but also revealed Septin 9 (SEPT9) as a novel candidate, in follow up study. These findings indicate a complex interaction between miR-148a dynamics and chief cell behavior, extending into gastric tissue injury and carcinogenesis. The planned *in vivo* studies using the miR-148aflox/flox mouse model aim to further delineate miR-148a's regulatory roles and its potential as a therapeutic target. Additionally, investigating miR-148a expression patterns throughout gastric

carcinogenesis will enhance our understanding of the molecular aspects of gastric cancer. This research direction is set to deepen our understanding of the molecular dynamics of gastric pathologies and may lead to innovative therapeutic approaches for gastric cancer.

2) Telocyte Involvement in Metaplasia Development:

The research presented in this thesis has highlighted the crucial involvement of telocytes in the development of gastric metaplasia. As telocytes are a relatively new cell type, their further characterization within the gastric stroma is essential. Future studies should focus on identifying specific markers that differentiate telocytes from other stromal cells within their microenvironment. Moreover, an in-depth examination of the signaling pathways and molecular interactions between telocytes and epithelial cells, both in normal gastric homeostasis and during metaplasia progression, is necessary. Understanding how changes in telocyte distribution and their secretory profiles influence metaplastic development could reveal novel targets for therapeutic intervention. Additionally, exploring the role of telocytes as potential biomarkers for early detection of metaplastic changes and their progression to dysplasia could yield important scientific insights. Such studies would significantly expand our understanding of telocytes in gastric pathologies. This line of research is essential for deepening our knowledge of the cellular dynamics within the gastric microenvironment, particularly how telocytes contribute to the onset and development of metaplasia. Expanding our comprehension of these aspects will be crucial in advancing the broader scientific field of gastric metaplasia and its underlying mechanisms.

Characterization of Telocytes in the Stomach

The characterization of telocytes within the gastric microenvironment is a crucial aspect of understanding metaplasia development. While immune cells and fibroblasts have known roles in responding to mucosal changes and shaping the extracellular matrix, telocytes emerge as a significant yet less understood component. These cells have the potential to be crucial in maintaining tissue homeostasis and may play a key role in the response to tissue damage that leads to metaplastic transformations.

In addition to the previously mentioned markers, further exploration into the unique characteristics and functions of telocytes in the stomach is imperative, particularly for human tissue samples, where FOXL1 staining is not available. Identifying specific markers for telocytes is essential, especially considering that PDGFRα alone may not be sufficient due to its expression in various cell populations within the gastrointestinal tract. Previous studies have reported the presence of both PDGFRα-high and PDGFRα-low cells in the stroma of the small and large intestine, indicating the need for additional markers (McCarthy et al., 2020; Melissari et al., 2021). Despite their significance, telocytes have not yet been included in standard histological textbooks, underscoring the novelty of this research area (Klein et al., 2021).

Further analysis and validation studies, such as those utilizing single-cell RNA sequencing, are essential to explore the diversity of stromal cell populations within the gastric microenvironment and their roles in metaplasia. In our lab, we have identified four distinct subpopulations of fibroblasts in the human stomach, which notably includes a telocyte-like population (Lee et al., 2023). This specific subpopulation is characterized by elevated levels of *BMP4*, *WNT4*, and *WNT5A*, which aligns with the expression patterns of *Wnt5a* in mouse telocytes as documented in Chapter 3 of this thesis. These parallel observations suggest a

potential similarity between mouse gastric telocytes and human telocyte-like fibroblasts, thereby providing a promising direction for further detailed characterization of telocytes and other stromal cell types using available sequencing data. Utilizing the insights gained from existing sequencing data, our future research aims to determine the complex interplay within these stromal cell populations, enhancing our understanding of their roles in the progression of gastric metaplasia.

In our ongoing studies, we are closely examining various stromal cell populations in the mouse stomach. Our aim is to delineate how these cells present themselves in a state of normal homeostasis, and then to examine their transformation as they undergo changes during the development of metaplasia, and ultimately, their progression to dysplasia. Through immunofluorescence staining for α-smooth muscle actin (αSMA), we have identified that Foxl1+/PDGFRα+ double-positive telocytes form a distinct population separate from myofibroblasts, aligning with observations in the small intestine (Figure 22A) (Aoki et al., 2016). Interestingly, the co-expression of FOXL1 and αSMA was observed in DMP-777 treated stomachs, suggesting dynamic changes in stromal composition in response to gastric injury. This finding indicates a potential adaptive or reactive role of telocytes in response to tissue damage, which could be pivotal in understanding their function in gastric pathologies.

We also investigated the relationship between FOXL1+/PDGFRα+ double-positive telocytes and periostin (POSTN) and tissue factor (F3), markers associated with tissue repair and extracellular matrix remodeling (Figure 22B, C) (Bernier-Latmani et al., 2022; Kinchen et al., 2018). The observed overlap of POSTN and F3 with telocytes in injured tissue reinforces the hypothesis that telocytes play a significant role in the gastric tissue remodeling process, especially during the transition from normal to metaplastic glands. Understanding the functional

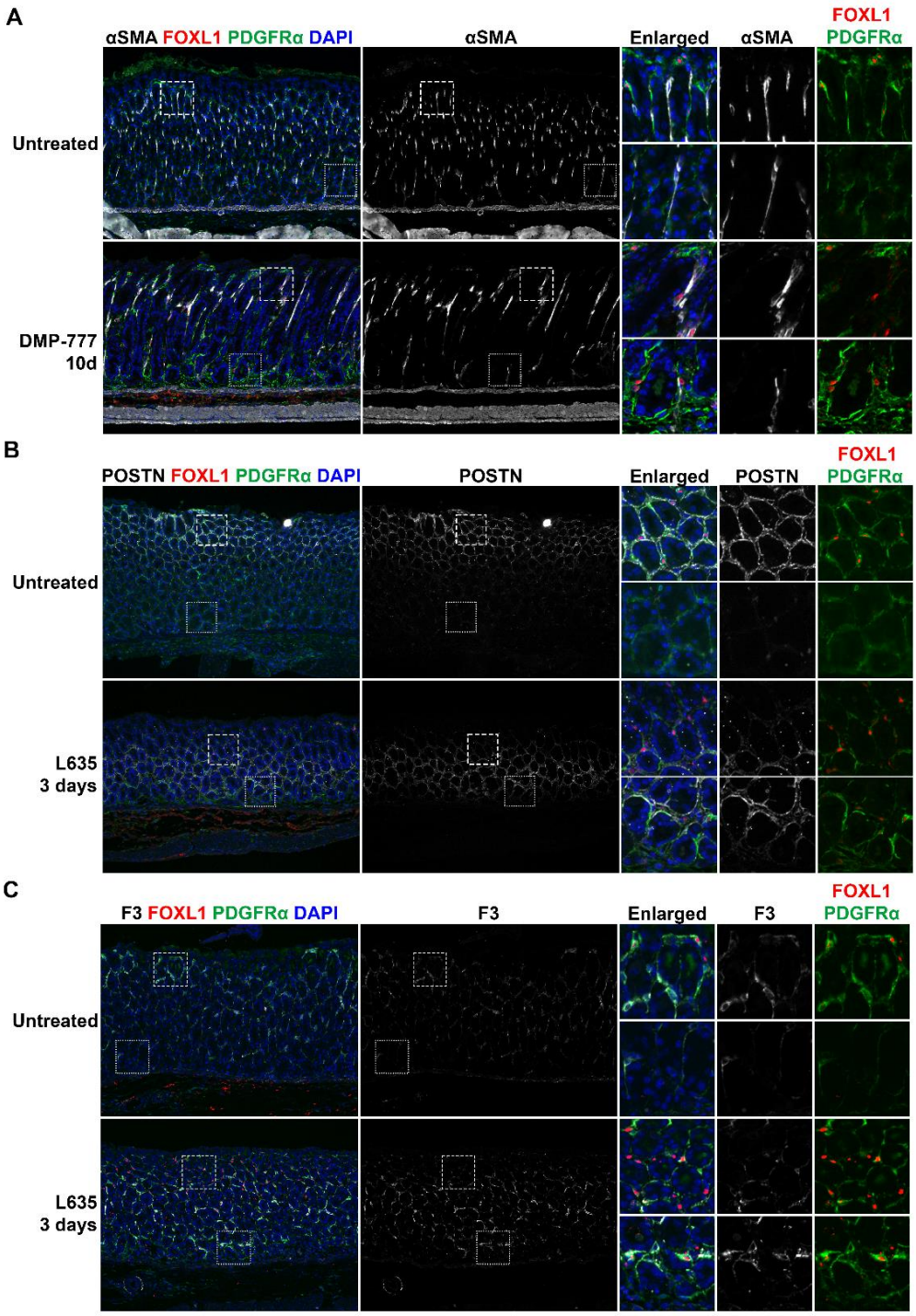

Figure 22. FOXL1+/PDGFRα+ double-positive telocytes with other cell markers in stroma.
A) IF staining for αSMA (white), FOXL1 (red), PDGFRα (green) and DAPI (blue). Telocytes are distinct from myofibroblasts, identified by αSMA staining. However, in DMP-777 treated stomach, a cell population positive for FOXL1 and αSMA but negative for PDGFRα was observed.
E) IF staining for POSTN (white), FOXL1 (red), PDGFRα (green) and DAPI (blue). POSTN staining exhibits partial overlap with telocytes.
E) IF staining for F3 (white), FOXL1 (red), PDGFRα (green) and DAPI (blue). There is an observable overlap between F3 and PDGFRα in the staining.

role of these markers and how telocytes contribute to tissue repair and remodeling could provide essential insights into the cellular mechanisms driving metaplasia.

For specific investigation in the context of gastric metaplasia and telocyte function, examining the expression and function of R-spondin 3 (RSPO3) in the stomach presents another intriguing area for future studies. RSPO3, recognized for its crucial role in stem cell turnover and tissue repair, is expressed in telocytes within the intestinal crypts (Aoki et al., 2016). In the stomach, RSPO3 expression increases in response to *H. pylori* infection and parietal cell loss, indicating its critical involvement in the gastric injury response (Fischer et al., 2022; Sigal et al., 2017). Moreover, the absence of RSPO3 in mice correlates with reduced glandular hyperproliferation after injury, emphasizing the importance of RSPO3 in gastric tissue repair and the maintenance of epithelial proliferative capacity post-injury (Fischer et al., 2022). These observations suggest that RSPO3 plays a pivotal role in gastric tissue dynamics, particularly in response to injury and repair. Investigating the dynamics of RSPO3 in telocytes could offer insights into their role in regulating gastric epithelial cell behavior under metaplasia-inducing conditions. This investigation could advance our understanding of the cellular and molecular mechanisms underlying metaplasia development.

However, the challenge remains in clearly distinguishing telocytes due to the overlapping expression of certain markers with other cell types. For instance, the use of CD34, a known marker of telocytes, as a marker for telocytes in gastric lamina propria is complicated by its prevalent expression in endothelial cells within the gastric tissue. While CD34+/PDGFRα+ cells do exist and exhibit the elongated network phenotype characteristic of telocytes, they do not consistently co-express FOXL1. This discrepancy highlights the complexity of accurately identifying telocytes and underscores the necessity for more definitive and specific markers. The

identification of such markers would not only clarify the role of telocytes in the gastric microenvironment but also aid in distinguishing them from other stromal cells, particularly in the context of metaplasia and dysplasia.

Through these studies, we aim to build a more comprehensive picture of the stromal cell dynamics within the gastric microenvironment, particularly focusing on the role and characteristics of telocytes. By deciphering the unique properties and interactions of these cells, we hope to gain a deeper understanding of their involvement in gastric tissue homeostasis and pathology.

The Isolation of Telocytes

In the evolving field of telocyte research, several studies have reported the isolation of telocytes, primarily based on their distinctive morphological characteristics (Hatta et al., 2012; Sanches et al., 2017; Song et al., 2019). A key feature of these isolated telocytes, consistent with *in situ* observations, was the presence of telopode-like extended processes. Despite these advances, a significant gap remains in our understanding, partly due to the lack of successful *in vitro* culturing of telocytes. While primary culture characterizations have provided some insights, these have been largely limited to morphological observations.

Amidst these developments, a critical perspective has been presented by Varga et al., addressing a fundamental concern in telocyte research (Varga et al., 2019). They argued that the long cytoplasmic processes, often considered a hallmark of telocytes, may not be a unique characteristic exclusive to these cells *in vitro*. Their observation suggests that such morphological traits can also arise in other cell populations, particularly under conditions of metabolic stress or long-term culture. This phenomenon has been observed in fibroblasts and

somatic stem cells after prolonged cultivation, raising questions about the specificity of this morphological feature for telocytes *in vitro*. This critique underscores the necessity for a more rigorous and multifaceted approach to telocyte identification, moving beyond mere morphological characterization. The reliance on long cytoplasmic processes as a definitive marker in culture could lead to misinterpretation, given that other cell types may exhibit similar features under certain conditions. Therefore, there must be an emphasis on the importance of identifying unique molecular markers that can reliably distinguish telocytes from other cell populations, especially in *in vitro* settings. Accurate identification and characterization of telocytes are essential for elucidating their roles in tissue homeostasis, repair, and pathogenesis.

Distribution and Functional Role of Telocytes in the Stomach

This thesis presented a comparative analysis of telocyte distribution and functional dynamics within the gastrointestinal tract, focusing on the distinctive localization and signaling roles of telocytes in the stomach. A noteworthy difference was observed in the spatial distribution of telocytes in the stomach versus the intestine. In the stomach, telocytes predominantly occupied the upper regions of the gland in normal homeostasis, notably absent from the gland base. This contrasts with the distribution in the intestine, where telocytes were dispersed throughout the small intestine, forming a subepithelial sheath that enveloped the entire epithelial lining. Further, an intriguing aspect of telocytes in the small intestine was their compartmentalized function in producing distinct signaling molecules (Shoshkes-Carmel et al., 2018). This specialization was evident in the crypts and villi, where telocytes exhibited differential secretion profiles, contributing to the unique microenvironmental dynamics of these regions.

Translating these observations to the gastric context, it becomes imperative to investigate whether a similar pattern of functional specialization exists among gastric telocytes. In the normal stomach, telocytes are primarily located in the isthmus, but during the development of metaplasia, a new population of telocytes emerges at the gland base. This shift in distribution raises the question of whether these distinct populations of gastric telocytes, those in the isthmus versus those newly emerging at the gland base, differ in their secretory profiles and signaling molecule production. Similar to the intestinal telocytes, gastric telocytes may exhibit compartmentalized signaling functions, with those in the isthmus expressing different molecules compared to those at the base.

The examination of differential signaling molecule production by telocytes in various regions of the gastric gland, particularly in the context of metaplasia, would provide insights into the role of these cells in gastric tissue dynamics. Such findings could elucidate the mechanisms by which telocytes contribute to the maintenance of gastric homeostasis and their involvement in the development of metaplasia. Understanding these aspects is crucial for deepening our understanding of telocyte biology and function in the stomach.

Telocyte Proliferation Dynamics During Metaplasia Development in the Stomach

This thesis illustrated the dynamic response of telocytes in the stomach during the onset of metaplasia, especially following mucosal damage. There is a growing body of evidence, both from this research and other studies across various tissues, supporting the role of telocytes in tissue recovery and regeneration as a response to injury (Cretoiu et al., 2016; Pomerleau et al., 2023; Wang et al., 2014; Wang et al., 2020). Notably, an increase in telocyte numbers has been consistently observed in the context of gastric injury and subsequent metaplastic development, aligning with their proposed regenerative function. However, an intriguing observation emerged

during the examination of telocyte proliferation using immunofluorescence staining for the proliferation marker, Ki67.

Despite the apparent increase in telocyte numbers post-injury, it was rare to find FOXL1+/PDGFRα+ double-positive telocytes that were also positive for Ki67. This finding was somewhat unexpected, considering the clear increase in telocyte count following gastric damage. The scarcity of proliferating telocytes was consistently noted even when examining successive time points with progressive treatment using DMP-777 and L635, which further complicated our understanding of telocyte proliferation during gastric injury and metaplasia.

To gain deeper insights into the proliferation of telocytes, I propose an experimental approach using BrdU labeling. BrdU, a thymidine analog, can be incorporated into the DNA of dividing cells during the S phase of the cell cycle, thereby serving as an effective marker for cell proliferation. A pulse and chase experiment could be performed with BrdU labeling during the phases of mucosal damage, to track the proliferation of telocytes more accurately. This approach can determine the temporal and spatial patterns of telocyte proliferation in response to gastric injury. The results from this experiment are expected to shed light on the kinetics of telocyte proliferation in response to gastric injury and contribute to a better understanding of their role in gastric tissue regeneration and metaplasia.

Telocyte Redistribution and Clearance Post-Recovery

In this thesis, I have demonstrated the dynamic response of telocytes to mucosal injury and their role in the development of gastric metaplasia. There was an expansion and extension of telocytes during the injury and metaplasia phase, followed by a reversion to their baseline levels upon mucosal recovery. This dynamic behavior raises intriguing questions about the fate and

behavior of telocytes after the recovery, and the investigation of telocyte clearance from the metaplastic cell niche and their redistribution during the recovery phase is needed.

One hypothesis is the potential migration of telocytes. It is possible that telocytes at the base of the gastric gland migrate back to the isthmus region post-recovery. This would imply a dynamic repositioning capability of telocytes in response to tissue homeostasis demands. Another aspect to consider is the possibility of telocyte apoptosis or other mechanisms of clearance from the basal region. Understanding the process by which telocytes are removed or redistributed following metaplasia resolution could provide insights into the regenerative and homeostatic mechanisms of the gastric mucosa.

To explore these hypotheses, I propose utilizing the Foxl1-CreERT2;R26R-tdTomato model. This model would be employed with the induction of metaplasia through acute drug treatment, DMP-777 or L635, followed by the administration of tamoxifen to label Foxl1-expressing telocytes. After the induction, the treatment would be ceased to allow for mucosal recovery. The subsequent tracing and analysis of the labeled telocytes in the recovered stomach would offer critical insights into their spatial and functional dynamics during the recovery process. This investigation will not only illuminate the fate of telocytes post-recovery but also contribute to our understanding of gastric tissue recovery mechanisms. Deciphering the processes underlying telocyte clearance and redistribution could add a significant dimension to our current understanding of gastric telocytes and their role in tissue homeostasis and regeneration.

Telocyte Depletion and Its Implications in Gastric Metaplasia

Previous research has established the crucial role of FOXL1+ telocytes in maintaining intestinal stem cell niches. Particularly, the ablation of FOXL1+ mesenchymal cells in the

intestine led to disrupted proliferation of intestinal stem cells, underscoring the importance of FOXL1+ telocytes in supporting intestinal stem cells (Aoki et al., 2016). In Foxl1–hDTR mice, where Foxl1+ telocytes were depleted using diphtheria toxin, a marked disruption in epithelial integrity and a cessation of stem cell proliferation were observed. This disruption was linked to a loss of active Wnt signaling, a pathway critical for stem cell maintenance and proliferation (Shoshkes-Carmel et al., 2018).

Moreover, Foxl1 expression has been shown to have functional significance beyond serving as a telocyte marker. Foxl1$^{-/-}$ mice displayed structural abnormalities in stomach epithelia, including elongated glands and increased proliferation, suggesting the potential development of metaplasia (Perreault et al., 2001). This implies a vital role for telocytes, and particularly Foxl1 expression, in maintaining gastric tissue homeostasis.

Considering these findings, conducting similar experiments using Foxl1-CreERT2;R26R-DTA mice would be insightful for studying telocyte functions in the stomach. I hypothesize that, parallel to the intestine, telocyte depletion in the stomach would disrupt progenitor cell proliferation. Furthermore, in the depletion model, where telocyte function is compromised, the inability of normal progenitor cells to proliferate could lead to the development of metaplasia, with a proliferative metaplastic cell population emerging and recruiting other stromal cells.

To further explore the role of telocytes in gastric metaplasia, future research should investigate the effects of telocyte depletion during the induction of metaplasia. Conducting such studies is crucial for understanding the role of telocytes in the formation of a metaplastic niche within the gastric mucosa. It will be particularly interesting to observe whether the depletion of telocytes leads to the development of a proliferative metaplastic niche or if other stromal cells

compensate for this loss, allowing metaplastic niche formation and supporting the growth of metaplastic cells.

In conclusion, this thesis has established a foundational understanding of telocyte involvement in metaplasia development in the stomach, paving the way for numerous research opportunities. Future studies should focus on the detailed characterization of telocytes in the gastric lamina propria, identifying specific markers that distinguish them from other stromal cells and investigating their interactions with epithelial cells during metaplasia progression. Additionally, investigating the effects of telocyte depletion and on the development of metaplasia will be crucial in understanding their functional role within the gastric microenvironment. The pursuit for a comprehensive understanding of gastric telocytes is expected to yield fundamental insights into gastric homeostasis and carcinogenesis, ultimately contributing to the advancement of gastric cancer research.

REFERENCES

Ajani, J. A., D'Amico, T. A., Bentrem, D. J., Chao, J., Cooke, D., Corvera, C., . . . Pluchino, L. A. (2022). Gastric Cancer, Version 2.2022, NCCN Clinical Practice Guidelines in Oncology. *J Natl Compr Canc Netw*, *20*(2), 167-192. https://doi.org/10.6004/jnccn.2022.0008

Albulescu, R., Tanase, C., Codrici, E., Popescu, D. I., Cretoiu, S. M., & Popescu, L. M. (2015). The secretome of myocardial telocytes modulates the activity of cardiac stem cells. *J Cell Mol Med*, *19*(8), 1783-1794. https://doi.org/10.1111/jcmm.12624

Annibale, B., Esposito, G., & Lahner, E. (2020). A current clinical overview of atrophic gastritis. *Expert Rev Gastroenterol Hepatol*, *14*(2), 93-102. https://doi.org/10.1080/17474124.2020.1718491

Aoki, R., Shoshkes-Carmel, M., Gao, N., Shin, S., May, C. L., Golson, M. L., . . . Kaestner, K. H. (2016). Foxl1-expressing mesenchymal cells constitute the intestinal stem cell niche. *Cell Mol Gastroenterol Hepatol*, *2*(2), 175-188. https://doi.org/10.1016/j.jcmgh.2015.12.004

Banan, B., Beckstead, J. A., Dunavant, L. E., Sohn, Y., Adcock, J. M., Nomura, S., . . . Fingleton, B. (2020). Development of a novel murine model of lymphatic metastasis. *Clin Exp Metastasis*, *37*(2), 247-255. https://doi.org/10.1007/s10585-020-10025-3

Bartel, D. P. (2004). MicroRNAs: genomics, biogenesis, mechanism, and function [Research Support, Non-U.S. Gov't Research Support, U.S. Gov't, P.H.S. Review]. *Cell*, *116*(2), 281-297. http://www.ncbi.nlm.nih.gov/pubmed/14744438

Bei, Y., Wang, F., Yang, C., & Xiao, J. (2015). Telocytes in regenerative medicine. *J Cell Mol Med*, *19*(7), 1441-1454. https://doi.org/10.1111/jcmm.12594

Benjamini, Y., & Hochberg, Y. (1995). Controlling the False Discovery Rate: A Practical and Powerful Approach to Multiple Testing. *Journal of the Royal Statistical Society, Series B (Statistical Methodology)*(57), 289–300. https://doi.org/https://doi.org/10.1111/j.2517-6161.1995.tb02031.x

Bernier-Latmani, J., Mauri, C., Marcone, R., Renevey, F., Durot, S., He, L., . . . Petrova, T. V. (2022). ADAMTS18(+) villus tip telocytes maintain a polarized VEGFA signaling domain and fenestrations in nutrient-absorbing intestinal blood vessels. *Nat Commun*, *13*(1), 3983. https://doi.org/10.1038/s41467-022-31571-2

Bertaux-Skeirik, N., Wunderlich, M., Teal, E., Chakrabarti, J., Biesiada, J., Mahe, M., . . . Zavros, Y. (2017). CD44 variant isoform 9 emerges in response to injury and contributes to the regeneration of the gastric epithelium. *J Pathol*, *242*(4), 463-475. https://doi.org/10.1002/path.4918

Biffi, G., & Tuveson, D. A. (2021). Diversity and Biology of Cancer-Associated Fibroblasts. *Physiol Rev*, *101*(1), 147-176. https://doi.org/10.1152/physrev.00048.2019

Blaser, M. J., & Parsonnet, J. (1994). Parasitism by the "slow" bacterium Helicobacter pylori leads to altered gastric homeostasis and neoplasia. *J Clin Invest*, *94*(1), 4-8. https://doi.org/10.1172/JCI117336

Bockerstett, K. A., Lewis, S. A., Noto, C. N., Ford, E. L., Saenz, J. B., Jackson, N. M., . . . DiPaolo, R. J. (2020). Single-Cell Transcriptional Analyses Identify Lineage-Specific Epithelial Responses to Inflammation and Metaplastic Development in the Gastric Corpus. *Gastroenterology*, *159*(6), 2116-2129 e2114. https://doi.org/10.1053/j.gastro.2020.08.027

Bredemeyer, A. J., Geahlen, J. H., Weis, V. G., Huh, W. J., Zinselmeyer, B. H., Srivatsan, S., . . .

Mills, J. C. (2009). The gastric epithelial progenitor cell niche and differentiation of the zymogenic (chief) cell lineage. *Dev Biol*, *325*(1), 211-224. https://doi.org/S0012-1606(08)01279-7 [pii]
10.1016/j.ydbio.2008.10.025
Burclaff, J., Osaki, L. H., Liu, D., Goldenring, J. R., & Mills, J. C. (2017). Targeted Apoptosis of Parietal Cells Is Insufficient to Induce Metaplasia in Stomach. *Gastroenterology*, *152*(4), 762-766 e767. https://doi.org/10.1053/j.gastro.2016.12.001
Busada, J. T., Ramamoorthy, S., Cain, D. W., Xu, X., Cook, D. N., & Cidlowski, J. A. (2019). Endogenous glucocorticoids prevent gastric metaplasia by suppressing spontaneous inflammation. *J Clin Invest*, *129*(3), 1345-1358. https://doi.org/10.1172/JCI123233
Busuttil, R. A., & Boussioutas, A. (2009). Intestinal metaplasia: a premalignant lesion involved in gastric carcinogenesis. *J Gastroenterol Hepatol*, *24*(2), 193-201. https://doi.org/10.1111/j.1440-1746.2008.05774.x
Caldwell, B., Meyer, A. R., Weis, J. A., Engevik, A. C., & Choi, E. (2022). Chief cell plasticity is the origin of metaplasia following acute injury in the stomach mucosa. *Gut*, *71*(6), 1068-1077. https://doi.org/10.1136/gutjnl-2021-325310
Calin, G. A., & Croce, C. M. (2006). MicroRNA signatures in human cancers. *Nat Rev Cancer*, *6*(11), 857-866. https://doi.org/10.1038/nrc1997
Cao, H., Liu, Z., Wang, R., Zhang, X., Yi, W., Nie, G., . . . Zhu, M. (2017). miR-148a suppresses human renal cell carcinoma malignancy by targeting AKT2. *Oncol Rep*, *37*(1), 147-154. https://doi.org/10.3892/or.2016.5257
Cho, Y. M., Kim, T. M., Hun Kim, D., Hee Kim, D., Jeong, S. W., & Kwon, O. J. (2016). miR-148a is a downstream effector of X-box-binding protein 1 that silences Wnt10b during adipogenesis of 3T3-L1 cells. *Exp Mol Med*, *48*, e226. https://doi.org/10.1038/emm.2016.3
Choi, E., Hendley, A. M., Bailey, J. M., Leach, S. D., & Goldenring, J. R. (2016). Expression of Activated Ras in Gastric Chief Cells of Mice Leads to the Full Spectrum of Metaplastic Lineage Transitions. *Gastroenterology*, *150*(4), 918-930 e913. https://doi.org/10.1053/j.gastro.2015.11.049
Choi, E., Means, A. L., Coffey, R. J., & Goldenring, J. R. (2019). Active Kras Expression in Gastric Isthmal Progenitor Cells Induces Foveolar Hyperplasia but Not Metaplasia. *Cell Mol Gastroenterol Hepatol*, *7*(1), 251-253 e251. https://doi.org/10.1016/j.jcmgh.2018.09.007
Correa, P., & Piazuelo, M. B. (2012). The gastric precancerous cascade. *J Dig Dis*, *13*(1), 2-9. https://doi.org/10.1111/j.1751-2980.2011.00550.x
Correa, P., Piazuelo, M. B., & Wilson, K. T. (2010). Pathology of gastric intestinal metaplasia: clinical implications. *Am J Gastroenterol*, *105*(3), 493-498. https://doi.org/10.1038/ajg.2009.728
Cretoiu, D., Xu, J., Xiao, J., & Cretoiu, S. M. (2016). Telocytes and Their Extracellular Vesicles-Evidence and Hypotheses. *Int J Mol Sci*, *17*(8), 1322. https://doi.org/10.3390/ijms17081322
Diesenberg, K., Beerbaum, M., Fink, U., Schmieder, P., & Krauss, M. (2015). SEPT9 negatively regulates ubiquitin-dependent downregulation of EGFR. *J Cell Sci*, *128*(2), 397-407. https://doi.org/10.1242/jcs.162206
Eda, A., Osawa, H., Yanaka, I., Satoh, K., Mutoh, H., Kihira, K., & Sugano, K. (2002). Expression of homeobox gene CDX2 precedes that of CDX1 during the progression of

intestinal metaplasia. *J Gastroenterol*, *37*(2), 94-100. https://doi.org/10.1007/s005350200002
Esquela-Kerscher, A., & Slack, F. J. (2006). Oncomirs - microRNAs with a role in cancer [Research Support, N.I.H., Extramural Research Support, U.S. Gov't, Non-P.H.S. Review]. *Nat Rev Cancer*, *6*(4), 259-269. https://doi.org/10.1038/nrc1840
Eulalio, A., Huntzinger, E., & Izaurralde, E. (2008). Getting to the root of miRNA-mediated gene silencing. *Cell*, *132*(1), 9-14. https://doi.org/10.1016/j.cell.2007.12.024
Fischer, A. S., Mullerke, S., Arnold, A., Heuberger, J., Berger, H., Lin, M., . . . Sigal, M. (2022). R-spondin/YAP axis promotes gastric oxyntic gland regeneration and Helicobacter pylori-associated metaplasia in mice. *J Clin Invest*, *132*(21). https://doi.org/10.1172/JCI151363
Fox, J. G., Li, X., Cahill, R. J., Andrutis, K., Rustgi, A. K., Odze, R., & Wang, T. C. (1996). Hypertrophic gastropathy in Helicobacter felis-infected wild-type C57BL/6 mice and p53 hemizygous transgenic mice. *Gastroenterology*, *110*(1), 155-166. https://doi.org/10.1053/gast.1996.v110.pm8536852
Fox, J. G., Wang, T. C., Rogers, A. B., Poutahidis, T., Ge, Z., Taylor, N., . . . Peek, R. M., Jr. (2003). Host and microbial constituents influence Helicobacter pylori-induced cancer in a murine model of hypergastrinemia. *Gastroenterology*, *124*(7), 1879-1890. https://doi.org/10.1016/s0016-5085(03)00406-2
Gailhouste, L., Gomez-Santos, L., Hagiwara, K., Hatada, I., Kitagawa, N., Kawaharada, K., . . . Ochiya, T. (2013). miR-148a plays a pivotal role in the liver by promoting the hepatospecific phenotype and suppressing the invasiveness of transformed cells. *Hepatology*, *58*(3), 1153-1165. https://doi.org/10.1002/hep.26422
Go, S. I., Ko, G. H., Lee, W. S., Kim, R. B., Lee, J. H., Jeong, S. H., . . . Ha, W. S. (2016). CD44 Variant 9 Serves as a Poor Prognostic Marker in Early Gastric Cancer, But Not in Advanced Gastric Cancer. *Cancer Res Treat*, *48*(1), 142-152. https://doi.org/10.4143/crt.2014.227
Goldenring, J. R. (2018). Pyloric metaplasia, pseudopyloric metaplasia, ulcer-associated cell lineage and spasmolytic polypeptide-expressing metaplasia: reparative lineages in the gastrointestinal mucosa. *J Pathol*, *245*(2), 132-137. https://doi.org/10.1002/path.5066
Goldenring, J. R. (2023). Spasmolytic polypeptide-expressing metaplasia (SPEM) cell lineages can be an origin of gastric cancer. *J Pathol*, *260*(2), 109-111. https://doi.org/10.1002/path.6089
Goldenring, J. R., & Mills, J. C. (2022). Cellular Plasticity, Reprogramming, and Regeneration: Metaplasia in the Stomach and Beyond. *Gastroenterology*, *162*(2), 415-430. https://doi.org/10.1053/j.gastro.2021.10.036
Goldenring, J. R., Nam, K. T., & Mills, J. C. (2011). The origin of pre-neoplastic metaplasia in the stomach: chief cells emerge from the Mist. *Exp Cell Res*, *317*(19), 2759-2764. https://doi.org/10.1016/j.yexcr.2011.08.017
Goldenring, J. R., Nam, K. T., Wang, T. C., Mills, J. C., & Wright, N. A. (2010). Spasmolytic polypeptide-expressing metaplasia and intestinal metaplasia: time for reevaluation of metaplasias and the origins of gastric cancer. *Gastroenterology*, *138*(7), 2207-2210, 2210 e2201. https://doi.org/10.1053/j.gastro.2010.04.023
Gonzalez, C. A., Sanz-Anquela, J. M., Gisbert, J. P., & Correa, P. (2013). Utility of subtyping intestinal metaplasia as marker of gastric cancer risk. A review of the evidence. *Int J Cancer*, *133*(5), 1023-1032. https://doi.org/10.1002/ijc.28003

Gu, S., & Kay, M. A. (2010). How do miRNAs mediate translational repression? *Silence*, *1*(1), 11. https://doi.org/10.1186/1758-907X-1-11
Ha, M., & Kim, V. N. (2014). Regulation of microRNA biogenesis. *Nat Rev Mol Cell Biol*, *15*(8), 509-524. https://doi.org/10.1038/nrm3838
Halldorsdottir, A. M., Sigurdardottrir, M., Jonasson, J. G., Oddsdottir, M., Magnusson, J., Lee, J. R., & Goldenring, J. R. (2003). Spasmolytic polypeptide-expressing metaplasia (SPEM) associated with gastric cancer in Iceland. *Dig Dis Sci*, *48*(3), 431-441. http://www.ncbi.nlm.nih.gov/pubmed/12757153
Hata, M., Kinoshita, H., Hayakawa, Y., Konishi, M., Tsuboi, M., Oya, Y., . . . Koike, K. (2020). GPR30-Expressing Gastric Chief Cells Do Not Dedifferentiate But Are Eliminated via PDK-Dependent Cell Competition During Development of Metaplasia. *Gastroenterology*, *158*(6), 1650-1666 e1615. https://doi.org/10.1053/j.gastro.2020.01.046
Hatta, K., Huang, M. L., Weisel, R. D., & Li, R. K. (2012). Culture of rat endometrial telocytes. *J Cell Mol Med*, *16*(7), 1392-1396. https://doi.org/10.1111/j.1582-4934.2012.01583.x
Hayakawa, Y., Ariyama, H., Stancikova, J., Sakitani, K., Asfaha, S., Renz, B. W., . . . Wang, T. C. (2015). Mist1 Expressing Gastric Stem Cells Maintain the Normal and Neoplastic Gastric Epithelium and Are Supported by a Perivascular Stem Cell Niche. *Cancer Cell*, *28*(6), 800-814. https://doi.org/10.1016/j.ccell.2015.10.003
Ishimoto, T., Nagano, O., Yae, T., Tamada, M., Motohara, T., Oshima, H., . . . Saya, H. (2011). CD44 variant regulates redox status in cancer cells by stabilizing the xCT subunit of system xc(-) and thereby promotes tumor growth. *Cancer Cell*, *19*(3), 387-400. https://doi.org/10.1016/j.ccr.2011.01.038
Jiang, Q., He, M., Ma, M. T., Wu, H. Z., Yu, Z. J., Guan, S., . . . Wei, M. J. (2016). MicroRNA-148a inhibits breast cancer migration and invasion by directly targeting WNT-1. *Oncol Rep*, *35*(3), 1425-1432. https://doi.org/10.3892/or.2015.4502
Karam, S. M., & Leblond, C. P. (1993). Dynamics of epithelial cells in the corpus of the mouse stomach. III. Inward migration of neck cells followed by progressive transformation into zymogenic cells. *Anat.Rec.*, *236*, 297-313.
Kesisova, I. A., Robinson, B. P., & Spiliotis, E. T. (2021). A septin GTPase scaffold of dynein-dynactin motors triggers retrograde lysosome transport. *J Cell Biol*, *220*(2). https://doi.org/10.1083/jcb.202005219
Kinami, S., Saito, H., & Takamura, H. (2021). Significance of Lymph Node Metastasis in the Treatment of Gastric Cancer and Current Challenges in Determining the Extent of Metastasis. *Front Oncol*, *11*, 806162. https://doi.org/10.3389/fonc.2021.806162
Kinchen, J., Chen, H. H., Parikh, K., Antanaviciute, A., Jagielowicz, M., Fawkner-Corbett, D., . . . Simmons, A. (2018). Structural Remodeling of the Human Colonic Mesenchyme in Inflammatory Bowel Disease. *Cell*, *175*(2), 372-386 e317. https://doi.org/10.1016/j.cell.2018.08.067
Kinoshita, H., Hayakawa, Y., Niu, Z., Konishi, M., Hata, M., Tsuboi, M., . . . Koike, K. (2018). Mature gastric chief cells are not required for the development of metaplasia. *Am J Physiol Gastrointest Liver Physiol*, *314*(5), G583-G596. https://doi.org/10.1152/ajpgi.00351.2017
Klein, M., Csobonyeiova, M., Danisovic, L., Lapides, L., & Varga, I. (2022). Telocytes in the Female Reproductive System: Up-to-Date Knowledge, Challenges and Possible Clinical Applications. *Life (Basel)*, *12*(2). https://doi.org/10.3390/life12020267
Klein, M., Csobonyeiova, M., Ziaran, S., Danisovic, L., & Varga, I. (2021). Cardiac Telocytes 16

Years on-What Have We Learned So Far, and How Close Are We to Routine Application of the Knowledge in Cardiovascular Regenerative Medicine? *Int J Mol Sci*, *22*(20). https://doi.org/10.3390/ijms222010942

Lau, W. M., Teng, E., Chong, H. S., Lopez, K. A., Tay, A. Y., Salto-Tellez, M., . . . Chan, S. L. (2014). CD44v8-10 is a cancer-specific marker for gastric cancer stem cells. *Cancer Res*, *74*(9), 2630-2641. https://doi.org/10.1158/0008-5472.CAN-13-2309

Lee, H. J., Nam, K. T., Park, H. S., Kim, M. A., Lafleur, B. J., Aburatani, H., . . . Goldenring, J. R. (2010). Gene expression profiling of metaplastic lineages identifies CDH17 as a prognostic marker in early stage gastric cancer. *Gastroenterology*, *139*(1), 213-225 e213. https://doi.org/10.1053/j.gastro.2010.04.008

Lee, S. H., Contreras Panta, E. W., Gibbs, D., Won, Y., Min, J., Zhang, C., . . . Goldenring, J. R. (2023). Apposition of Fibroblasts With Metaplastic Gastric Cells Promotes Dysplastic Transition. *Gastroenterology*, *165*(2), 374-390. https://doi.org/10.1053/j.gastro.2023.04.038

Lee, S. H., Jang, B., Min, J., Contreras-Panta, E. W., Presentation, K. S., Delgado, A. G., . . . Goldenring, J. R. (2022). Up-regulation of Aquaporin 5 Defines Spasmolytic Polypeptide-Expressing Metaplasia and Progression to Incomplete Intestinal Metaplasia. *Cell Mol Gastroenterol Hepatol*, *13*(1), 199-217. https://doi.org/10.1016/j.jcmgh.2021.08.017

Lee, S. R., Kim, H. O., Son, B. H., Shin, J. H., & Yoo, C. H. (2012). Prognostic significance of the metastatic lymph node ratio in patients with gastric cancer. *World J Surg*, *36*(5), 1096-1101. https://doi.org/10.1007/s00268-012-1520-5

Lennerz, J. K., Kim, S. H., Oates, E. L., Huh, W. J., Doherty, J. M., Tian, X., . . . Mills, J. C. (2010). The transcription factor MIST1 is a novel human gastric chief cell marker whose expression is lost in metaplasia, dysplasia, and carcinoma. *Am J Pathol*, *177*(3), 1514-1533. https://doi.org/10.2353/ajpath.2010.100328

Lennerz, J. K. M., Kim, S., Oates, E. L., Huh, W. J., Dherty, J. M., Tian, X., . . . Mills, J. C. (2010). The transcription factor MIST1 is a novel human gastric chief cell marker whose expression is lost in metaplasia, dysplasia and carcinoma. *Amer. J. Pathol.*, *177*, 1514-1533.

Leushacke, M., Tan, S. H., Wong, A., Swathi, Y., Hajamohideen, A., Tan, L. T., . . . Barker, N. (2017). Lgr5-expressing chief cells drive epithelial regeneration and cancer in the oxyntic stomach. *Nat Cell Biol*, *19*(7), 774-786. https://doi.org/10.1038/ncb3541

Li, B., Wang, W., Li, Z., Chen, Z., Zhi, X., Xu, J., . . . Xu, Z. (2017). MicroRNA-148a-3p enhances cisplatin cytotoxicity in gastric cancer through mitochondrial fission induction and cyto-protective autophagy suppression. *Cancer Lett*, *410*, 212-227. https://doi.org/10.1016/j.canlet.2017.09.035

Liu, L., Ye, J. X., Qin, Y. Z., Chen, Q. H., & Ge, L. Y. (2015). Evaluation of miR-29c, miR-124, miR-135a and miR-148a in predicting lymph node metastasis and tumor stage of gastric cancer. *Int J Clin Exp Med*, *8*(12), 22227-22236. https://www.ncbi.nlm.nih.gov/pubmed/26885198

Long, X. R., He, Y., Huang, C., & Li, J. (2014). MicroRNA-148a is silenced by hypermethylation and interacts with DNA methyltransferase 1 in hepatocellular carcinogenesis. *Int J Oncol*, *44*(6), 1915-1922. https://doi.org/10.3892/ijo.2014.2373

Maekita, T., Nakazawa, K., Mihara, M., Nakajima, T., Yanaoka, K., Iguchi, M., . . . Ushijima, T. (2006). High levels of aberrant DNA methylation in Helicobacter pylori-infected gastric

mucosae and its possible association with gastric cancer risk. *Clin Cancer Res*, *12*(3 Pt 1), 989-995. https://doi.org/10.1158/1078-0432.CCR-05-2096

Marshall, B. J., Armstrong, J. A., McGechie, D. B., & Glancy, R. J. (1985). Attempt to fulfil Koch's postulates for pyloric Campylobacter. *Med J Aust*, *142*(8), 436-439. https://doi.org/10.5694/j.1326-5377.1985.tb113443.x

Marshall, B. J., & Warren, J. R. (1984). Unidentified curved bacilli in the stomach of patients with gastritis and peptic ulceration. *Lancet*, *1*(8390), 1311-1315. https://doi.org/10.1016/s0140-6736(84)91816-6

Matsushima, K., Isomoto, H., Inoue, N., Nakayama, T., Hayashi, T., Nakayama, M., . . . Kohno, S. (2011). MicroRNA signatures in Helicobacter pylori-infected gastric mucosa. *Int J Cancer*, *128*(2), 361-370. https://doi.org/10.1002/ijc.25348

McCarthy, N., Manieri, E., Storm, E. E., Saadatpour, A., Luoma, A. M., Kapoor, V. N., . . . Shivdasani, R. A. (2020). Distinct Mesenchymal Cell Populations Generate the Essential Intestinal BMP Signaling Gradient. *Cell Stem Cell*, *26*(3), 391-402 e395. https://doi.org/10.1016/j.stem.2020.01.008

Melissari, M. T., Henriques, A., Tzaferis, C., Prados, A., Sarris, M. E., Chalkidi, N., . . . Koliaraki, V. (2021). Col6a1(+)/CD201(+) mesenchymal cells regulate intestinal morphogenesis and homeostasis. *Cell Mol Life Sci*, *79*(1), 1. https://doi.org/10.1007/s00018-021-04071-7

Meyer, A. R., Engevik, A. C., Madorsky, T., Belmont, E., Stier, M. T., Norlander, A. E., . . . Goldenring, J. R. (2020). Group 2 Innate Lymphoid Cells Coordinate Damage Response in the Stomach. *Gastroenterology*, *159*(6), 2077-2091 e2078. https://doi.org/10.1053/j.gastro.2020.08.051

Meyer, A. R., Engevik, A. C., Willet, S. G., Williams, J. A., Zou, Y., Massion, P. P., . . . Goldenring, J. R. (2019). Cystine/Glutamate Antiporter (xCT) Is Required for Chief Cell Plasticity After Gastric Injury. *Cell Mol Gastroenterol Hepatol*, *8*(3), 379-405. https://doi.org/10.1016/j.jcmgh.2019.04.015

Meyer, A. R., & Goldenring, J. R. (2018). Injury, repair, inflammation and metaplasia in the stomach. *J Physiol*, *596*(17), 3861-3867. https://doi.org/10.1113/JP275512

Mills, J. C., & Sansom, O. J. (2015). Reserve stem cells: Differentiated cells reprogram to fuel repair, metaplasia, and neoplasia in the adult gastrointestinal tract. *Sci Signal*, *8*(385), re8. https://doi.org/10.1126/scisignal.aaa7540

Motoyama, K., Inoue, H., Nakamura, Y., Uetake, H., Sugihara, K., & Mori, M. (2008). Clinical significance of high mobility group A2 in human gastric cancer and its relationship to let-7 microRNA family. *Clin Cancer Res*, *14*(8), 2334-2340. https://doi.org/10.1158/1078-0432.CCR-07-4667

Naeli, P., Winter, T., Hackett, A. P., Alboushi, L., & Jafarnejad, S. M. (2023). The intricate balance between microRNA-induced mRNA decay and translational repression. *FEBS J*, *290*(10), 2508-2524. https://doi.org/10.1111/febs.16422

Nakajima, T., Yamashita, S., Maekita, T., Niwa, T., Nakazawa, K., & Ushijima, T. (2009). The presence of a methylation fingerprint of Helicobacter pylori infection in human gastric mucosae. *Int J Cancer*, *124*(4), 905-910. https://doi.org/10.1002/ijc.24018

Nam, K. T., Lee, H. J., Mok, H., Romero-Gallo, J., Crowe, J. E., Jr., Peek, R. M., Jr., & Goldenring, J. R. (2009). Amphiregulin-deficient mice develop spasmolytic polypeptide expressing metaplasia and intestinal metaplasia. *Gastroenterology*, *136*(4), 1288-1296. https://doi.org/10.1053/j.gastro.2008.12.037

Nam, K. T., Lee, H. J., Sousa, J. F., Weis, V. G., O'Neal, R. L., Finke, P. E., . . . Goldenring, J. R. (2010). Mature chief cells are cryptic progenitors for metaplasia in the stomach. *Gastroenterology*, *139*(6), 2028-2037 e2029. https://doi.org/10.1053/j.gastro.2010.09.005

National Cancer Institute. (2023). Retrieved April 2023 from Surveillance, Epidemiology, and End Results (SEER) Program. Cancer Stat Facts: Stomach Cancer. 2021. Accessed July 9, 2021. Available at: https://seer.cancer.gov/statfacts/html/stomach.html

Niwa, T., Tsukamoto, T., Toyoda, T., Mori, A., Tanaka, H., Maekita, T., . . . Ushijima, T. (2010). Inflammatory processes triggered by Helicobacter pylori infection cause aberrant DNA methylation in gastric epithelial cells. *Cancer Res*, *70*(4), 1430-1440. https://doi.org/10.1158/0008-5472.CAN-09-2755

Nomura, S., Yamaguchi, H., Ogawa, M., Wang, T. C., Lee, J. R., & Goldenring, J. R. (2005). Alterations in gastric mucosal lineages induced by acute oxyntic atrophy in wild-type and gastrin-deficient mice. *Am J Physiol Gastrointest Liver Physiol*, *288*(2), G362-375. https://doi.org/10.1152/ajpgi.00160.2004

Nozaki, K., Ogawa, M., Williams, J. A., LaFleur, B. J., Ng, V., Drapkin, R. I., . . . Goldenring, J. R. (2008). A molecular signature of gastric metaplasia arising in response to acute parietal cell loss. *Gastroenterology.*(134), 511-521.

Peng, L., Liu, Z., Xiao, J., Tu, Y., Wan, Z., Xiong, H., . . . Xiao, W. (2017). MicroRNA-148a suppresses epithelial-mesenchymal transition and invasion of pancreatic cancer cells by targeting Wnt10b and inhibiting the Wnt/beta-catenin signaling pathway. *Oncol Rep*, *38*(1), 301-308. https://doi.org/10.3892/or.2017.5705

Perdigoto, C. N., Valdes, V. J., Bardot, E. S., & Ezhkova, E. (2014). Epigenetic regulation of epidermal differentiation. *Cold Spring Harb Perspect Med*, *4*(2). https://doi.org/10.1101/cshperspect.a015263

Perreault, N., Katz, J. P., Sackett, S. D., & Kaestner, K. H. (2001). Foxl1 controls the Wnt/beta-catenin pathway by modulating the expression of proteoglycans in the gut. *J Biol Chem*, *276*(46), 43328-43333. https://doi.org/10.1074/jbc.M104366200

Petersen, C. P., Meyer, A. R., De Salvo, C., Choi, E., Schlegel, C., Petersen, A., . . . Goldenring, J. R. (2018). A signalling cascade of IL-33 to IL-13 regulates metaplasia in the mouse stomach. *Gut*, *67*(5), 805-817. https://doi.org/10.1136/gutjnl-2016-312779

Petersen, C. P., Mills, J. C., & Goldenring, J. R. (2017). Murine Models of Gastric Corpus Preneoplasia. *Cell Mol Gastroenterol Hepatol*, *3*(1), 11-26. https://doi.org/10.1016/j.jcmgh.2016.11.001

Petersen, C. P., Weis, V. G., Nam, K. T., Sousa, J. F., Fingleton, B., & Goldenring, J. R. (2014). Macrophages promote progression of spasmolytic polypeptide-expressing metaplasia after acute loss of parietal cells. *Gastroenterology*, *146*(7), 1727-1738 e1728. https://doi.org/10.1053/j.gastro.2014.02.007

Pomerleau, V., Nicolas, V. R., Jurkovic, C. M., Faucheux, N., Lauzon, M. A., Boisvert, F. M., & Perreault, N. (2023). FOXL1+ Telocytes in mouse colon orchestrate extracellular matrix biodynamics and wound repair resolution. *J Proteomics*, *271*, 104755. https://doi.org/10.1016/j.jprot.2022.104755

Popescu, L. M., & Faussone-Pellegrini, M. S. (2010). TELOCYTES - a case of serendipity: the winding way from Interstitial Cells of Cajal (ICC), via Interstitial Cajal-Like Cells (ICLC) to TELOCYTES. *J Cell Mol Med*, *14*(4), 729-740. https://doi.org/10.1111/j.1582-4934.2010.01059.x

Qiu, X., Zhu, H., Liu, S., Tao, G., Jin, J., Chu, H., . . . Zhang, Z. (2017). Expression and

prognostic value of microRNA-26a and microRNA-148a in gastric cancer. *J Gastroenterol Hepatol*, *32*(4), 819-827. https://doi.org/10.1111/jgh.13533

Ramsey, V. G., Doherty, J. M., Chen, C. C., Stappenbeck, T. S., Konieczny, S. F., & Mills, J. C. (2007). The maturation of mucus-secreting gastric epithelial progenitors into digestive-enzyme secreting zymogenic cells requires Mist1. *Development*, *134*(1), 211-222. http://www.ncbi.nlm.nih.gov/entrez/query.fcgi?cmd=Retrieve&db=PubMed&dopt=Citation&list_uids=17164426

Ricci, E. P., Limousin, T., Soto-Rifo, R., Rubilar, P. S., Decimo, D., & Ohlmann, T. (2013). miRNA repression of translation in vitro takes place during 43S ribosomal scanning. *Nucleic Acids Res*, *41*(1), 586-598. https://doi.org/10.1093/nar/gks1076

Riera, K. M., Jang, B., Min, J., Roland, J. T., Yang, Q., Fesmire, W. T., . . . Goldenring, J. R. (2020). Trop2 is upregulated in the transition to dysplasia in the metaplastic gastric mucosa. *J Pathol*, *251*(3), 336-347. https://doi.org/10.1002/path.5469

Rosa, I., Marini, M., & Manetti, M. (2021). Telocytes: An Emerging Component of Stem Cell Niche Microenvironment. *J Histochem Cytochem*, *69*(12), 795-818. https://doi.org/10.1369/00221554211025489

Roth, K. A., Kapadia, S. B., Martin, S. M., & Lorenz, R. G. (1999). Cellular immune responses are essential for the development of Helicobacter felis-associated gastric pathology. *J Immunol*, *163*(3), 1490-1497. https://www.ncbi.nlm.nih.gov/pubmed/10415051

Sakamoto, N., Naito, Y., Oue, N., Sentani, K., Uraoka, N., Zarni Oo, H., . . . Yasui, W. (2014). MicroRNA-148a is downregulated in gastric cancer, targets MMP7, and indicates tumor invasiveness and poor prognosis. *Cancer Sci*, *105*(2), 236-243. https://doi.org/10.1111/cas.12330

Sanches, B. D. A., Maldarine, J. S., Zani, B. C., Tamarindo, G. H., Biancardi, M. F., Santos, F. C. A., . . . Taboga, S. R. (2017). Telocytes play a key role in prostate tissue organisation during the gland morphogenesis. *J Cell Mol Med*, *21*(12), 3309-3321. https://doi.org/10.1111/jcmm.13234

Schmidt, P. H., Lee, J. R., Joshi, V., Playford, R. J., Poulsom, R., Wright, N. A., & Goldenring, J. R. (1999). Identification of a metaplastic cell lineage associated with human gastric adenocarcinoma. *Lab Invest*, *79*(6), 639-646. https://www.ncbi.nlm.nih.gov/pubmed/10378506

Sepulveda, A. R., & Patil, M. (2008). Practical approach to the pathologic diagnosis of gastritis. *Arch Pathol Lab Med*, *132*(10), 1586-1593. https://doi.org/10.5858/2008-132-1586-PATTPD

Shao, L., Li, P., Ye, J., Chen, J., Han, Y., Cai, J., & Lu, X. (2018). Risk of gastric cancer among patients with gastric intestinal metaplasia. *Int J Cancer*, *143*(7), 1671-1677. https://doi.org/10.1002/ijc.31571

Sharma, P., & Montgomery, E. (2013). Gastrointestinal dysplasia. *Pathology*, *45*(3), 273-285. https://doi.org/10.1097/PAT.0b013e32835f21d7

Shimizu, T., Sohn, Y., Choi, E., Petersen, C. P., Prasad, N., & Goldenring, J. R. (2020). Decrease in MiR-148a Expression During Initiation of Chief Cell Transdifferentiation. *Cell Mol Gastroenterol Hepatol*, *9*(1), 61-78. https://doi.org/10.1016/j.jcmgh.2019.08.008

Shoshkes-Carmel, M., Wang, Y. J., Wangensteen, K. J., Toth, B., Kondo, A., Massasa, E. E., . . . Kaestner, K. H. (2018). Subepithelial telocytes are an important source of Wnts that supports intestinal crypts. *Nature*, *557*(7704), 242-246. https://doi.org/10.1038/s41586-018-0084-4

Sigal, M., Logan, C. Y., Kapalczynska, M., Mollenkopf, H. J., Berger, H., Wiedenmann, B., . . . Meyer, T. F. (2017). Stromal R-spondin orchestrates gastric epithelial stem cells and gland homeostasis. *Nature*, *548*(7668), 451-455. https://doi.org/10.1038/nature23642

Slaby, O., Srovnal, J., Radova, L., Gregar, J., Juracek, J., Luzna, P., . . . Ehrmann, J. (2015). Dynamic changes in microRNA expression profiles reflect progression of Barrett's esophagus to esophageal adenocarcinoma. *Carcinogenesis*, *36*(5), 521-527. https://doi.org/10.1093/carcin/bgv023

Song, D., Xu, M., Qi, R., Ma, R., Zhou, Y., Wu, D., . . . Wang, X. (2019). Influence of gene modification in biological behaviors and responses of mouse lung telocytes to inflammation. *J Transl Med*, *17*(1), 158. https://doi.org/10.1186/s12967-019-1870-y

Sousa, J. F., Nam, K. T., Petersen, C. P., Lee, H. J., Yang, H. K., Kim, W. H., & Goldenring, J. R. (2016). miR-30-HNF4gamma and miR-194-NR2F2 regulatory networks contribute to the upregulation of metaplasia markers in the stomach. *Gut*, *65*(6), 914-924. https://doi.org/10.1136/gutjnl-2014-308759

Sun, J., Zheng, M. Y., Li, Y. W., & Zhang, S. W. (2020). Structure and function of Septin 9 and its role in human malignant tumors. *World J Gastrointest Oncol*, *12*(6), 619-631. https://doi.org/10.4251/wjgo.v12.i6.619

Sung, H., Ferlay, J., Siegel, R. L., Laversanne, M., Soerjomataram, I., Jemal, A., & Bray, F. (2021). Global Cancer Statistics 2020: GLOBOCAN Estimates of Incidence and Mortality Worldwide for 36 Cancers in 185 Countries. *CA Cancer J Clin*, *71*(3), 209-249. https://doi.org/10.3322/caac.21660

Tang, H., Deng, M., Tang, Y., Xie, X., Guo, J., Kong, Y., . . . Xie, X. (2013). miR-200b and miR-200c as prognostic factors and mediators of gastric cancer cell progression. *Clin Cancer Res*, *19*(20), 5602-5612. https://doi.org/10.1158/1078-0432.CCR-13-1326

Tseng, C. W., Lin, C. C., Chen, C. N., Huang, H. C., & Juan, H. F. (2011). Integrative network analysis reveals active microRNAs and their functions in gastric cancer. *BMC Syst Biol*, *5*, 99. https://doi.org/10.1186/1752-0509-5-99

Tsukamoto, Y., Nakada, C., Noguchi, T., Tanigawa, M., Nguyen, L. T., Uchida, T., . . . Moriyama, M. (2010). MicroRNA-375 is downregulated in gastric carcinomas and regulates cell survival by targeting PDK1 and 14-3-3zeta. *Cancer Res*, *70*(6), 2339-2349. https://doi.org/10.1158/0008-5472.CAN-09-2777

Ueda, T., Volinia, S., Okumura, H., Shimizu, M., Taccioli, C., Rossi, S., . . . Croce, C. M. (2010). Relation between microRNA expression and progression and prognosis of gastric cancer: a microRNA expression analysis. *Lancet Oncol*, *11*(2), 136-146. https://doi.org/10.1016/S1470-2045(09)70343-2

Vannucchi, M. G., Traini, C., Manetti, M., Ibba-Manneschi, L., & Faussone-Pellegrini, M. S. (2013). Telocytes express PDGFRalpha in the human gastrointestinal tract. *J Cell Mol Med*, *17*(9), 1099-1108. https://doi.org/10.1111/jcmm.12134

Varga, I., Polak, S., Kyselovic, J., Kachlik, D., Danisovic, L., & Klein, M. (2019). Recently Discovered Interstitial Cell Population of Telocytes: Distinguishing Facts from Fiction Regarding Their Role in the Pathogenesis of Diverse Diseases Called "Telocytopathies". *Medicina (Kaunas)*, *55*(2). https://doi.org/10.3390/medicina55020056

Wada, T., Ishimoto, T., Seishima, R., Tsuchihashi, K., Yoshikawa, M., Oshima, H., . . . Nagano, O. (2013). Functional role of CD44v-xCT system in the development of spasmolytic polypeptide-expressing metaplasia. *Cancer Sci*, *104*(10), 1323-1329. https://doi.org/10.1111/cas.12236

Wang, F., Song, Y., Bei, Y., Zhao, Y., Xiao, J., & Yang, C. (2014). Telocytes in liver regeneration: possible roles. *J Cell Mol Med*, *18*(9), 1720-1726. https://doi.org/10.1111/jcmm.12355
Wang, L., Song, D., Wei, C., Chen, C., Yang, Y., Deng, X., & Gu, J. (2020). Telocytes inhibited inflammatory factor expression and enhanced cell migration in LPS-induced skin wound healing models in vitro and in vivo. *J Transl Med*, *18*(1), 60. https://doi.org/10.1186/s12967-020-02217-y
Wang, T. C., Goldenring, J. R., Dangler, C., Ito, S., Mueller, A., Jeon, W. K., . . . Fox, J. G. (1998). Mice lacking secretory phospholipase A2 show altered apoptosis and differentiation with Helicobacter felis infection. *Gastroenterology*, *114*(4), 675-689. https://doi.org/10.1016/s0016-5085(98)70581-5
Weis, V. G., Petersen, C. P., Mills, J. C., Tuma, P. L., Whitehead, R. H., & Goldenring, J. R. (2014). Establishment of novel in vitro mouse chief cell and SPEM cultures identifies MAL2 as a marker of metaplasia in the stomach. *Amer. J. Physiol.: GI & Liver Physiol.*, *307*(8), G777-792.
Weis, V. G., Petersen, C. P., Weis, J. A., Meyer, A. R., Choi, E., Mills, J. C., & Goldenring, J. R. (2016). Maturity and age influence chief cell ability to transdifferentiate into metaplasia. *Am J Physiol Gastrointest Liver Physiol*, *312*, G67-G76. https://doi.org/10.1152/ajpgi.00326.2016
Weis, V. G., Sousa, J. F., LaFleur, B. J., Nam, K. T., Weis, J. A., Finke, P. E., . . . Goldenring, J. R. (2013). Heterogeneity in mouse spasmolytic polypeptide-expressing metaplasia lineages identifies markers of metaplastic progression. *Gut*, *62*(9), 1270-1279. https://doi.org/10.1136/gutjnl-2012-302401
Willet, S. G., Lewis, M. A., Miao, Z. F., Liu, D., Radyk, M. D., Cunningham, R. L., . . . Mills, J. C. (2018). Regenerative proliferation of differentiated cells by mTORC1-dependent paligenosis. *EMBO J*, *37*(7). https://doi.org/10.15252/embj.201798311
Wu, T., Qu, L., He, G., Tian, L., Li, L., Zhou, H., . . . Sun, Y. (2016). Regulation of laryngeal squamous cell cancer progression by the lncRNA H19/miR-148a-3p/DNMT1 axis. *Oncotarget*, *7*(10), 11553-11566. https://doi.org/10.18632/oncotarget.7270
Yamaguchi, H., Goldenring, J. R., Kaminishi, M., & Lee, J. R. (2002). Identification of spasmolytic polypeptide expressing metaplasia (SPEM) in remnant gastric cancer and surveillance postgastrectomy biopsies. *Dig Dis Sci*, *47*(3), 573-578. http://www.ncbi.nlm.nih.gov/pubmed/11911345
Yan, J., Guo, X., Xia, J., Shan, T., Gu, C., Liang, Z., . . . Jin, S. (2014). MiR-148a regulates MEG3 in gastric cancer by targeting DNA methyltransferase 1. *Med Oncol*, *31*(3), 879. https://doi.org/10.1007/s12032-014-0879-6
Yu, B., Lv, X., Su, L., Li, J., Yu, Y., Gu, Q., . . . Liu, B. (2016). MiR-148a Functions as a Tumor Suppressor by Targeting CCK-BR via Inactivating STAT3 and Akt in Human Gastric Cancer. *PLoS One*, *11*(8), e0158961. https://doi.org/10.1371/journal.pone.0158961
Yum, M. K., Han, S., Fink, J., Wu, S. S., Dabrowska, C., Trendafilova, T., . . . Simons, B. D. (2021). Tracing oncogene-driven remodelling of the intestinal stem cell niche. *Nature*, *594*(7863), 442-447. https://doi.org/10.1038/s41586-021-03605-0
Zabaleta, J. (2012). MicroRNA: A Bridge from H. pylori Infection to Gastritis and Gastric Cancer Development. *Front Genet*, *3*, 294. https://doi.org/10.3389/fgene.2012.00294
Zheng, B., Liang, L., Wang, C., Huang, S., Cao, X., Zha, R., . . . Shi, Y. (2011). MicroRNA-148a suppresses tumor cell invasion and metastasis by downregulating ROCK1 in gastric cancer. *Clin Cancer Res*, *17*(24), 7574-7583. https://doi.org/10.1158/1078-0432.CCR-11-

1714
Zhou, J., Fan, X., Chen, N., Zhou, F., Dong, J., Nie, Y., & Fan, D. (2015). Identification of CEACAM5 as a Biomarker for Prewarning and Prognosis in Gastric Cancer. *J Histochem Cytochem*, *63*(12), 922-930. https://doi.org/10.1369/0022155415609098
Zhu, A., Xia, J., Zuo, J., Jin, S., Zhou, H., Yao, L., . . . Han, Z. (2012). MicroRNA-148a is silenced by hypermethylation and interacts with DNA methyltransferase 1 in gastric cancer. *Med Oncol*, *29*(4), 2701-2709. https://doi.org/10.1007/s12032-011-0134-3
Zhu, Y., Gu, L., Li, Y., Lin, X., Shen, H., Cui, K., . . . Li, Y. (2017). miR-148a inhibits colitis and colitis-associated tumorigenesis in mice. *Cell Death Differ*, *24*(12), 2199-2209. https://doi.org/10.1038/cdd.2017.151